Modeling the Gram-Negative Bacterial Cell Envelope:

A New Approach for Permeability Investigations of Anti-Infectives

DISSERTATION

zur Erlangung des Grades

des Doktors der Naturwissenschaften

der Naturwissenschaftlich-Technischen Fakultät

der Universität des Saarlandes

von

Florian Gräf

Saarbrücken

2017

Tag des Kolloquiums:	13.07.2017

Dekan:	Prof. Dr. Guido Kickelbick

Vorsitzender:	Prof. Dr. Guido Kickelbick

Berichterstatter:	Prof. Dr. Claus-Michael Lehr
Prof. Dr. Rolf Hartmann

Akademischer Mitarbeiter:	Dr. Stefan Boettcher

Für meine Familie!!!

‘‘Dolor hic tibi proderit olim.’’

-Ovid-

Table of contents

Short summary

Antibiotics have to permeate across or into the bacterial cell envelope in order to reach their target sites. The Gram-negative bacterial cell envelope however works as a formidable barrier, often limiting sufficient antibiotic drug levels. An in-depth understanding of anti-infective permeation processes into or across the envelope (structure-permeability relationships) would therefore be of considerable interest allowing for complementary information to established efficacy testing (structure-activity relationships), together facilitating a more rational and optimized drug design process. While currently available approaches do provide insight into permeation processes, they demonstrate several shortcomings such as a non-representative composition or the inability to provide quantitative permeation data. Hence, a divisible model of the Gram-negative bacterial cell envelope, specifically designed to yield quantitative kinetically- and spatially-resolved permeation data was developed. A step by step approach was adopted, modeling each component of the tripartite structure individually followed by a final combination step. Permeability investigations showed model predictability for bacterial uptake as well as the advantage of in-depth characterization of permeation processes, enabling assessment of *in bacterio* activity on the basis of degree of passive compound permeability. Hence, the overall envelope model constitutes a valuable tool for the development of novel antibiotics.

Kurzzusammenfassung

Antibiotika müssen in die bakterielle Zellwand gelangen bzw. diese passieren um ihren Wirkort zu erreichen. Gerade die Zellwand gramnegativer Bakterien weist in diesem Zusammenhang eine ausgeprägte Barrierefunktion auf, welche hinreichende antibiotische Substanzspiegel stark limitiert. Ein tiefergehendes Verständnis derartiger Permeationsprozesse (Struktur-Permeations-Beziehung) wäre daher von großem Interesse. Diese Informationen würden zusammen mit etablierten Effektivitätsuntersuchungen (Struktur-Aktivitäts-Beziehung) einen optimierten Wirkstoffentwicklungsprozess ermöglichen. Existierende, bakterielle Modelle ermöglichen bereits einen Einblick in Permeationsvorgänge, jedoch sehen sich diese mit diversen Unzulänglichkeiten konfrontiert. So weisen die meisten eine nicht repräsentative Zusammensetzung auf und ermöglichen es in den meisten Fällen nicht, quantitative Permeationsdaten zu generieren. Daher wurde im Rahmen dieser Doktorarbeit ein Modell der gramnegativen bakteriellen Zellwand entwickelt, welches speziell entworfen wurde um quantitative, kinetische sowie räumlich aufgelöste Permeationsdaten zu erhalten. Durchgeführte Permeabilitätsstudien zeigten die Vorhersagekraft des entwickelten Models für die Substanzaufnahme in Bakterien, sowie die Möglichkeit die Aktivität von antibiotisch wirksamen Substanzen auf der Basis ihrer Modellpermeabilität vorherzusagen. Das entwickelte Modell stellt daher ein interessantes Instrument für die Entwicklung neuer Antibiotika dar.

1. General introduction

Parts of this chapter have been published in:

F. Graef, S. Gordon, C.-M. Lehr, Anti-infectives in Drug Delivery − Overcoming the Gram-Negative Bacterial Cell Envelope, *Curr. Top. Microbiol. Immunol.*, 2016 (epub ahead of print 1-22) and Anti-infectives in Drug Delivery − Overcoming the Gram-Negative Bacterial Cell Envelope, in: *How to Overcome the Antibiotic Crisis: Facts, Challenges, Technologies and Future Perspectives*, Springer International Publishing, (2016) 475-496.

The authors made the following contributions:

F. Graef   conducted literature research, created outline, wrote manuscript

S. Gordon   wrote manuscript

C.-M. Lehr   wrote manuscript

Content and figures reproduced with permission from Springer.

1.1   Mammalian epithelia as biological barriers

Mammalian epithelial cells of the for instance skin, the intestine or the lungs work as an interface with the outside world, responsible for regulating water hemostasis as well as controlling the exchange of solutes and oxygen, respectively [1]. However, such epithelial cell layers additionally have an important and pronounced protective function, acting as 'outside-in' as well as 'inside-out' barrier. Thus, only smaller molecules with specific characteristics are able to enter the cell interior via passive permeation or receptor mediated processes. The successful permeation or transport of drugs across such biological barriers in order to be bioavailable therefore represents a major challenge in the field of drug delivery.

1.2   Methods to investigate permeation across mammalian biological barriers

In vitro models mimicking mammalian biological barriers, which are capable of presenting accurate, reproducible and ethically preferable testing alternatives to the use of animal models, are from enormous interest for researchers from both industrial and academic surroundings. Such *in vitro* setups are employed to evaluate absorption processes within the evaluation of drug absorption, distribution, metabolism and excretion (ADME) across various mammalian biological barriers. An overview of commonly used experimental setups as well as a more detailed description of the system and its applications, which was employed in this doctoral thesis as support to construct the bacterial envelope model, will therefore be given in the following sections 1.2.1 and 1.2.2.

1.2.1   Overview of existing mammalian *in vitro* model setups

The majority of existing *in vitro* modeling approaches are similar in design, basically consisting of two compartments (donor and acceptor) separated by a representation of the relevant barrier, across which the permeation of the compound of interest is studied.

The first approach which has to be mentioned is the Franz diffusion cell model, depicted in Figure 1.1A, as the state of the art system to investigate dermal absorption of drugs or drug formulations [2]. The cells are usually made of glass and can be subdivided into flow-through [3] and static [4] systems. The donor and acceptor compartments are separated by excised skin of animal (e.g. porcine) or human origin. Furthermore, the Franz diffusion cell was recently used together with the so-called Permeapad™, an artificial, biomimetic membrane mimicking the small intestine [5, 6] to study passive permeation processes.

Another approach widely used to construct *in vitro* permeation models is the parallel artificial membrane permeability assay (PAMPA), initially developed to predict intestinal drug absorption. It was described for the first time in 1998 by Kansy *et al.* [7]. The setup is generally designed on a 96-well microtiter plate. Donor and acceptor compartments are separated by an artificial membrane system composed of a porous microfilter soaked in small fractions of phospholipids (PLs) dissolved in organic solvents (Figure 1.1B). In the case of the original system, filter supports are soaked with an *n*-dodecane solution containing 10% (w/v) egg lecithin [7], the reason why the approach is also referred to as the 'egg-PAMPA'. The PAMPA system has undergone tremendous advancements in recent years. One of the first modifications constituted the addition of cholesterol to egg lecithin in order to more closely mimic the high content of sterols in mammalian membranes [8]. The so-called DOPC-PAMPA uses dioleoylphosphatidylcholine (DOPC) dissolved in *n*-dodecane, as a synthetic lipid source, in comparison to egg-lecithin, which often presents batch-wise quality differences [9, 10]. The double sink PAMPA (DS-PAMPA) [11, 12], containing an artificial membrane based on lecithin dissolved in *n*-dodecane with an additional pH gradient between donor and acceptor compartments to mimic the pH difference between gastrointestinal tract and bloodstream, can be seen as a further

development. Other improvements or alterations which should be mentioned are the hexadecane membrane PAMPA (HDM-PAMPA) [13], only employing *n*-hexadecane without PLs, and the biomimetic PAMPA (BM-PAMPA), where a more relevant PL mixture, dissolved in 1,7-octadiene is used as an artificial membrane system [14, 15]. The employment of hydrophilic filter materials, such as polyvinylidene fluoride (PVDF) constitutes another variation, allowing for higher permeation rates and lower experimental times [16] in contrast to the usually used lipophilic filter material. The PAMPA system was furthermore advanced in order to investigate passive permeation across biological barriers other than the intestine, such as the skin [17] and the blood-brain barrier [18]. Another modification of the PAMPA system by Chen *et al.*, uses a different construction of the respective barrier, which is rather constructed in the pores of the filter support as a lipid-oil-lipid trilayer structure [19].
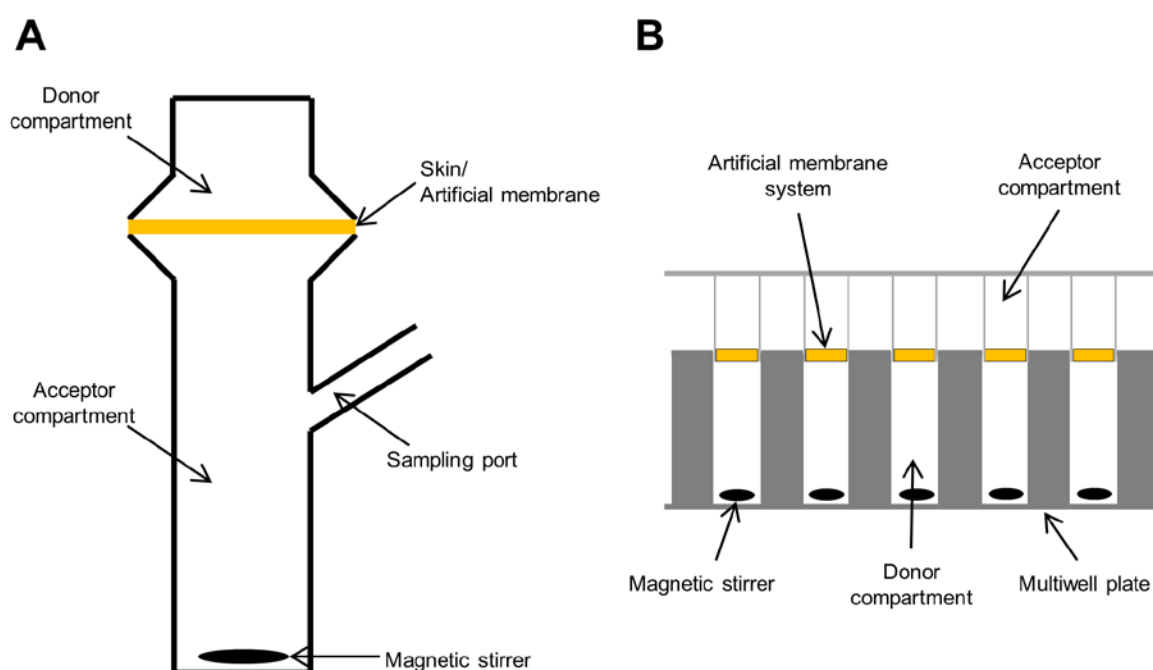
Figure 1.1: Schematic of a static Franz diffusion cell (A, modified from reference [2]) and the PAMPA system (B, modified from reference [19]).

The third approach which has to be mentioned is the Transwell® system, being widely used as a support system for cell-based as well as cell-free *in vitro* models. The system as such, together with its applications and parameters which need to be considered when performing transport studies will be discussed in more detail in the following section 1.2.2.

1.2.2 The Transwell® system and its applications

As already mentioned, the Transwell® system, depicted in Figure 1.2, constitutes a system commonly employed in cell culture work for permeation assessment. It consists of a cell culture plate together with corresponding filter inserts, which are available in different membrane materials and filter membrane pore sizes. The inserts are used as support for seeded cell layers or prepared artificial membranes, and separate the culture plate wells into donor (apical) and acceptor (basolateral) compartments.

The existing Transwell®-based approaches can basically be differentiated into cell-based and cell-free assays. When studying orally-applied drugs, the Caco-2 cell line [20, 21] represents the most commonly utilized cell type cultured as a monolayer on the filter inserts for subsequent permeation assessment. The cell line was originally isolated from colon adenocarcinoma cells from a Caucasian male. The permeation data obtained from Caco-2 cells has been shown to correlate with human intestinal absorption [21] and encompasses not only aspects of passive permeation, but also of active efflux, due to the presence of P-glycoprotein, an advantage in comparison to cell-free assays. However, the long cultivation time (approximately 21 days) required for the cell monolayer to reach confluency can be regarded as a disadvantage of this cell-based approach as well as of cell-based approaches in general. Other cell lines which are used in the Transwell® setup are alveolar epithelial cells like Calu-3 [22] or bronchial epithelial cells such as A549 [23] or the so-called human Alveolar Epithelial Lentivirus immortalized (hAELVi) cells [24]. In addition, the filter inserts also served as supports for the development of advanced and complex cell models, such as a previously developed 3D triple-culture mimicking the inflamed intestinal mucosa [25].

The Transwell® system has furthermore been employed in the development of cell-free permeation models, initially developed to investigate passive intestinal permeation. The so-called phospholipid-vesicle based permeation assay (PVPA) [26] uses PLs (originally egg-PLs) to prepare liposomes, which are employed as a transfer tool to coat filter inserts, leading to the formation of an artificial membrane structure without the use of organic solvents. The preparation procedure has been shown to result in a tight and robust barrier resistant to agitation and pH changes [27-

29]. The composition of PLs utilized for PVPA preparation has also been furthermore modified, employing for instance PL compositions which more closely mimic the intestinal PL composition [30], or PLs which allow for mimicking and studying permeation across other barriers such as the skin [31, 32].
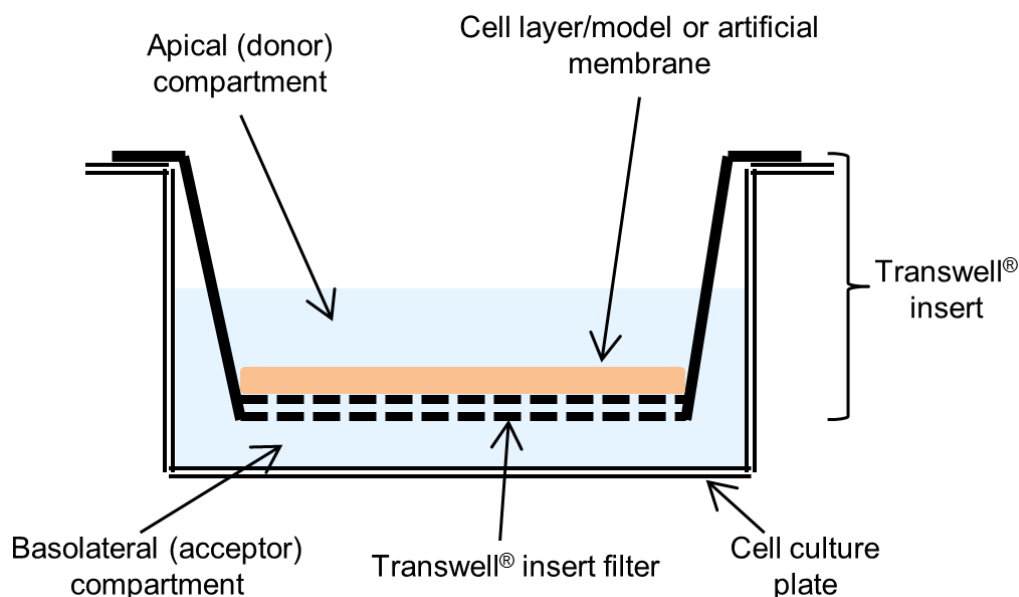
Figure 1.2: Schematic of the Transwell® cell culture system.

For the performance of Transwell®-based transport experiments buffer systems are mostly chosen in order to ensure a physiologically-relevant pH (and, in cell-based assays, a continued cell viability). However, before starting the experiment it must be ensured that the utilized compound or drug is completely soluble in the appointed buffer system. In addition, the used buffer system should not affect or alter the integrity of the employed model membrane. When studying passive permeation, it additionally has to be guaranteed that the drug concentration in the basolateral compartment does not exceed 10% of the drug concentration initially present in the apical compartment. The maintenance of these so-called sink conditions throughout the duration of the transport study ensures a continued concentration gradient, serving as a driving force for passive permeation processes [33]. After the addition of the test compound into the donor/apical compartment, samples are withdrawn from the acceptor/basolateral compartment at desired timescales and subsequently analyzed for the cumulative amount of permeated substance. In order to guarantee a

homogeneous distribution of the drug and to reduce the thickness of the unstirred water layer [33], plates are placed on an orbital shaker between sample collection time points. Furthermore, the whole system has to be thermostatically controlled throughout the experiment in order to sufficiently mimic *in vivo* temperature conditions.

1.3 The Gram-negative bacterial cell envelope as a bioavailability-limiting barrier

In clear contrast to mammalian biological barriers, the Gram-negative bacterial cell envelope consists of three principal layers: the inner (IM) and the outer membrane (OM), separated by the periplasm [34]. This complex structure works intrinsically as a significant biological barrier [35], protecting bacteria against their hostile environment. With respect to anti-infective therapy, it should be considered therefore that the efficacy of antibiotics may not just limited by an inadequate human bioavailability (e.g. due to insufficient permeation across the intestinal membrane) − anti-infective compounds are additionally confronted with the permeation-limiting ability of the envelope barrier [36], which has to be sufficiently overcome in order for anti-infective agents to be able to reach their bacterial target sites and exert their effect. This requirement highlights the presence of an additional, bacteria-related bioavailability issue [35]. The achievement of sufficient anti-infective levels at the site of action can also be further hindered by the development of bacterial resistance mechanisms, such as the production of enzymes like ß-lactamase [37]. An overview of the major structural envelope components, including occurring envelope modifications responsible for emerging resistance as well as the role of passive permeation into bacterial cells regarding anti-infective efficacy will be discussed in the following subsections.

1.3.1   The intrinsic barrier function of the envelope

The Gram-negative bacterial cell envelope, depicted in Figure 1.3, exhibits a tripartite structure. Beginning from the cytoplasmic region and proceeding outward, the IM represents the first of the three discrete layers. It constitutes a PL bilayer, being mainly composed of phosphatidylethanolamine (PE), phosphatidylglycerol (PG) and cardiolipin. The IM furthermore houses transmembrane proteins, for instance AcrB as the IM part of an efflux pump system, which will be described in more detail later in this section. Proceeding further outward, the periplasmic space (PS) represents the second structural unit, incorporating the peptidoglycan cell wall, which is much thinner in Gram-negative bacteria compared to Gram-positives.
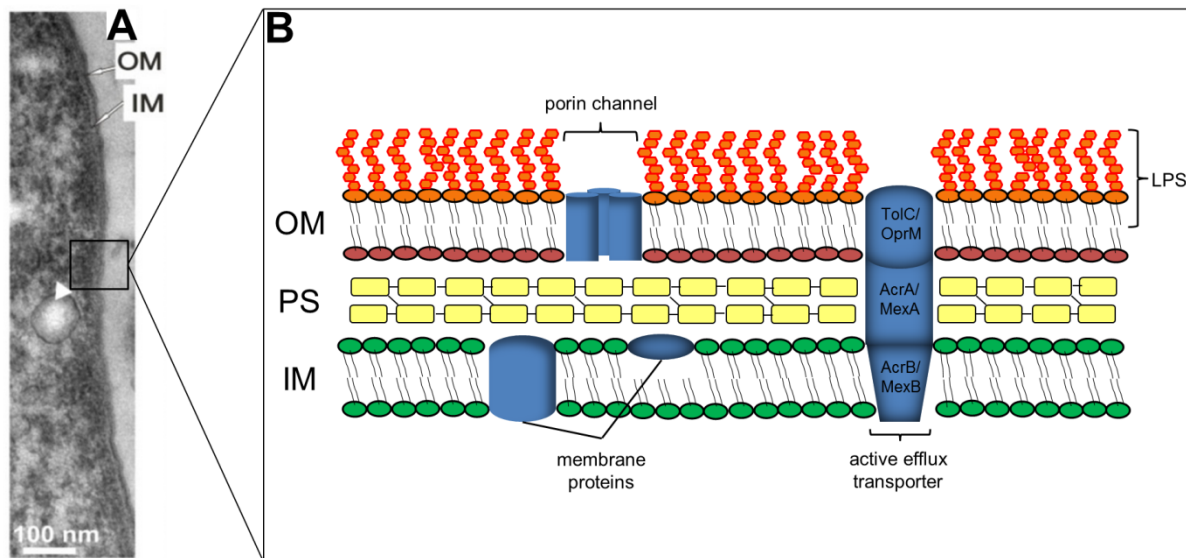
Figure 1.3: Transmission electron microscopy image of the Gram-negative bacterial cell (A) and schematic overview of the cell envelope highlighting the most important structural components (B). (A) adapted from [38]. Reproduced from [35] with permission from Springer.

Peptidoglycan as such consists of repeating disaccharide units, made of N-acetyl glucosamine and N-acetyl muramic acid, which are cross-linked by peptide side chains [39]. Peptidoglycan is responsible for imparting rigidity to bacterial cells, and therefore for sustaining cell shape and structure. The periplasm is additionally known to be an aqueous compartment showing a higher viscosity in contrast to the cytoplasm, acting as an area of high metabolic activity due to the presence of various proteins. In addition, factors of defense mechanisms such as ß-lactamase are

located in this region [34, 40]. The OM constitutes the outermost component of the tripartite structure. It is composed of a PL containing inner leaflet (IL) and a lipopolysaccharide (LPS)-containing outer leaflet (OL), hence shows an asymmetric structure. Molecules of LPS can themselves be subdivided into three major structural regions − the lipid A region (containing a phosphorylated glucosamine with saturated acyl chains which binds LPS to the IL), a core polysaccharide and the O-antigen [41]. The association of LPS molecules is strengthened by the presence of divalent cations such as calcium or magnesium in the surrounding medium, interacting in an electrostatic manner with present negative charges (on phosphate groups) in LPS molecules. The saturated nature of acyl chains within the lipid A region additionally leads to the molecule exhibiting a gel-like structure, responsible for limiting the permeation of hydrophobic compounds. In addition, outer membrane proteins (OMPs) which span the entire OM, such as porins, are incorporated into this membrane structure. Porins control the passive permeation of hydrophilic compounds, allowing small molecules such as mono- or disaccharides to pass but limiting the permeation of molecules larger in size than approximately 700 dalton [34]. The OM structure therefore constitutes an intricate barrier with a considerable ability to limit the permeation of both hydrophilic and lipophilic compounds. Moreover, active efflux transporters can additionally be present in the envelope structure, as referred to above. Most of these transport systems belong to the resistance-nodulation-cell division superfamily. They generally span the entire envelope structure, and are divided into subunits each located within different envelope layers (e.g. AcrB-AcrA-TolC or MexB-MexA-OprM efflux systems, where specified subunits are located in IM-PS-OM regions, respectively). The described pump systems are an effective efflux mechanism, mediating the excretion of anti-infectives in an energy-dependent manner [42].

1.3.2 The role of the envelope in mediating antimicrobial resistance

Bacterial resistance mechanisms can basically be clustered into categories of: (i) protection of targets by structural or expression modifications, (ii) enzymatic

degradation of antibiotics and (iii) alteration of the envelope barrier function [43]. The latter category will be further discussed as the most relevant mechanism for this doctoral thesis. The occurrence of increased efflux together with reduced uptake of anti-infectives, resulting in inadequate intracellular drug levels, can be regarded as the main results of resistance-mediated envelope modifications. The enhancement of anti-infective efflux arises due to an efflux pump overexpression – such pumps generally have a broad range of action and are therefore able to mediate efflux to various antibiotic classes [44]. In contrast, the alteration of OMP copy number or conformation, together with modifications in the LPS structure, lead to a reduced antibiotic uptake. Porins (such as OmpF), the most commonly occurring OMPs, can be downregulated even to the extent of non-expression within the OM structure [45]. In addition, a narrowing of porin channels has been reported in resistant organisms, resulting in a decreased permeation of large, hydrophilic compounds [46]. Structural modifications of LPS molecules have furthermore been shown to facilitate increased barrier properties of the envelope by means of reducing the negative net charge present in the molecule, leading to a decreased permeation of cationic anti-infectives [42].

1.3.3   The impact of passive anti-infective permeation on efficacy

Active transport, mediated by bacterial cell envelope transmembrane proteins, plays an important role in anti-infective permeation. However, passive permeation of anti-infectives, not only through porins but also across envelope membrane structures, also plays a role in the level of efficacy of anti-infectives – as such, its characterization can be considered to be of great value [47]. The ability to discriminate between passive membrane permeation and active protein-mediated transport may also be useful, for example by aiding in the differentiation of compounds which are simply poorly permeable, from compounds which actually have good membrane permeability but do not appear to reach or be retained at their target site due to active efflux. Furthermore, downregulation of porin protein expression in the OM has already been mentioned as a common bacterial resistance strategy; this occurrence creates an even greater justification for why information on passive trans-

membrane permeation is highly relevant and important. Existing models which allow for investigation of aspects of both active and passive transport pathways will therefore be discussed below.

1.4 Existing modeling approaches for characterization of bacterial transport

As discussed above, the Gram-negative bacterial cell envelope is capable of limiting the ability of anti-infectives to reach their target sites due to its intrinsic barrier function, as well as through upregulation of resistance mechanisms. As a result, the cell envelope is concluded to be an important delimiter of anti-infective bioavailability. It is therefore of considerable interest, in addition to commonly performed efficacy testing, to obtain a more detailed understanding of antibiotic trafficking processes into or across the envelope structure. A more in-depth characterization of such mechanisms would be of great value within anti-infective compound development processes. Modeling approaches which aim to mimic the cell envelope structure for the purpose of permeability testing could facilitate a more rational anti-infective drug design, and furthermore may help to improve intrinsic delivery problems. Existing approaches for modeling the cell envelope can generally be clustered into *in vitro*, *in silico* and *in bacterio* approaches, each of which will be described and evaluated in the following sections.

1.4.1 *In vitro* approaches

The variety of existing *in vitro* models provides insights into interactions between anti-infectives and bacterial cell envelope components as well as transport processes. They are mainly based on electrophysiological, vesicle-based and Langmuir trough approaches, which will be further discussed below.

1.4.1.1   Electrophysiological studies

Electrophysiological studies are employed to investigate the transport of anti-infective compounds through single channel-forming proteins – in the context of bacterial transport studies, these studies generally focus on the use of porins as a subset of outer membrane proteins. The porin OmpF, responsible for controlling the passive permeation of several antibiotics such as ß-lactams and quinolones across the OM, is most frequently employed in this respect. The experimental setup of a bacteria-relevant electrophysiology study, which is schematically depicted in Figure 1.4A, is generally based on the reconstitution of single porin channels into planar lipid bilayers, mostly consisting of phosphatidylcholine (PC). The setup is prepared by bursting porin-containing proteoliposomes across an aperture within a glass support [48]. An ion flux can subsequently be detected across the inserted porin channel, after applying an external voltage across the aperture-spanning membrane. Information about the channel structure and its functional properties under various experimental conditions (e.g. different pH) can be obtained as a result of the strength of the resulting current. The experimental setup has further been automated [49] and transferred into glass nanopipets, enabling rapid screening and additionally facilitating a higher bilayer stability [50]. The application of high-resolution ion-current fluctuation analysis additionally allows for investigation of anti-infective passage kinetics through reconstituted single porin channels [51], detecting the permeation processes by decreasing current levels as a result of porin channel occlusion by the respective, permeating compound. The determination of direct translocation of charged molecules is therefore additionally possible. Furthermore, the combination of electrophysiological studies with molecular dynamics (MD) simulations facilitates the identification of specific porin transport pathways [52, 53]. The obtained information resulting from such combinational approaches allows for insights into porin channel structure modification-related resistance mechanisms. As an example, simple modification of the OmpF channel constriction zone (the narrowest point in the channel) was shown to result in a drastic decrease of anti-infective translocation [54].

1.4.1.2   Liposomal assays

Existing liposome-based assays generally facilitate investigation of the permeabilizing effect of anti-infectives on lipid membranes, as well as their own permeation into such model structures. Herein, the so-called liposome swelling assays and liposome leakage studies need to be mentioned. Both utilize uni- or multilamellar vesicles consisting of single PLs, such as PE or PC (porins can additionally be incorporated) [45], PL mixtures, or PL-LPS mixtures, attempting to mimic OM components. In addition, fluorescent dyes or polymers are incorporated in the aqueous compartment or the bilayer of such vesicles, in order to allow for an indirect detection of permeation of the compound of interest by means of fluorescence analysis or by tracking changes in optical density (OD). Both approaches employ a similar principle for permeation detection; a general experimental setup utilizing OD measurements as read-out for the degree of permeation will therefore be further described in detail. A polymer-containing liposome dispersion is mixed together with the anti-infective of interest under isosmotic conditions. A swelling of the vesicles occurs due to water influx into the liposomes, as a result of an occurring osmotic gradient caused by the permeation of the compound of interest. The swelling of the liposomes can furthermore cause a burst of the vesicles leading to a release of the incorporated polymer, detectable as a decrease in OD (Figure 1.4B). If however, the anti-infective is not able to penetrate into the bilayer structure the OD remains unchanged. Both, liposomal leakage studies and swelling assays can be used to investigate direct membrane disrupting effects of proteins such as lamB and surfactant protein A or antimicrobial peptides (AMPs) [55-57]. In addition, as referred to above, the composition of liposomes used in such assays has been optimized in some cases in order to more closely imitate the OM composition. In such cases LPS or PL-LPS mixtures were employed, additionally allowing for the investigation of OM-specific phenomena such as PL-LPS interactions. Within this, the investigation of the lateral structure of such model membranes revealed LPS molecules to form gel-like lipid domains, whose size is dependent on the chemical structure and concentration of employed LPS molecules. These optimized setups could therefore facilitate a broader understanding of the OM

organization, or occurring modulations within the OM structure during the development of resistance mechanisms [58, 59].
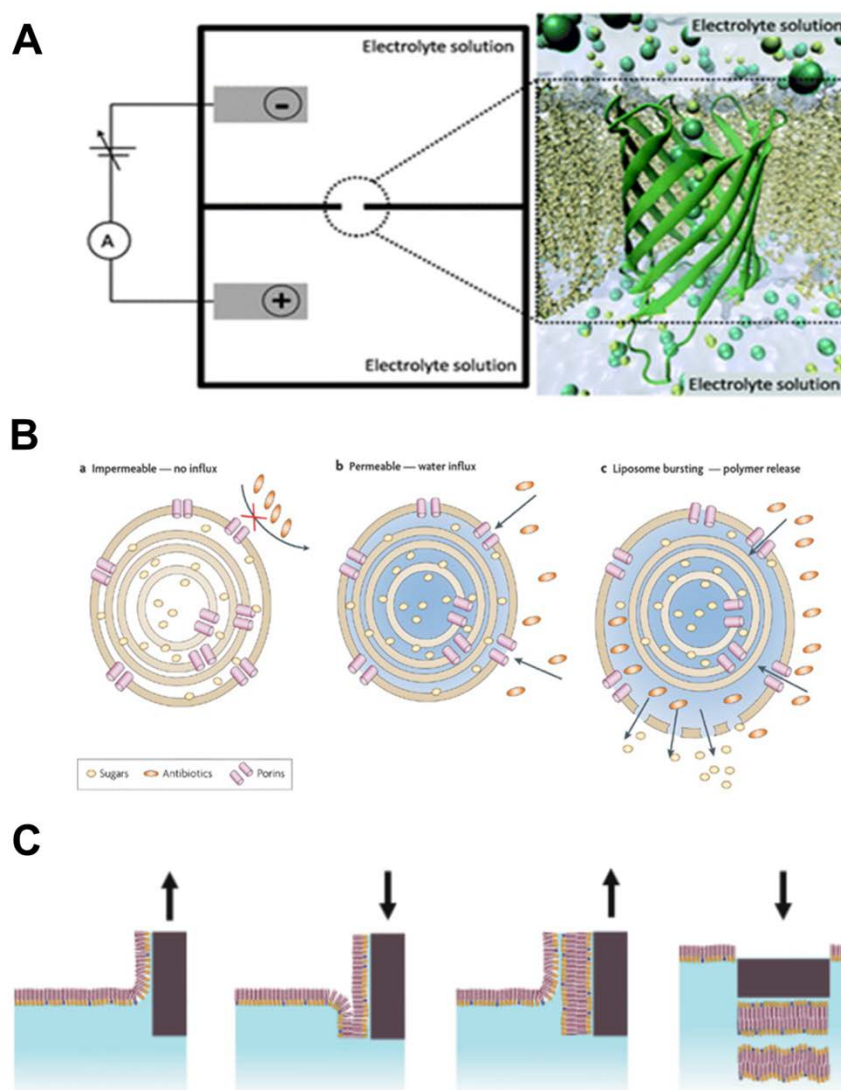
Figure 1.4: Schematic overview of *in vitro* approaches to produce bacterial membrane models, for the characterization of drug interaction and transport. (A) The experimental setup for electrophysiology studies, (B) the principle of a liposome swelling assay (C) and the Langmuir-based preparation procedure for preparing floating lipid bilayers are shown. (A) is adapted from [60] with permission of the royal Society of Chemistry. (B) is reproduced from [51] with permission from Macmillan Publishers Ltd: (Nature Reviews Microbiology) Pages *et al.* 2008. (C) is reproduced from [61] with permission from Springer.

In addition to investigating anti-infective transport by indirectly assessing their effects on vesicular lipid structures, the accumulation or uptake of anti-infectives into membrane-mimicking vesicles can be studied in a direct manner. In this respect, the anti-infective of interest, being either fluorescent or fluorescently labeled, is incubated with vesicles. Anti-infective uptake into the liposomes or the accumulation within the

lipid membrane is then measured via fluorescence microscopy or nucleic magnetic resonance spectroscopy [62, 63].

1.4.1.3   Langmuir trough-based approaches

Langmuir-based approaches are in general used for the preparation of mono- or bilayers of amphiphilic compounds. Monolayers can be deposited on water or buffer surfaces via Langmuir film balances or troughs. Bilayers however are often prepared as so-called supported lipid bilayers (SLBs) via the Langmuir-Blodgett (LB, either alone or in combination with the Langmuir-Schaefer (LS)) deposition technique using lipid vesicles which are fused onto solid supports (silicon, mica or gold) [64]. Mono- or bilayer structures can be utilized to study the organization of and interactions within such model membranes, as well as the impact of e.g. AMPs or proteins on model membrane integrity. Like many of the approaches discussed herein, Langmuir-based approaches were originally applied to study interactions within mammalian lipid-based membranes. However, mono- and/or bilayers made of bacteria-specific raw materials which furthermore mimic the envelope structure, in particular the asymmetric nature of the OM are of considerable interest in current anti-infective research. An advancement in Langmuir models with respect to a more biomimetic structural setup constitutes the preparation of so-called floating lipid bilayers. The approach combines three vertical LB depositions together with one horizontal LS deposition (Figure 1.4C), leading to a lipid bilayer floating at a distance of 2-3 nm from the SLB [61, 65]. Langmuir-derived bilayers, in an attempt to mimic the bacterial envelope, are often made from PC-PG mixtures to allow for consideration of negative charges as present in the envelope structure. Negatively charged bilayers have been used to investigate the effect of AMPs on the envelope, revealing a higher affinity to such model membranes in contrast to membranes solely consisting of electroneutral, mammal-relevant PLs like PC, and as a result an enhanced disordering and disruptive effect [55, 66]. The incorporation of porin channels, such as the aforementioned OmpF, into Langmuir-produced monolayers made of PG represents a further advancement. These OM models enable investigation of the initial interaction of antimicrobial proteins such as colicins with OmpF responsible for its

translocation across the OM [67]. Furthermore, LPS as the major OM component has been used for monolayer formation at the air-liquid interface, to produce a more accurate model of the OM and to provide insights into the orientation of LPS as well as on the structure at the air-liquid interface [68]. A more complex model setup of the OM combines a PC-containing IL (prepared via LB deposition on a solid support) together with an overlying rough strain LPS-containing (missing the O-antigen) OL (prepared via LS deposition). The model more closely mimics the asymmetric nature of the OM and was furthermore shown to describe the molecular mechanism of OM destabilization resulting from the removal of divalent cations, initially present in surrounding media [69, 70]. Another setup, being so far the closest to Langmuir-based modeling approach combines a PC self-assembled monolayer on a gold support with an overlying floating bilayer consisting of a dipalmitoylphosphatidylcholine (DPPC) IL and a rough strain LPS-containing OL (prepared via LB and LS deposition). The model was shown to exhibit an asymmetric structure. In addition, neutron reflectometry was used to study OM integrity alterations on a molecular scale as a result of treating the model membrane with ethylenediaminetetraacetic acid (EDTA), and AMPs such as lysozyme [71].

1.4.2   *In silico* approaches

In addition to the so-far described *in vitro* models, *in silico* approaches are also employed for investigation of the impact and interaction of PL species and/or LPS within simulated models. The simulations generally aim to generate accurate IM and OM mimics, with respect to both composition and structure. Furthermore, *in silico* methods are used to study the interaction of anti-infective with, or their translocation across, porins (see section 1.4.1.1). Such methods are additionally used to screen compound libraries to determine antibiotic activity as a function of quantitative structure-activity relationships (SARs) via the definition of topological descriptors, which represent values correlating chemical properties with biologic activity [72] and physicochemical parameters.

As an example, *in silico* approaches have been used to simulate an IM model consisting of PE and PG in a relatively accurate physiological ratio of 3:1, to elucidate

the intramembrane interactions between PLs. The study revealed H-bond formation between PE and PG as the main occurring interaction. Moreover, the simulation showed that the presence of PG in the IM is chiefly responsible for mediating an increased membrane stability, due to its ability to limit PE motion along the artificial membrane [73, 74]. IM model simulations have also advanced further, incorporating additional PLs. For instance, interactions within single cardiolipin bilayers were investigated [75], as well as the behavior of heterogeneous PL mixtures exhibiting different acyl chain length [76].

OM simulations have also been widely performed, initially based on LPS alone, followed by combinations of LPS together with PL to accurately reflect the asymmetric nature of the OM. These simulations generally focus on investigating the interaction between LPS molecules within the OM, the mediation of OM barrier properties as a result of the stabilizing effect of divalent cations, and the impact of OM enzymes and proteins on membrane integrity [77-79].

IM and OM simulations have furthermore been used to study the interactions of AMPs with the envelope [80]. MD simulations were additionally employed in studies elucidating the molecular and rate-limiting interactions of anti-infective permeation through porin channels on an atomic scale. Such investigations allow for a better understanding of how alterations in the porin constriction zone affect anti-infective permeation, as well as for general insights into anti-infective translocation pathways [54, 81, 82]. Moreover, *in silico* screening has been used to define quantitative SARs of anti-infective compounds by assessing the impact of physicochemical properties such as molecular weight and lipophilicity on anti-infective activity [83, 84].

1.4.3   *In bacterio* approaches

In bacterio studies, which assess the uptake/permeation of antibiotics into relevant bacteria, are of enormous interest as such a setup constitutes the most relevant condition for bacterial permeation assessment. Within such assays, a large number of relevant bacteria are typically incubated with the antibiotic of interest. Bacteria are then washed to remove the remaining extracellular and adherent antibiotic fraction,

followed by lysis of the cells and direct quantification of the amount of intracellular drug [85, 86]. In general, very sensitive quantification methods are required due to very low accumulated compound levels. Liquid chromatography-tandem mass spectrometry (LC-MS/MS) therefore constitutes the method of choice in most such cases. Another existing assay uses an indirect quantification of antibiotic uptake. Within the scope of this approach, bacterial cells are incubated with the anti-infective compound of interest, followed by centrifugation. The drug amount in the supernatant is subsequently quantified via LC-MS/MS to determine the change of extracellular drug concentration, serving as a parameter for the uptake into bacterial cells [87]. However, the accuracy of such approaches is hampered by the potential for insufficient removal of adherent antibiotic; they furthermore do not allow for a quantification process with single-cell resolution. For this reason, methods employing deep ultraviolet (DUV) fluorescence as well as a combination of a DUV fluorescence microscope together with a synchrotron beamline have subsequently been employed. Such approaches facilitate the quantification of fluorescent or fluorescently labeled compounds at a single cell level of resolution, and have been applied in the course of antibiotic uptake comparisons of wild-type to mutant/resistant strains [88-90]. Although such approaches constitute considerable advancements in the area of *in bacterio* models, most approaches are limited to an inside-outside distinction of antibiotic location. In addition, a higher degree of spatial resolution of antibiotic permeation remains extremely difficult [91]. Further shortcomings of current *in bacterio* models, as well as other envelope modeling approaches, are discussed below.

1.5   Shortcomings of existing approaches

All modeling approaches or assays described above in section 1.4 facilitate a better understanding of anti-infective permeation, as well as the interaction of anti-infectives with selected structural components of the Gram-negative bacterial cell envelope. Nevertheless, drawbacks and unmet needs can be stated for all the discussed and currently employed model categories. In general, the described *in vitro* and *in silico* approaches mostly approximate the IM or OM, rather than a combination of these

membranes as in the overall envelope structure. Moreover, most of the models deviate in their employed PL composition from that found in Gram-negative bacterial cells and do furthermore not reflect the envelope structure, in particular the asymmetric nature of the OM. In the case of the few existing overall envelope mimics, the obtainable data is limited to the description of intramembrane interactions or explanations of membrane disrupting processes. In addition, the majority of the existing approaches aiming to investigate permeation processes allow for a qualitative analysis of anti-infective permeation rather than for a quantitative one, mainly due to quantification method-based difficulties with respect to scale and resolution− there is a paucity of overall envelope models which can specifically be used to investigate anti-infective permeation processes in a quantitative manner. *In bacterio assays* have been shown to provide detailed and in some cases quantitative permeation data; however, the obtained data mostly rely on calculation of an average permeability within a bacterial cell population. In addition, such approaches are often associated with time consuming and laborious setup procedures, which do not allow for the obtainment of spatially-resolved permeation data. Such approaches furthermore enable in only a few cases the extent of anti-infective compound remaining within the envelope structure in the course of permeability investigations to be discerned.

1.6   Aims of the thesis

Anti-infective compounds need to sufficiently permeate into or across the bacterial cell envelope in order to reach their target and exert their effect. The numerous described bacterial envelope modeling approaches (*in vitro*, *in silico* and *in bacterio*) were developed and advanced over the last decades, allowing for a certain level of assessment with respect to how the Gram-negative bacterial cell envelope limits antibiotic permeation. However, all approaches – even *in bacterio* assays, as the most representative means for anti-infective permeability assessment − present several shortcomings and unmet needs (see section 1.5). It was therefore hypothesized that structurally-accurate *in vitro* envelope models, specifically designed to facilitate investigation of passive anti-infective permeation data (as initial

step) in a kinetically and time-resolved manner would be beneficial; as such permeation data would allow for a more in-depth and information-rich evaluation of anti-infective permeation processes and therefore allow for a more purposeful and rational design of novel drug candidates, in addition to existing efficacy testing.

In light of this hypothesis, the aims of this thesis were (i) to develop an *in vitro* permeation model of the overall Gram-negative bacterial cell envelope, by modeling each part of the structure individually followed by a final combination step. The model should further (ii) more accurately represent the tripartite structure of the envelope, and consist of physiologically-relevant raw materials; (iii) should be capable of providing quantitative permeation data in a kinetically- and spatially-resolved manner; and (iv) should yield permeation data predictive of bacterial uptake as well as complementary to the *in bacterio* activity of anti-infective compounds.

Based on the aims, the thesis will be structured in three main chapters:

    a)   **Modeling the Gram-negative bacterial inner membrane**

    b)   **Modeling the Gram-negative bacterial outer membrane**

    c)   **Membrane combination and the overall cell envelope model**

2. Modeling the Gram-negative bacterial inner membrane

Parts of this chapter have been published in:

F. Graef, B. Vukosavljevic, J.P. Michel, M. Wirth, O. Ries, C. De Rossi, M. Windbergs, V. Rosilio, C. Ducho, S. Gordon, C.M. Lehr, The bacterial cell envelope as delimiter of anti-infective bioavailability - An *in vitro* permeation model of the Gram-negative bacterial inner membrane, *J. Control. Release*, 243 (2016) 214-224.

The authors made the following contributions:

F. Graef	planned and performed all experiments, analyzed data, wrote manuscript
B. Vukosavljevic	planned and performed confocal Raman investigations, analyzed these data, wrote manuscript
J.P. Michel	planned and performed Langmuir studies, analyzed these data, wrote manuscript
M. Wirth, O. Ries	synthesized muraymycin derivatives
C. De Rossi	assisted with analytical techniques
M. Windbergs	designed and planned confocal Raman investigations, wrote manuscript
V. Rosilio	designed and planned Langmuir studies, wrote manuscript
C. Ducho	designed and planned the vesicle-based assay comparison, wrote manuscript
S. Gordon	designed and planned the study, wrote manuscript
C.M. Lehr	designed and planned the study, wrote manuscript

Content and figures reproduced with permission from Elsevier.

2.1 Introduction

The design, preparation and characterization of a bacterial IM model, specifically tailored for the investigation of quantitative permeation kinetics, will be described in the following chapter. A Transwell®-based setup, as discussed in the introduction (see section 1.2.2) of this thesis, was chosen as a support for model preparation in order to mimic a conventional and robust approach widely used for permeability assessment across mammalian cell barriers [22]. The original PVPA approach [26], designed for the preparation of a mammalian lipid-based model of the small intestine, as also discussed in the previous chapter (see section 1.2.2) was adapted in order to prepare the IM model, employing a specific PL composition as present in the IM of representative Gram-negative strains such as *Escherichia coli* and *Pseudomonas aeruginosa* [92]. The resulting preparation procedure was further used for the production of a model solely based on PC, the major PL in mammalian cell membranes [26], as a comparator system, designed to illustrate the importance of using bacteria-relevant materials for IM model preparation. The IM and the mammalian lipid-based model ('mammalian comparator') were subsequently compared at each stage of IM characterization as well as in following permeability investigations. This comparison was conducted in order to clearly discern any lipid-dependent differences between the models regarding structure and function. Furthermore the comparison intents to ultimately demonstrate the need to adapt an already existing PVPA assay, employing bacteria-specific raw materials. In an initial step, employed PLs were analyzed and compared on the molecular scale. Further characterization on the model level addressed parameters such as integrity and robustness, as well as topography and thickness. In addition, sets of model compounds and anti-infectives were utilized to assess the impact of model PL composition on permeability behavior, and to investigate the existence of functional similarity of the IM model to the native IM. Such studies also aimed to highlight the ability of the developed IM model to provide quantitative and kinetically-resolved permeation data, a clear advantage in comparison to already existing bacterial assays.

2.2   Materials and Methods

2.2.1   Materials

The bacteria-relevant PLs (1-hexadecanoyl-2-(9*Z*-octadecenoyl)-*sn*-glycero-3-phosphoethanolamine (POPE), 1-hexadecanoyl-2-(9*Z*-octadecenoyl)-*sn*-glycero-3-phospho-(1'-*rac*-glycerol) (sodium salt) (POPG) and 1,1',2,2'-tetra-(9*Z*-octadecenoyl) cardiolipin (sodium salt) (CL) were purchased from Avanti Polar Lipids Inc. (Alabaster, Al, USA). Egg PC (Lipoid E 80) was kindly provided by Lipoid GmbH (Ludwigshafen, Germany). The commercially available Transwell® cell culture system (Transwell® permeable supports 3460) was purchased from Corning Inc. (Acton, MA, USA). All employed fluorescent dyes, ß-blockers and anti-infective compounds were purchased from Sigma-Aldrich Co. (St. Louis, MO, USA). Mobile phase components for ultra-high performance liquid chromatography (UHPLC) were purchased from VWR (Radnor, PA, USA). All other solvents and chemicals were of at least analytical grade.

2.2.2   Langmuir trough investigations

A thermostated Langmuir film trough (775.75 cm^2, Biolin Scientific, Finland) enclosed in a plexiglas box was used to perform surface pressure-area (π-A) measurements of lipid monolayers. Monolayers were composed of pure PC, the single bacteria-relevant PLs (POPE, POPG, CL) and a 70:20:10 (POPE:POPG:CL) weight mixture, representative of the Gram-negative IM composition [92]. All experiments were conducted at 294 and 303 K (21 ± 1 °C and 30 ± 1 °C respectively). A chloroform-methanol mixture (9:1 v/v) was used to prepare PL solutions of 1x10^{15} molecules µl^{-1}. PLs were then spread at the air/buffer interface, followed by subphase cleaning by suction. The system was left for 15 min to allow for complete organic solvent evaporation. A speed of 5 Å^2*molecule^{-1}*min^{-1} was used for monolayer compression. The reported results constitute mean from two individual experiments. The surface

compressional moduli (K) from obtained monolayers were calculated according to equation 1:

$$K = -A^* \left(\frac{d\pi}{dA} \right) \tag{1}$$

where A is the PL molecular area (Å^2), $d\pi$ the surface pressure change (mN/m) and dA the change in molecular area.

Furthermore, the area occupied by PL molecules in the bacterial PL mixture monolayer, at each surface pressure (π), was calculated according to the additivity rule, shown in equation 2:

$$[A_{TH}]_\pi = [X_{POPE}\ A_{POPE} + X_{POPG}\ A_{POPG} + X_{CL}\ A_{CL}]_\pi \tag{2}$$

where $[A_{TH}]_\pi$ is the theoretical molecular area, X the PL molar fraction and A the PL molecular area in the pure PL monolayer.

The excess molecular areas ΔA^{EXC} were then calculated from A_M-A_{TH} representing the difference between experimental (A_M) and theoretical (A_{TH}) molecular area values. Calculated deviations of A_M from A_{TH} (as calculated from the additivity rule, equation 2) can be related to the quality of PL mixing. In this respect, negative deviations from the additivity rule imply good mixing, whereas positive deviations reflect of area expansion and unfavorable interactions between the PLs, resulting in poor mixing [93].

The free energy of mixing ΔG^M was calculated according to the equation 3 [94]:

$$\Delta G^M = \Delta G^{EXC} + \Delta G^{IDEAL} \tag{3}$$

where ΔG^{EXC} is the excess free energy (shown in equation 4) and ΔG^{IDEAL} is the free energy of mixing (shown below in equation 5) for an ideal mixture:

$$\Delta G^{EXC} = \int_0^\pi \Delta A^{EXC}\, d\pi \tag{4}$$

$$\Delta G^{IDEAL} = RT\, (X_{POPE} \ln X_{POPE} + X_{POPG} \ln X_{POPG} + X_{CL} \ln X_{CL}) \tag{5}$$

in the above, R is the universal gas constant and T the absolute temperature.

2.2.3   Liposome preparation and characterization

Both IM and mammalian comparator models were prepared using an adapted version of the PVPA approach [26]. In order to provide a means for depositing PLs onto Transwell® filter inserts, liposomes of the appropriate PLs were first produced via the lipid film hydration method [95]. In this respect, the bacteria-relevant PL mixture of POPE:POPG:CL (70:20:10 weight ratio) was utilized to produce liposomes for IM model preparation, while PC as mammal-relevant PL was employed to produce liposomes for preparation of the mammalian comparator model. In both cases, PLs were dissolved in a chloroform-methanol mixture (3:1 v/v, 5 ml). Using a Rotavapor R-205 (Büchi Labortechnik GmbH, Essen, Germany), the organic solvent mixture was then removed under reduced pressure for 1 h at 200 mbar, followed by an additional 30 min at 40 mbar (at 70 °C in the case of the bacteria-specific PL mixture, and at 55 °C for the mammal-specific PL) to form a thin lipid film. The lipid film was rehydrated using phosphate-buffered saline (PBS; adjusted to pH 7.4) containing 10% (v/v) ethanol, resulting in a 6% (w/v total PL) liposome dispersion. Liposomes were subsequently sonicated for 1 h and extruded 10 times, at the same temperature as used for the above corresponding lipid film formation step, using a Liposofast L-50 extruder (Avestin Europe GmbH, Mannheim, Germany). Liposomes were subsequently analyzed regarding their hydrodynamic diameter and size distribution using dynamic light scattering. Surface charge (ζ-potential) was also determined via laser doppler micro-electrophoresis (Zetasizer Nano ZS, Malvern Instruments, UK).

2.2.4   Model preparation procedure

Both, IM and mammalian comparator models were then similarly prepared via three consecutive cycles of respective liposome addition (75 µl in each cycle) onto Transwell® filter inserts, followed by centrifugation (30 min, 1040 g; Hettich Rotina 420 R, Hettich GmbH, Tuttlingen, Germany) and oven-drying (50 min, 50 °C). The procedure was completed by a freeze-thaw cycle (-80 °C, 20 min; 45 °C for 20 min).

2.2.5 Electrical resistance (ER) measurements

Simulated transport experiments were performed in which model membranes were exposed to Krebs-Ringer buffer (KRB; adjusted to pH 7.4; 37 °C) over a time period of 5 h. Resistance (R; Ω) was measured at regular time intervals, using a handheld chopstick electrode (STX-2) together with an epithelial voltohmmeter (EVOM, World Precision Instruments, Berlin, Germany). Cell culture plates supporting IM and mammalian comparator models were stored on an orbital shaker (IKA®-Werke GmbH and Co KG, Staufen, Germany) set at 150 rpm and kept in an incubator at 37 °C between the measurements. The electrical resistance (ER) of each model at measured time points was calculated via equation 6:

$$ER\ (\Omega*cm^2) = (R_{\text{insert with model membrane}}/R_{\text{blank insert}})*1.12\ cm^2 \tag{6}$$

where $1.12\ cm^2$ represents the surface area of the Transwell® filter insert.

2.2.6 Confocal Raman microscopy

A WITec alpha 300R + imaging system (WITec GmbH, Ulm, Germany) with an Olympus 50 x objective (N.A. 0.35) was used to study the model integrity of IM and mammalian comparator lipid layers. A diode laser with a wavelength of 785 nm (50 mW) served as the excitation source. The IM and the mammalian comparator model were analyzed in both the freshly prepared state, as well as following 5 h incubation in KRB (adjusted to pH 7.4; 37 °C), without any further sample alteration. A confocal pinhole of 100 μm was used to reject signals from out-of-focus regions. The entire model membrane area was analyzed in all cases, recording Raman spectra every 100 μm (along the x- and y-axis) with an integration time of 4 s. Background subtraction and cosmic ray removal were applied to all obtained spectra. Spectra were subsequently processed using hierarchical cluster and basis analysis, serving as multivariate approaches for data processing, followed by conversion into spatially-resolved false-color images using WITec Project Plus software (WITec GmbH, Ulm, Germany).

2.2.7   Laser scanning interferometry

A LEXT OLS4000 3D Laser Measuring Microscope (Olympus AG, Tokyo, Japan), with a 405 nm semiconductor laser and a 20 x objective lens was used for model topography analysis. Transwell[®] filter insert membranes with respective PL coatings were cut out of the plastic surround and subsequently fixed on sample holders. Representative membrane areas each with an image size of 5.6 mm^2 were examined. The model center was defined as surface area (1) and centers of additional analyzed regions were set at a distance of 3000 μm from the upper (2), right (3), bottom (4) and left (5) boundary of the model surface.

2.2.8   Scanning electron microscopy (SEM) and cryogenic (cryo)-SEM

For the purpose of scanning electron microscopy (SEM) analysis, freshly prepared model membranes were initially freeze-dried (Christ alpha 2-4 plus, Martin Christ Gefriertrocknungsanlagen GmbH, Osterode am Harz, Germany), following which Transwell[®] filter insert membranes with respective PL coatings were removed from the plastic holder surround. Transwell[®] filter membranes themselves were then carefully removed from freeze-dried membrane models, and vertical cross-sections of models were prepared using a scalpel. Cross-sections were sputtered with gold, vertically placed on sample grids and analyzed via SEM (Zeiss EVO HD 15, Carl Zeiss AG, Oberkochen, Germany). For cryogenic (cryo)-SEM investigations, model membranes were frozen in liquid nitrogen, followed by the preparation of cross-sections as for conventional SEM. Samples were subsequently cryo-coated using a fracture coater (MED 020, Leica microsystems GmbH, Wetzlar, Germany) and imaged via a Quanta™ FEG 3 d SEM (FEI, Hillboro, Oregon, USA) in order to investigate inner model morphology.

2.2.9   Permeability investigations

Transport studies were performed to investigate permeability behavior across the IM and mammalian comparator model. Fluorescent dyes and ß-blockers served as model compounds (Table 2.1), while ciprofloxacin and minocycline (with or without 1 h model pre-incubation of 15.4 µM polymyxin B (PMB)) were employed as anti-infective compounds. AlexaFluor[®] 488-labeled functionalized fatty acids of the muraymycin A series of nucleoside antibiotics together with the corresponding reference compound (both synthesized in-house in accordance with Ries *et. al* [63]), were further utilized as anti-infective compound-derived structures. Transwell[®] filter inserts with model membrane coatings were placed in cell culture plates and pre-incubated with pre-warmed KRB (pH 7.4; 37 °C) for 30 min to rehydrate and equilibrate the membrane system. KRB was then removed and 520 µl of model or anti-infective compound solutions in KRB (at concentrations calculated in order to ensure sink conditions and adjusted to pH 7.4) was added to the apical compartment of each Transwell[®] system (Table 2.1). A volume of 1.5 ml pre-warmed KRB was added to the basolateral compartment. A 20 µl volume of compound solution was then directly removed from the apical (donor) compartment in order to allow for precise determination of the start concentration. Samples of 200 µl were taken from the basolateral (acceptor) compartment after 0, 0.5, 1, 1.5, 2, 2.5, 3.5 and 4.5 h for the quantification of permeated compound amounts (see section 2.2.10). A 200 µl volume of pre-warmed KRB was added to the basolateral (acceptor) compartment after each sampling, to maintain sink conditions. Cell culture plates with model-supporting Transwell[®] filter inserts were placed on an orbital shaker (IKA[®] - Werke GmbH und Co KG, Staufen, Germany) set at 150 rpm and kept in an incubator at 37 °C (CO_2: 5%) for the entire experiment run time.

2.2.10   Quantification of permeated compound amounts

2.2.10.1   Fluorescence quantification

A plate reader (Tecan Infinite$^®$ M200, Tecan GmbH, Crailsheim, Germany) was used to determine the permeated amounts of calcein, fluorescein, rhodamine 123, rhodamine B, rhodamine B isothiocyanate and AlexaFluor$^®$ 488-labeled fatty acid moieties as well as the corresponding reference compound (Table 2.1).

2.2.10.2   UHPLC quantification

The permeated amount of ß-blockers, ciprofloxacin and minocycline was quantified using a Dionex Ulitmate$^®$ 3000 UHPLC with an RP-18 column (Accucore™, 150 mm x 2.1 mm; 2.6 µm; Thermo Fisher Scientific Co., Waltham, MA, USA). A binary solvent mixture (A = 36.36 mM Na_2HPO_4 + 33.4 mM trimethylamine adjusted to pH 3; B = acetonitrile) was used in the case of the ß-blockers. The employed flow rate and resulting retention time (RT) differed between compounds (Table 2.1), whereas the column oven temperature was set to 40 °C in all cases. Ciprofloxacin and minocycline quantification was also performed using a binary solvent system (A = 0.02 M Na_2HPO_4 adjusted to pH 2.7; B = acetonitrile) in different ratios, resulting in different RTs (Table 2.1). The column oven temperature was set to 25 °C for ciprofloxacin and 40 °C for minocycline.

Table 2.1: Quantification parameters of employed compounds. Adapted from [96] with permission from Elsevier.

Compound	Initial donor concentration (µM)	λ_{exc} (nm) – λ_{em} (nm)	λ_{max} (nm)	Binary solvent system (A:B)	Flow rate (ml min^{-1})	Retention time (min)
Calcein	22	470 - 530	-	-	-	-
Fluorescein	26.6	485 - 530	-	-	-	-
Rhodamine 123	14.4	540 - 580	-	-	-	-
Rhodamine B	130.4	540 - 600	-	-	-	-
Rhodamine B isothiocyanate	116.6	540 - 600	-	-	-	-
AlexaFluor® 488-labeled moieties	1.27	470 - 520	-	-	-	-
Atenolol	3.6	-	280	90:10	0.2	1.4
Metoprolol	16.4	-	280	70:30	0.4	1.1
Timolol	7.8	-	280	80:20	0.4	1.7
Nadolol	5.7	-	280	85:15	0.2	3.1
Acebutolol	0.89	-	235	70:30	0.2	2.2
Alprenolol	4	-	270	65:35	0.4	1.4
Ciprofloxacin	0.06	-	280	77:23	0.2	3.6
Minocycline	2.19	-	270	80:20	0.2	4.2

2.2.10.3   Calculation of permeated compound amounts

The permeated amount was calculated in the case of all tested compounds according to calibration curves created from samples of standard concentration. The permeated, cumulative amount was then plotted as a function of time.

The slope of the linear region of this curve represents the compound flux rate, which was used to calculate the apparent permeability coefficient (P_{app}) via equation 7:

$$P_{app} \text{ (cm/s)} = J / (A * c_0) \tag{7}$$

where J is the substance flux (mg/s), A the surface of the Transwell® filter insert (cm^2) and c_0 the initial compound concentration in the apical compartment (mg/ml).

2.2.11 Statistical analysis

Where suitable, presented numerical data represent the mean ± standard error of the mean (SE). Student's t-test was used to evaluate significant differences (* = $P < 0.05$, *** = $P < 0.001$). All tests were calculated with the software SigmaPlot (version 12.5, Systat Software, Inc., San Jose, California, USA).

2.3 Results and discussion

2.3.1 Bacteria- and mammal- relevant PL interfacial behavior comparison

The interfacial behavior of the bacterial IM-specific PLs POPE, POPG and CL alone, the ternary blend (in a relevant 70:20:10 weight ratio) and PC as mammal-relevant PL were studied via the Langmuir trough technique. Surface pressure-area measurements of respective monolayers were performed in order firstly to demonstrate the miscibility of the bacterial ternary mixture, and secondly to determine any notable differences between the bacterial mixture and PC monolayers at the molecular level. The measurements were first performed at 21 °C, and then at 30 °C, the latter representing a more physiologically relevant temperature and the maximum temperature able to be applied in the experimental setup without the occurrence of buffer evaporation, which would lead to inaccuracies. The obtained measurements were used to construct surface pressure isotherms, which were

subsequently used to calculate the compressibility moduli of investigated PL monolayers.

As visible in Figure 2.1A, surface pressure isotherms of the ternary bacterial PL mixture, measured at 21 °C, appeared to be in-between those of the pure components.
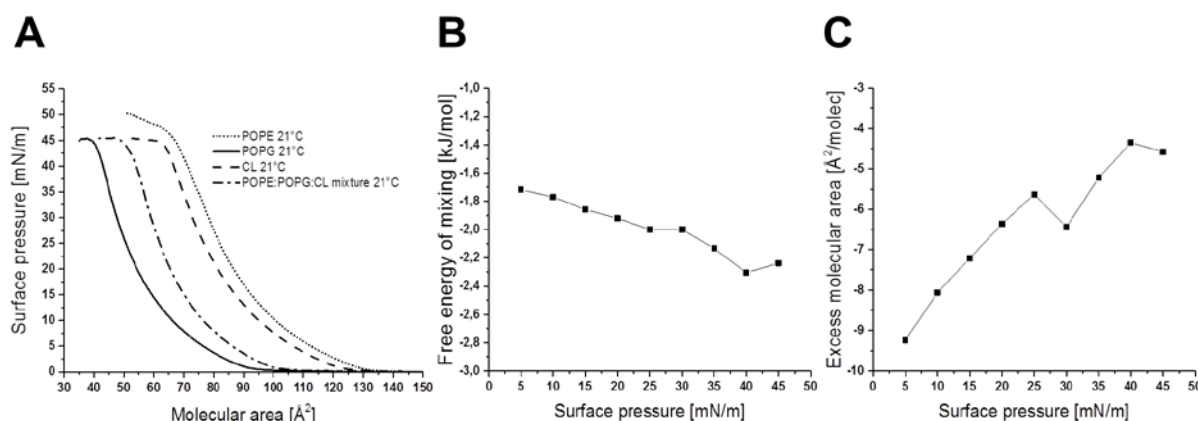

Figure 2.1: Comparison of the isotherms for pure bacteria-relevant PLs and the IM relevant mixture (A), together with the free energy of mixing (ΔG^M) (B) and the excess molecular area (ΔA^{EXC}) (C) with respect to surface pressure of the ternary IM-representative PL blend. Reproduced from [96] with permission from Elsevier.

The interfacial behavior of the ternary mixture monolayers is therefore influenced by the presence of POPG and CL, and is not solely dependent on its major component POPE. The observed impact of POPG and CL on the interfacial behavior, together with the calculated negative free energy of mixing (Figure 2.1B) and negative excess molecular area (Figure 2.1C) of the ternary mixture monolayer, further conclusively demonstrate a good miscibility of the ternary bacterial mixture at all studied surface pressures.

The ternary bacterial PL blend and pure PC monolayers revealed similar collapse pressures (π_c) at both measured temperatures (Figure 2.2A), with values of approximately 44 mN m^{-1} (Table 2.2). However, the larger molecular areas of the mixture monolayers in comparison to those of pure PC (derived from the respective isotherms) at pressure onset (A_{onset}) and collapse (A_c), indicate a more expanded state of the bacterial PL blend monolayers relative to the pure PC (Table 2.2).
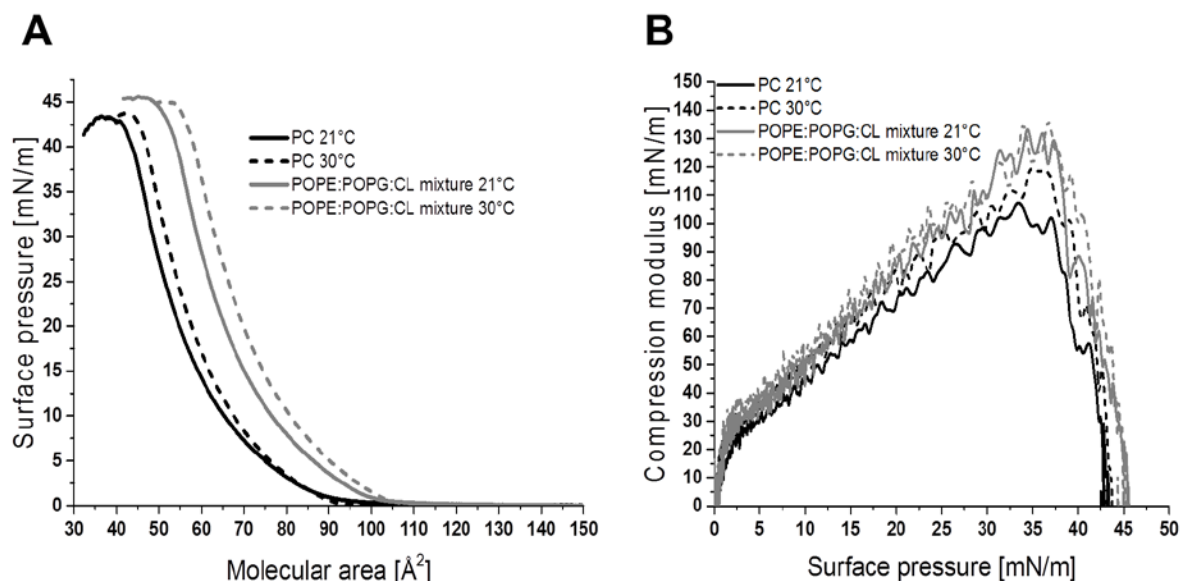
Figure 2.2: Compression isotherms for the IM-specific PL mixture (POPE:POPG:CL) and pure PC monolayers at 21 °C and 30 °C (A), showing differences in two-dimensional organization. Corresponding compressibility moduli as a function of surface pressure for both tested monolayers are additionally depicted (B). Reproduced from [96] with permission of Elsevier.

The physical state of PC and bacterial PL mixture monolayers as a function of surface pressure was furthermore determined by calculating the compressibility moduli. Compressibility moduli values below 12.5 mN/m indicate a gaseous phase of monolayers, while values in the range of 13-100 mN/m infer a liquid expanded (LE) state; values from 100 to 250 mN/m account for a liquid condensed (LC) physical state, while values above 250 mN/m demonstrate a solid state of monolayers [97]. The physical state of PLs at surface pressures of 25-35 mN/m is of particular interest, as this range correlates with the internal lateral pressure of natural membranes [98]. As can be seen from Figure 2.2B at both investigated temperatures, POPE:POPG:CL monolayers were observed to be in LC state within the pressure range of 25-35 mN/m, whereas PC monolayers were found to be in an LE state, only reaching the LC state at higher pressure values of 30-38 mN/m. The performed interfacial analysis therefore revealed the bacterial ternary blend monolayers as being slightly more rigid and greater in molecular area in comparison to those of PC – this provides a first indication of differences between bacterial IM- and mammalian-specific PLs on a molecular scale.

Table 2.2: Characteristic parameters of compression isotherms, comparing the IM-relevant POPE:POPG:CL mixture to PC at 21 °C and 30 °C. Reproduced from [96] with permission from Elsevier.

Applied Temperature (°C)	Monolayer	A_{onset} (Å^2)	A_c (Å^2)	π_c (mN/m)
21	POPE:POPG:CL	103.0	51.6	45.4
21	PC	97.5	43.5	42.9
30	POPE:POPG:CL	107.5	55.8	44.9
30	PC	92.3	45.4	43.5

2.3.2   IM and mammalian comparator model preparation

Following the initially conducted interfacial behavior comparison, the 70:20:10 (weight ratio) mixture of POPE:POPG:CL was used to prepare the bacterial IM model, while PC was used for production of the mammalian comparator model. Both models were prepared via the PVPA [26], a two-step approach, starting with the preparation of liposomes (made of the PLs of interest) which are used in the second step as transfer tool to deposit PLs onto Transwell® filter inserts without the use of organic solvents, via a repeated coating procedure. Prepared POPE:POPG:CL and PC liposomes, although serving only as deposition tool, were nevertheless analyzed regarding their hydrodynamic diameter and surface charge in order to prove a consistent outcome of liposome production. An acceptable variability of the z-average and surface charge was observed in the case of both liposome formulations (Table 2.3), while differences in liposome size comparing bacterial and mammalian lipid liposomes could be considered as an outcome of the previously observed PL differences on the molecular level, especially with respect to the lipid packing.

Table 2.3: Z-average (nm) and surface charge (ζ-potential, mV) of POPE:POPG:CL (bacteria-specific) and PC (mammal-specific) liposomes. Values represent mean ± SE from 4 batches, each measured in triplicate. Reproduced from [96] with permission from Elsevier.

Liposome Formulation	z-average (nm)	ζ-potential (mV)
POPE:POPG:CL	413.5 ± 13.7	-31.3 ± 1.4
PC	665.8 ± 30.4	-4.9 ± 0.3

While the initial PVPA model consisted of PC alone [27, 28, 99], the major aim of the work within this chapter was to design a robust and stable model of the bacterial IM using the physiologically-relevant 70:20:10 mixture of bacteria-specific PLs. Therefore, the PVPA preparation procedure was first adapted and optimized to the use of POPE:POPG:CL. The finalized procedure was then transferred to the preparation of the mammalian model, employing PC, in order to obtain a comparator which was truly and directly comparable. The preparation method was optimized to ultimately obtain a model with sufficient barrier properties as well as stability with respect to buffer exposure, as would occur during transport studies. Hence, the liposome deposition and coating parameters were refined to fulfill these requirements, by means of tracking the influence of parameter changes on model barrier function via ER measurements during simulated transport experiments (KRB, pH 7.4, 37 °C, 5 h). ER as such constitutes a parameter which is commonly employed to examine barrier properties of cell-free [26] and cell-based [100] permeation models. A resistance value of 400 Ω*cm^2 was set as a commonly accepted minimum indicating sufficient barrier properties in cell-based models [22, 100]. The final, optimized preparation procedure, depicted in Figure 2.3, consisted of three consecutive cycles of liposome addition onto Transwell® filter inserts, followed by centrifugation and drying as well as a final freeze-thaw cycle as shown to promote liposome fusion and formation of a confluent PL layer [27].
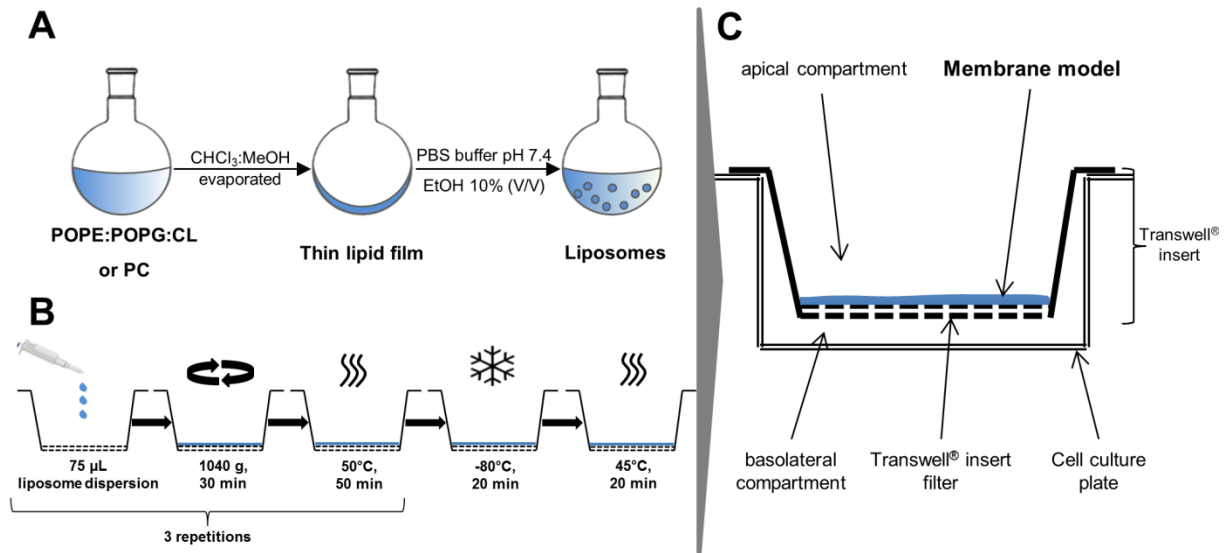
Figure 2.3: Schematic of the two-step PVPA model preparation procedure, consisting of liposome preparation (A) and subsequent coating with liposome dispersions to form IM and mammalian comparator models (B). The final model setup (blue) placed on top of a Transwell® filter insert is additionally shown (C). Reproduced from [96] with permission from Elsevier.

ER measurements of the final, optimized bacterial IM model showed sufficient values always higher than the set and accepted minimum throughout the conducted simulated transport experiments (Figure 2.4), as well as no visible detachment of lipid coating. The same observations could be made in the case of the identically prepared mammalian comparator model (data not shown).
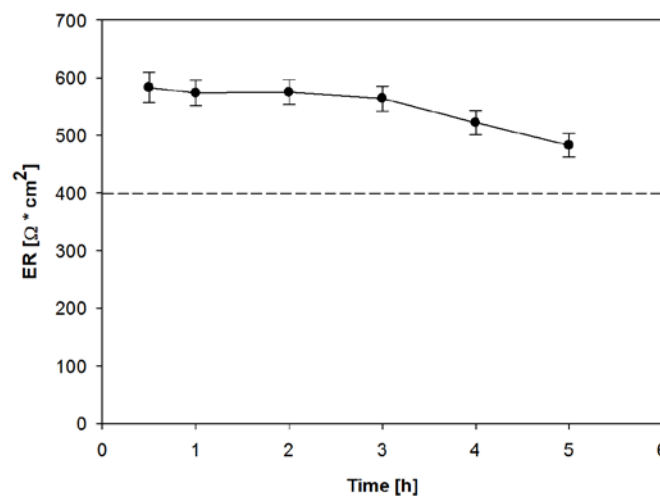
Figure 2.4: Blank corrected ER values of the bacterial IM model. The high and relatively constant ER profile indicates sufficient and continued model barrier properties. The dashed line indicates the accepted minimum ER level of live cell-based models such as Caco-2 cell monolayers, for reference. Values represent mean ± SE; n=6 from 2 individual experiments. Image reproduced from [96] with permission from Elsevier.

2.3.3   Model characterization and comparison

2.3.3.1   Model integrity assessment

As described, both IM and mammalian comparator models were shown to constitute stable and robust membrane structures with appreciable barrier function. However, any discontinuity present upon model preparation or occurring during transport experiments would potentially lead to overestimation of the permeated amount of tested drugs/compounds; it was therefore deemed necessary to further assess and conclusively demonstrate model integrity. Confocal Raman microscopy was therefore used as a chemically selective method to analyze the PL coating across the entire surface of both models following preparation, and after simulated transport experiments.

In light of the structured surface of the models, optical topography was applied before conducting confocal Raman microscopy analysis in order to allow for adjustment of focus based on model topography, and to allow for topography characterization of the entire model area. Topography profiles showed a lower surface height at the center compared to the edges in the case of both models (Figure 2.5), an observation which is in agreement with previous investigations and attributed to the model preparation procedure [101].
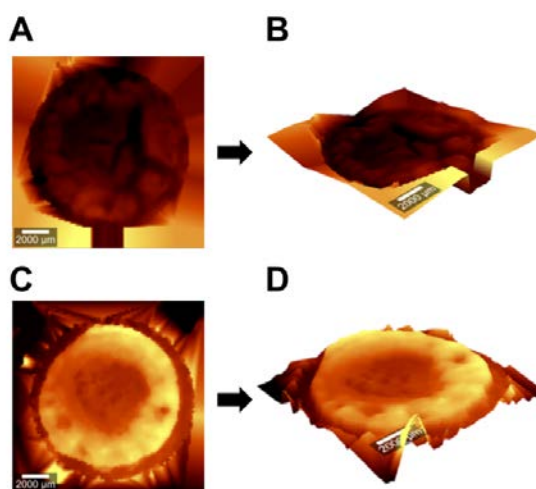
Figure 2.5: Two- and three-dimensional optical topography profiles of the overall model surface area in the case of the IM (A, B) and the mammalian comparator model (C, D). Reproduced from [96] with permission from Elsevier.

The individual Raman spectra of the polyester material of Transwell® filter inserts and the PLs of each membrane model, as recorded via confocal Raman spectroscopy, allow for label-free discrimination between these components, and consequently for the determination of the extent of PL coating of Transwell® filter inserts. Recorded Raman spectra were processed and converted into spatially-resolved false color images to allow for visualization of the PL coating integrity. A continuous PL coverage of Transwell® filter inserts without any lipid-free areas could be observed in the case of the bacterial IM model, after preparation (Figure 2.6A) as well as after model exposure to KRB for 5 h (Figure 2.6B). The same observations were made in the case of the mammalian comparator model; likewise analyzed following preparation (Figure 2.6C) and simulated transport experiments (Figure 2.6D). Raman signal intensity variations were seen to translate to color intensity gradients in false color images in some cases (especially in Figure 2.6D); however, the presence of the respective lipid-specific peaks, detected across the entire Transwell® filter insert area in both models before and after exposure to KRB, confirmed the PL layer as being continuous and intact in all cases. For illustrative purposes, the individual raw Raman spectra collected from the central and the outer region of coated filter membranes (marked by black and red crosses, respectively) are shown below each false color image in Figure 2.6. The confirmed integrity of both IM and mammalian comparator models, together with the above demonstrated appropriate and stable model barrier properties, therefore indicates a fitness for purpose of both models with respect to compound permeability investigations.
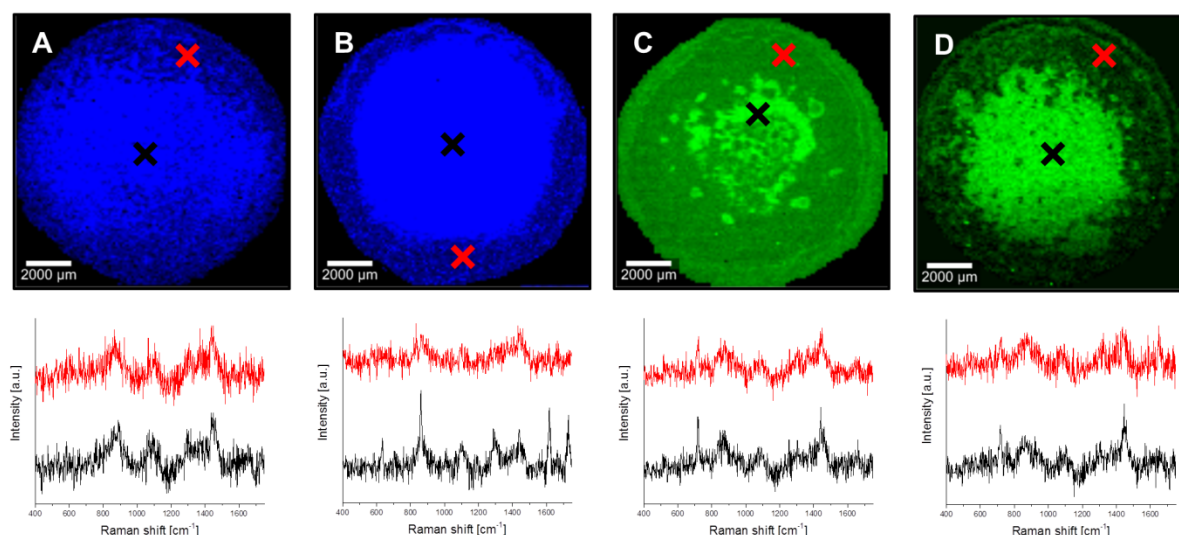
Figure 2.6: False color images with representative single Raman spectra of central and outer regions of coated Transwell® filter inserts, showing the IM model with bacteria-relevant lipids indicated in blue before (A) and after (B) exposure to KRB, as well as mammal-relevant lipids of the comparator model in green before (C) and after (D) exposure to transport buffer. The presence of lipid-specific Raman peaks in all single Raman spectra at 1440 cm^{-1} (in raw state without any further spectral manipulation, e.g. smoothing or subtraction) confirmed the overall lipid coverage. Color intensity differences represent the variation in Raman signal intensity, not a lesser degree of lipid coverage. Reproduced from [96] with permission from Elsevier.

2.3.3.2   In-depth model topography assessment

Following the confirmation of model suitability for permeability experiment conditions, the characterization focus shifted further towards comparison and distinction of model properties. In this regard, laser scanning interferometry was employed to obtain a more detailed insight into model topography profiles upon preparation, additional to the previously performed optical topography investigations in the course of confocal Raman analysis. Thus, the IM model and mammalian comparator model topography was analyzed at five representative areas (center, upper, right, bottom and left edge) with an image size of approximately 5.6 mm^2, corresponding to the maximum objective-mediated image size (Figure 2.7A). Differences in height maxima were observed comparing the center area of IM models, showing values of approximately 73 μm, to the edge areas, where maximum values up to 184 μm were observed (Figure 2.7B 1-5). In addition, the center region revealed a more uniform surface profile as compared to the edge areas. The analysis of the mammalian comparator model showed comparable height maxima likened to the IM model as well as the

same difference in surface profile uniformity comparing center to edge regions (Figure 2.7C 1-5), hence demonstrating a lack of notable differences in initial topography profiles of the bacterial IM and the mammalian comparator model.
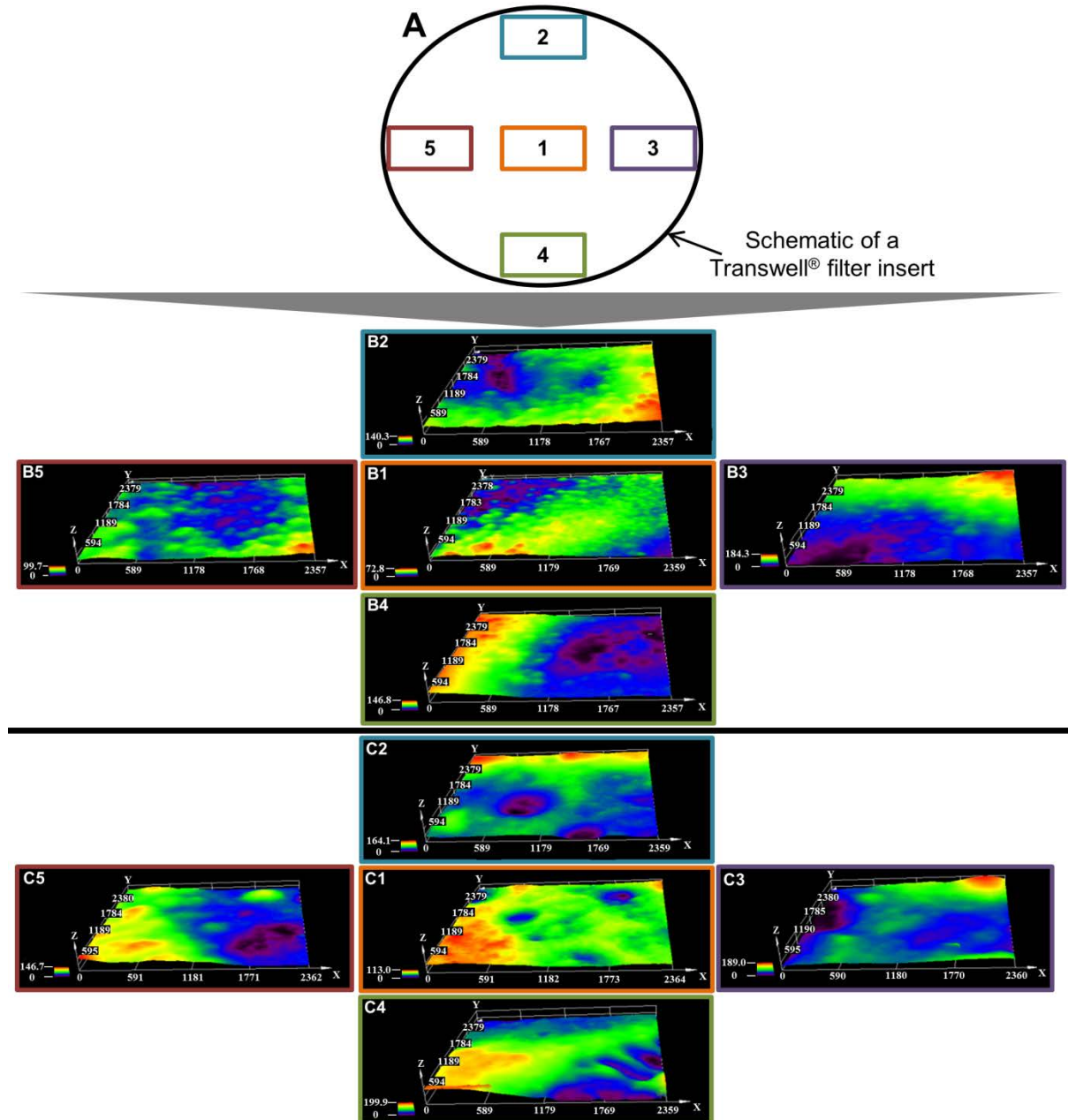

Figure 2.7: Schematic of the model surface showing the location of the representative imaged areas (A). Topography of the bacterial IM model imaged at the five representative model areas (center (B1), as well as upper (B2), right (B3), bottom (B4) and left (B5) edges) is shown. The same areas of the mammalian comparator model (center (C1), upper (C2), right (C3), bottom (C4) and left (C5) edges) were additionally imaged. Reproduced from [96] with permission from Elsevier.

2.3.3.3 Model thickness assessment

In addition to model integrity and topography, model thickness constitutes another parameter which can potentially influence the permeability behavior of tested compounds or drugs [102]. Thus, both bacterial IM and mammalian comparator models were analyzed and compared regarding their z-dimension using SEM. Freeze-dried vertical cross sections of the IM and mammalian comparator model were therefore placed in their original orientation on sample grids and subsequently imaged and sized. The analysis revealed a similar thickness of IM and mammalian comparator models, of approximately 160 µm (Figure 2.8A, B). While demonstrating comparability in this respect, SEM analysis indicated a difference between models in terms of inner morphology. Visualization of model cross-sections via cryo-SEM clearly showed a difference in internal structure when comparing the bacterial IM to mammalian comparator model (Figure 2.8C, D) most likely as a result of the differences in PL model composition.
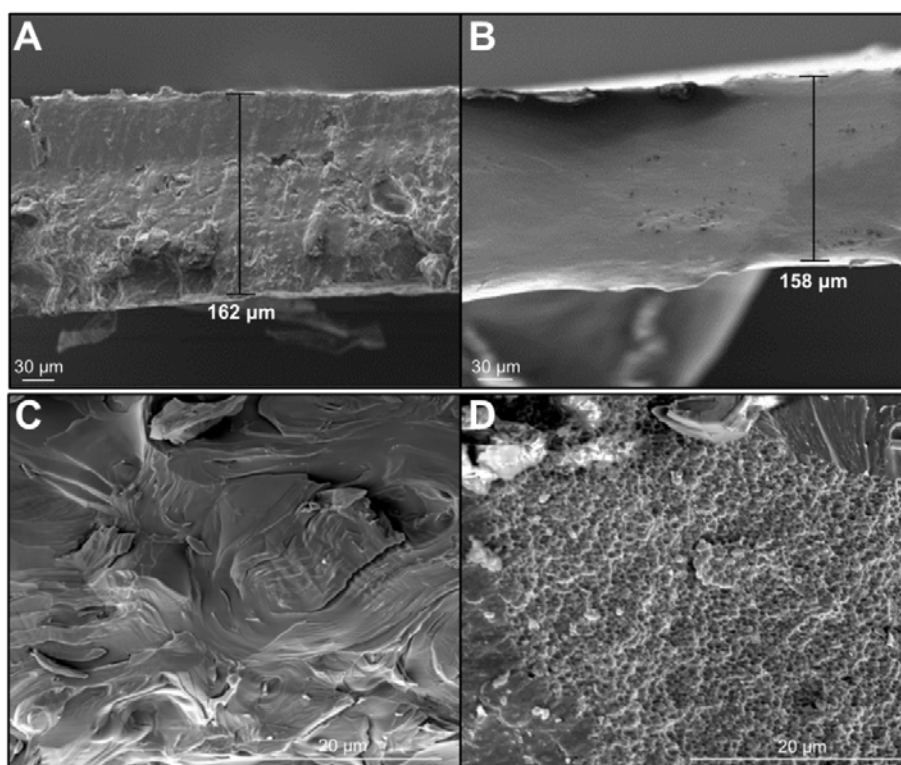
Figure 2.8: Representative SEM images of vertical cross sections of the bacterial IM (A) and mammalian comparator model (B) without underlying Transwell® filter. Images are representative of n=3 investigations, with mean values of 156 ± 18 µm and 165 ± 6 µm for the IM and mammalian comparator model respectively. Cryo-SEM cross section images of the bacterial IM (C) and mammalian comparator model (D) are also shown. Reproduced from [96] with permission from Elsevier.

2.3.4 Permeability investigations and comparison

2.3.4.1 Model compounds

The performed characterization of IM and mammalian comparator models revealed the suitability of both models for transport experiment conditions, as well as (required) similarities in properties such as thickness. In contrast, molecular level differences as well as differences in inner model morphology could be demonstrated, most likely as a result of the difference in employed PLs. As a next step, it was investigated whether these indicated PL-related differences could be linked to differences in the permeability behavior of tested compounds in the bacterial IM and mammalian comparator models, which would ultimately demonstrate the importance of employing bacterial IM-specific PLs in a physiologically-relevant ratio. A readily-quantifiable set of fluorescent dyes (Table 2.4), with a range of distribution coefficients at pH 7.4 (log $D_{(pH\ 7.4)}$) was chosen for a preliminary study aimed to prove this concept. Point-wise differences in compound P_{app} values with higher trend for permeation in the case of the bacterial IM as compared to the mammalian comparator model were obtained (Figure 2.9A), even in the case of the negatively charged dyes calcein and fluorescein − both of which could be hypothesized to interact with negatively charged IM-PLs (such as PG and CL) in a repulsive manner, actually leading to a low level of permeation [103].

Table 2.4: Important physicochemical parameters of employed fluorescent dyes and ß-blockers. Adapted from [96] with permission from Elsevier.

Compound	$\log D_{(pH\ 7.4)}$	Charge at pH 7.4	M_w (g/mol)	PSA (A^2)[c]	H-bond donors/ acceptors[c]
Calcein	-1.46[a]	-	622.5	232	6 / 5
Fluorescein	-0.43[a]	-	376.2	76	2 / 5
Rhodamine 123	1.17[a]	+	344.4	85.4	3 / 5
Rhodamine B	1.96[a]	+/-	479	52.8	1 / 5
Rhodamine B isothiocyanate	2.03[a]	+/-	536	86.5	1 / 7
Atenolol	-1.29[b]	not shown	266.3	94.6	3/4
Metoprolol	-0.16[b]	not shown	267.4	58.4	2/4
Timolol	0.03[b]	not shown	316.4	85.2	2/8
Nadolol	0.68[b]	not shown	309.4	88.8	4/5
Acebutolol	0.83[b]	not shown	336.4	92.8	3/5
Alprenolol	1.38[b]	not shown	249.3	43.7	2/3

[a] Values determined by the shake flask method (according to the OECD guideline for the testing of chemicals section 1: physical-chemical properties, test 107). [b] Values from Zhu *et al.* ([16]). [c] Values from Pubchem.

Following these initial results, it was decided to define a second, physicochemically-comparable compound set, which still exhibited a degree of variation in lipophilicity. Hence, a set of ß-blockers (Table 2.4) was utilized, constituting a compound class frequently employed for determination of the discriminatory capabilities of cell- [104] and lipid-based [7, 105] *in vitro* models. Employing ß-blockers furthermore allowed for a comparison of permeation data from the original PC-based PVPA to the current mammalian comparator model − this revealed an acceptable correlation with a coefficient of determination of 0.86, confirming the suitability of the mammalian comparator model to serve not only as a comparator for the bacterial IM, but also as an acceptable and relevant reference model.

ß-blocker permeability data again showed significant point-wise differences in P_{app} values comparing the bacterial IM to the mammalian comparator model with a trend for higher permeation across the former (Figure 2.9B). These observations were consistent over the entire range of compound lipophilicities, and furthermore confirm the impact of model PL composition on compound permeability.
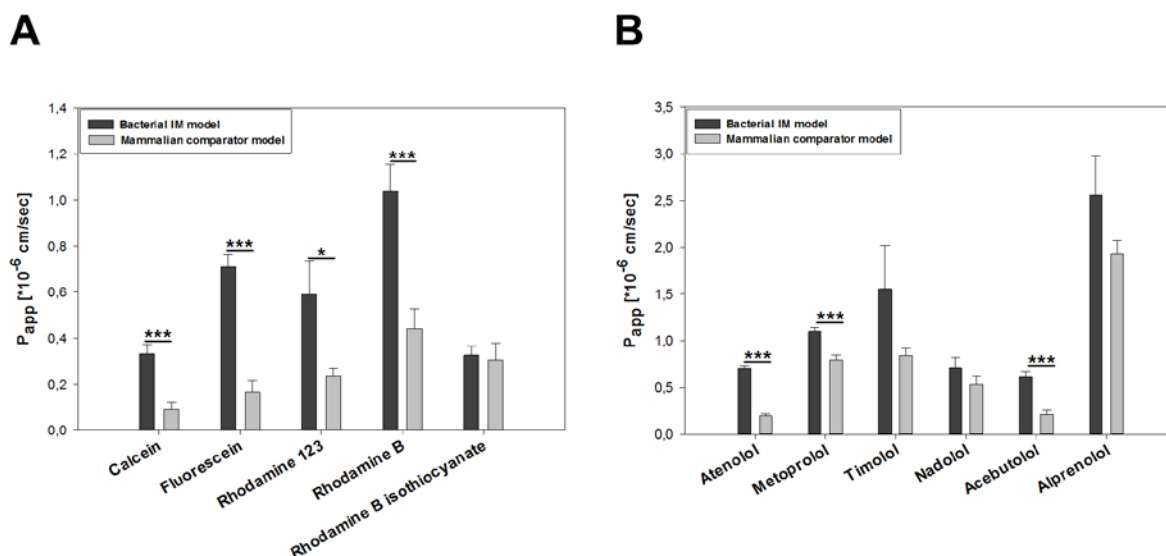

Figure 2.9: P_{app} values of fluorescent dyes (A) and ß-blockers (B), both in order of increasing lipophilicity, in the bacterial IM and mammalian comparator model. Values represent mean ± SE; n≥9 from 3 individual experiments; *=P<0.05, ***=P<0.001. Reproduced from [96] with permission from Elsevier.

2.3.4.2 Anti-infective compounds

In a next step, it was investigated whether the observed permeability differences of tested model compounds applied not only in the case of model compounds, but also with respect to actual anti-infectives. Hence, ciprofloxacin and minocycline, both intracellularly-targeting antibiotics [106], were chosen and tested for their ability to permeate across the bacterial IM as well as the mammalian comparator model. Permeability investigations revealed significant differences in P_{app} values, again with a trend for greater permeation across the IM model (Figure 2.10A), in accordance to the former obtained results of fluorescent dyes and ß-blockers (see section 2.3.4.1)

In a further step, it was assessed whether the IM model additionally shows a functional similarity to the native Gram-negative bacterial IM. For this purpose, PMB

was employed as an additional antibiotic, in conjunction with either ciprofloxacin or minocycline. The well-documented membrane disrupting effect of PMB is based on electrostatic interactions, occurring specifically at *in bacterio* assay concentrations [107], with acidic PLs such as POPG and CL, as present in the bacterial IM [108, 109]. This initial electrostatic interaction is followed by the insertion of PMB into the PL membrane, and pore formation which subsequently leads to a weakening of the membrane barrier function. In contrast, PMB does not electrostatically interact with electroneutral PLs such as PC [108], as present in the mammalian comparator model. Due to its permeabilizing effect, PMB may be applied in clinical settings together with other antibiotics, such as minocycline [110, 111], in order to increase intracellular drug levels by means of enhanced permeation. It was subsequently investigated whether the PL-selective membrane-disrupting behavior of PMB could also be observed in the current *in vitro* setups. Both bacterial IM and mammalian comparator models were incubated with PMB in a concentration shown previously to exhibit an IM permeabilizing effect in *E. coli*-based assays [108]. This was followed by the addition of ciprofloxacin or minocycline, the permeation of which was subsequently assessed. Both ciprofloxacin and minocycline showed significantly higher P_{app} values in the IM model as a result of PMB treatment, while no significant P_{app} increase was observed for either anti-infective in the mammalian comparator model following incubation with PMB (Figure 2.10B). The impact of PMB on the IM model barrier function and the corresponding lack of effect on the mammalian comparator model therefore illustrate the presence of a functional similarity between the IM model and the bacterial IM, further emphasizing the importance of employing bacteria-specific PLs in the IM model development.

A

B
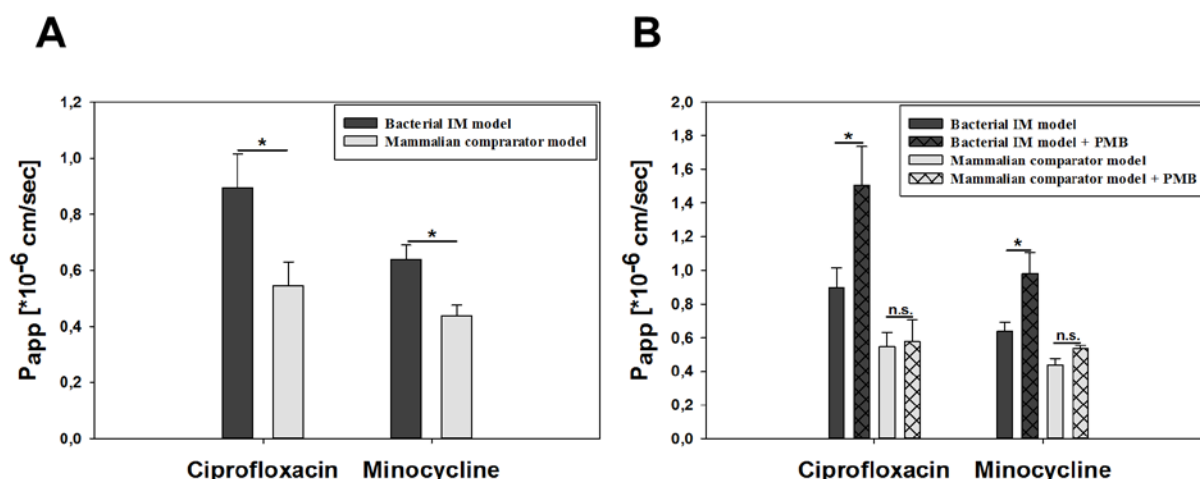
Figure 2.10: P_{app} values of ciprofloxacin and minocycline in the bacterial IM and mammalian comparator model are shown (A), and are compared with P_{app} values following pre-incubation of both models with PMB (B). Values represent mean ± SE; n=6 from 2 individual experiments; *=$P<0.05$, n.s. = not significant. Reproduced from [96] with permission from Elsevier.

2.3.5   Comparison to an established vesicle-based assay

After clearly illustrating the advantages of using the IM model over a standard, mammal membrane relevant model for assessing bacterial IM permeation, a small exploratory study was conducted, comparing the permeability data obtained from an established vesicle-based assay to that which can be derived from the IM model. The purpose of this comparison was to highlight the unique ability of the IM model to provide both quantitative and kinetically-resolved permeation data. For such a study, a hydroxyguanidine-functionalized fatty acid moiety derived from the muraymycin A-series of nucleoside antibiotics was selected, as a structure thought to mediate an enhanced permeation of the A-series members, and therefore their increased activity in comparison to other muraymycin classes [112]. Such a hydroxyguanidine-functionalized fatty acid moiety (linked to AlexaFluor 488® as a fluorophore) was previously investigated in a vesicle-based *in vitro* assay and compared to a reference compound (consisting of the fluorophore and linker, but lacking the functionalized motif) [63] to confirm this proposed effect of enhanced permeation of the A-series. The extent of permeation into the vesicles (which were not entirely composed of bacteria-relevant PLs) was measured by evaluating the fluorescence intensity inside vesicles relative to background, and was shown to be greater in the case of the functionalized fatty acid moiety in comparison to the reference compound. In addition,

the functionalized fatty acid was seen to accumulate at the surface of immobilized vesicles, immediately after its addition. However, insufficient assay sensitivity prevented the establishment of a correlation between the observed rapid accumulation, and the occurrence of a rapid permeation.

The same permeation comparison as conducted in the previous vesicle-based study, between hydroxyguanidine-functionalized fatty acid moiety and reference compound, was here conducted in the IM model. Significantly higher P_{app} values and higher permeation rates were seen in the IM model in the case of the functionalized fatty acid relative to the reference compound (Figure 2.11), a finding which is in accordance with the results of the vesicle-based study from Ries *et al.* [63]. In addition however, the ability of the IM model to provide quantitative, kinetically-resolved permeation data allows for a more in-depth characterization of these permeation processes in comparison to the vesicle-based assay. Herein, the noticeably high amount of permeated functionalized fatty acid at 0 h (Figure 2.11A) suggests that the previously observed effect of rapid accumulation does seem to correlate with an immediate phase of membrane permeation, followed by a second phase of permeation
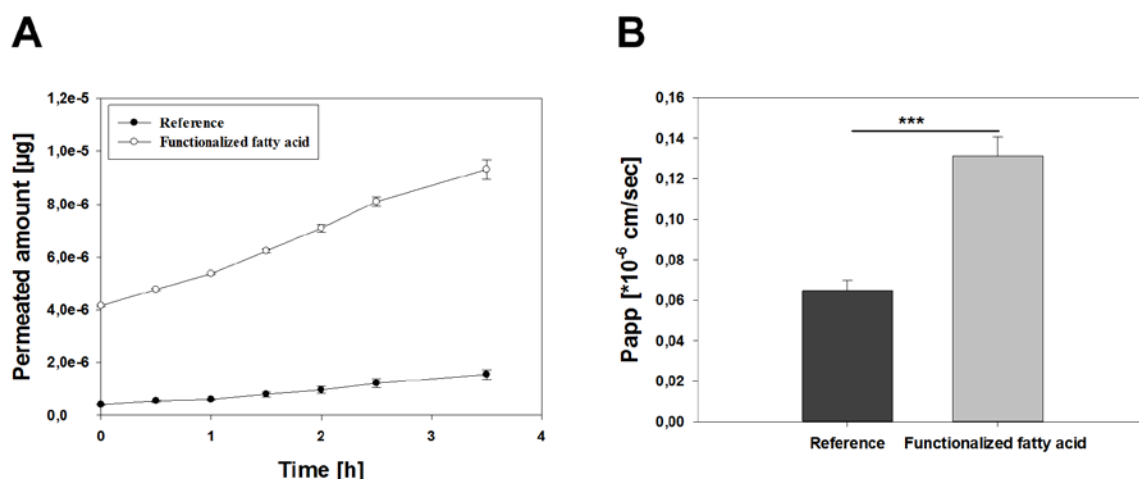
Figure 2.11: Permeation rate and extent of the hydroxyguanidinylated fatty acid and reference compound (A), showing a permeability enhancing effect of the functionalized fatty acid moiety. The finding is also reflected in the calculated P_{app} values (B), additionally highlighting the advantage of the IM model for quantification of permeation processes and assessment of the permeation kinetics of tested compounds. Values represent mean ± SE; n=9 from 3 individual experiments; ***=$P<0.001$. Reproduced from [96] with permission from Elsevier.

2.4   Conclusion

The second chapter describes the successful development of a stable, robust and reproducible model of the Gram-negative bacterial IM as a first step in an overall cell envelope modeling approach. The model is composed of bacteria IM-relevant PLs in a physiologically relevant ratio. Conducted characterization of the IM model and comparison to a similarly prepared PC-based mammalian comparator model revealed certain PL-related variances. Observed PL-related differences in model structure were eventually shown to translate into significant differences in the model function, with permeability behavior of employed model compounds as well as anti-infective shown to differ between bacterial IM and mammalian comparator model. This clearly illustrates the need to employ bacteria-specific raw materials in relevant ratios for the development of bacteria-specific permeation models. The ability of the IM model to facilitate a more information rich evaluation of permeation processes by providing quantitative data regarding the rate and extent of compound permeation was additionally illustrated. The development of the OM model as second step in the overall envelope modeling approach will be described in the following chapter.

3.   Modeling the outer membrane

<u>Personal contributions to this chapter were as follows:</u>

- ➢ Model development
- ➢ Performance, analysis and interpretation of SEM investigations
- ➢ Analysis and interpretation of CLSM investigations
- ➢ Interpretation of X-ray diffractometer measurements
- ➢ Performance, analysis and interpretation of all transport experiments
- ➢ Development of quantification methods
- ➢ Analysis and interpretation of all described results
- ➢ Writing of chapter

3.1   Introduction

The bacterial OM constitutes the first line of defense for Gram-negative bacteria, protecting them against their hostile environment. Considering the role of the OM as the outermost protective barrier, it is expected to be a more complex structure in contrast to the IM, which is very much the case – the OM constitutes as asymmetric bilayer, composed of a PL-containing (mainly POPE and POPG in a 90:10 weight ratio [113]) IL and a LPS-containing OL [34]. The latter structure is assumed to be chiefly responsible for limiting passive OM permeation [114]. The design of an OM model is reported in the following chapter, employing physiologically-relevant raw materials. The chief consideration in this process was to develop a model which mimics the asymmetric structure of the native OM, and which also shows a functional similarity to the bacterial OM.

The OM model was prepared on the same support system (Transwell® filter inserts) as used within the previously described IM model development, to allow for obtaining quantitative permeation data as well as for a subsequent combination of the individually-prepared model components into an overall envelope model (see chapter 4). The OM model preparation procedure consisted of a two-step approach, building the PL-containing IL on a Transwell® filter insert first, followed by the addition of the LPS-containing OL to obtain the entire, asymmetric OM model structure. The successful creation of IL and OL structures as well as the resulting OM model structure was investigated microscopically. This was followed by further characterization addressing OM model barrier properties as well as suitability for permeability experiment conditions. The interaction of agents such as EDTA and PMB with the OM model, as well as the permeation of the antibiotic vancomycin were then studied. EDTA [115, 116] and PMB [107, 117] are known to interact with and permeabilize the native OM, while vancomycin is known to be incapable to cross the native OM – assessment of whether similar effects were noted in the OM model therefore allowed for determination of the functional similarity of the OM model to the native OM. In addition, the permeability assessment of a set of novel anti-infective compounds revealed the advantage of quantitative model permeation data allowing for an in-depth characterization as well as to estimate *in bacterio* based activity data.

3.2 Materials and Methods

3.2.1 Materials

POPE and POPG were both purchased from Avanti Polar Lipids Inc. (see section 2.2.1). LPS (from *E.coli* 011:B4), either with or without a fluorescein isothiocyanate (FITC)-label, were purchased from Sigma-Aldrich Co. (St. Louis, MO, USA). Transwell® permeable supports 3460 were obtained from Corning Inc. (see section 2.2.1). Fluorescein, rhodamine 123, rhodamine B isothiocyanate and vancomycin were purchased from Sigma-Aldrich Co. (St. Louis, MO, USA). RNA polymerase (RNAP) inhibitors were synthesized in-house (compounds 229, 230 and 502 according to Hinsberger *et al.* [118]; compound 567 according to Elgaher *et al.* [119]). Mobile phase components for UHPLC and LC-MS/MS analysis were purchased from VWR (Radnor, PA, USA). All other solvents and chemicals were of at least analytical grade and were sourced from Sigma-Aldrich (St Louis, MO, USA).

3.2.2 OM model preparation

A 6 % (w/v) PL solution (90:10 weight ratio of POPE and POPG as a composition representative of *E. coli* [113]) was prepared in hexane and added in two cycles (37.5 µl, dried at 55 °C for 4 min) onto Transwell® filter inserts in order to form the IL of the bacterial OM. A 0.3 mg*ml^{-1} LPS solution (in water) was subsequently nebulized in 5 cycles (50 µl each) onto the IL using a Aerogen® Solo nebulizer (Aerogen Ltd., Galway, Ireland) together with an in-house developed nebulization chamber, followed by a final drying step of 5 min at 55 °C to form the OM model.

3.2.3   SEM investigations

For the purpose of SEM analysis, freshly prepared IL and OM model coatings on Transwell® filter inserts were cut out of the plastic holder surround, followed by the preparation of vertical cross-sections as described in section 2.2.8. Samples were subsequently sputtered with gold, positioned in a vertical manner on sample grids and imaged with a Zeiss EVO HD 15 (Carl Zeiss AG, Oberkochen, Germany) in order to investigate the thickness of the IL and OM model.

3.2.4   Confocal laser scanning microscopy (CLSM)

CLSM was employed to elucidate the integrity of the LPS-containing OL of the OM model. The OM model was prepared according to the procedure described in section 3.2.2, employing FITC-labeled LPS for imaging purposes. Prepared model coatings were imaged freshly after preparation, and following simulated transport experiments (incubation in KRB, adjusted to pH 7.4, 37 °C, for 5 h). Transwell® filters inserts with model coatings were cut out of plastic holder surrounds, fixed on glass slides (using an adhesive fixing agent) and subsequently analyzed using a Leica TCS SP8 AOBS/DMI8 confocal laser scanning microscope (Leica Microsystems GmbH, Wetzlar, Germany; λ_{exc}= 488 nm, λ_{em}= 545nm, 10x objective). In addition, 13 representative regions of interest (ROI) were defined across the entire model area with a size of approximately 3.24 mm^2 each, using the software LAS X (Leica Microsystems GmbH, Wetzlar, Germany). ROI were divided into 1800 vertical single measurements with a vertical measurement distance of 1.5 μm, thus covering the entire height of each ROI. The fluorescence intensity of FITC-labeled LPS was then measured at each of these points. In addition, IL samples were prepared and similarly imaged and analyzed, serving as negative controls.

3.2.5   Correlative microscopy

OM model samples were prepared as described in section 3.2.4 and subsequently sputter coated with gold (Quorum Q150R ES, Quorum Technologies Ltd., East Grinstead, UK). A Shuttle & Find™ extension with specialized sample holder (Carl Zeiss Microscopy GmbH, Germany) was used for both CLSM (Zeiss LSM 710, Jena, Germany) and SEM (Zeiss EVO HD 15, Carl Zeiss AG, Oberkochen, Germany) examinations, avoiding the need for further sample alteration, when switching between measurement methods. CLSM images (λ_{exc}= 488nm, λ_{em}= 540 nm) of OM samples were first taken, followed by SEM images, after sample transfer and calibration. CLSM and SEM images were then superimposed via the provided software (Zeiss Zen blue 2010; Carl Zeiss Microscopy GmbH, Germany) in a final step. The superimposed image was then examined in order to elucidate the LPS coverage in more depth, as compared to single CLSM investigations, as well as a function of the surface texture of the IL.

3.2.6   X-ray diffractometer (XRD)

3.2.6.1   XRD measurements

All OM samples were prepared on silicon wafers to allow for analysis, and were measured on an in-house fabricated diffractometer. In addition, IL samples were similarly prepared and analyzed for comparison purposes. A Cu K_α line with a wavelength of 1.541 Å was employed for the measurements. The incident beam was defined by the line focus of the X-ray tube and a slit of 0.1 mm, while the resolution was set to δ Q_z = 0.003 Å^{-1}. Following positioning of the sample the diffracted beam was monochromatized and detected by scintillation detectors. A nickel absorber was inserted into the diffracted beam in the case of low angles to prevent a saturation of the detector by high intensities.

All XRD experiments were performed in a humidity chamber, using water to adjust the relative humidity. The temperature within the chamber was controlled by a Haake

water bath (PSL Systemtechnik GmbH, Osterode am Harz Germany). Details on the in-house built instrument and its operational mode can be found in published literature [120].

3.2.6.2   XRD analysis

XRD curve peaks were evaluated by classical Fourier analysis [121], which provided an electron density profiles of a single lipid lamella (1D unit cell), S_{exp} (z) (equation 8):

$$S_{exp}(z) = \frac{2}{d_l} \sum_{n=1}^{n_{max}} F_n \cos\left(\frac{2\pi n z}{d_l}\right)$$ (8)

with z=0 being the center position of a lipid bilayer, and d_l the lamellar spacing.

The scaled structure factor F_n was calculated by using the Lorentz corrected integral intensity of a single Bragg peak of order n [121].

3.2.7   Permeability investigations

OL, IL and OM model-permeated amounts of fluorescein, rhodamine 123 and rhodamine B isothiocyanate were assessed, as model fluorescent dyes. IL and OM model-permeated amounts of vancomycin as well as selected members of the RNAP inhibitor class were also investigated, as anti-infective compounds. Solutions of fluorescent dyes and anti-infective compounds were prepared in KRB (pH 7.4), in the case of the RNAP inhibitors with an additional 2% dimethyl sulfoxide (DMSO) to guarantee compound solubility. Concentrations of prepared solutions were calculated in order to ensure sink conditions for permeation studies (see Table 2.1, section 2.2.10 for employed fluorescent dye concentrations; a 1.18 mM concentration was utilized in the case of vancomycin, and 50 µM solutions were prepared in the case of all RNAP inhibitors). OL, IL or OM models on Transwell® filter inserts were placed in cell culture plates and pre-incubated with pre-warmed KRB (pH 7.4, 37 °C) for 30 min for model rehydration and equilibration prior to transport studies. After KRB removal, 520 µl of fluorescent dye or drug solution was added to the apical compartment of

each culture plate well. A 1.5 ml volume of pre-warmed KRB was then added to the basolateral compartment. A 20 µl volume of the solution within the apical compartment was then immediately removed, and used to precisely measure the starting dye/drug concentration. Samples of 200 µl were taken from the basolateral compartment of each culture plate well at 0, 0.5, 1, 1.5, 2 and 2.5 h. A final time point of 2.5 was set in this respect to ensure the absence of any effect of DMSO on model integrity (data not shown). Samples collected from basolateral compartments were subsequently used to quantify the permeated amount of tested compounds over time (see section 3.2.8). The removed volume was always directly replaced with an equivalent volume of pre-warmed KRB in order to maintain sink conditions. Culture plates were placed on an orbital shaker (150 rpm) and kept in an incubator (at 37 °C, CO_2: 5%) throughout the entire transport experiment.

IL and OM transport studies employing EDTA and PMB as known bacterial OM permeabilizing agents were additionally conducted. In these studies, the above mentioned fluorescent dyes were again utilized as permeability markers. Transport studies assessing the impact of EDTA were carried out as described above, with the addition of 16 mM EDTA to donor compartment-applied fluorescent dye solutions. The procedure was slightly altered when conducting studies employing PMB. Briefly, model membranes were pre-incubated with pre-warmed KRB for 30 min followed by incubation for one hour with a 1.53 mM PMB solution, followed by washing with pre-warmed KRB. Permeability marker solution was then added to the apical compartment. Basolateral samples were subsequently collected after 0, 0.25, 0.5, 1, 1.5, 2 and 2.5 h.

3.2.8   Quantification of permeated compound amounts

3.2.8.1   Fluorescence quantification

A Tecan Infinite® M200 was used to determine the permeated amount of fluorescent dyes (for quantification parameters see Table 2.1, section 2.2.10).

3.2.8.2   UHPLC quantification

A UHPLC (Dionex Ulitmate® 3000; see section 2.2.10.2) with an Accucore™ column (RP 18, 150 mm x 2.1 mm, 2.6 µm, Thermo Fisher Scientific Co., Waltham, MA, USA) was used to quantify the permeated amount of vancomycin according to the method of Jesus Valle *et al.* [122] (RT = 2.53 min; flow rate = 0.4 ml min^{-1}).

3.2.8.3   LC-MS/MS quantification

A TSQ Quantum Access Max tandem quadrupole mass spectrometer coupled to an Accela UHPLC system, consisting of a quaternary mixing pump with a built-in solvent degassing system, thermostated autosampler and column oven (all from Thermo Fisher Scientific, Waltham, MA, USA), was used to quantify the permeated amount of RNAP inhibitors. An Accucore™ RP column (150 mm x 2.1mm, 2.6 µm, Thermo Fisher Scientific, Waltham, MA, USA) was used. Column oven temperature was set to 30 °C. The standard software Xcalibur™ (Thermo Fisher Scientific, Waltham, MA, USA) was used to operate the system. Quantification was performed using a binary solvent mixture (A: water + 0.1% formic acid; B: acetonitrile + 0.1% formic acid) in gradient runs. In the case of compounds 229, 230 and 502, component B of the mobile phase was increased from an initial value of 30% to 100 % in 3 min, and then kept constant for 2 min. In the case of compound 567, the percentage of B was increased from 50% to 100% in 1 min and kept constant for 2 min. Flow rate was set to 350 µl min^{-1}, spray voltage to 4500 mV and capillary temperature to 330 °C in all cases. Analysis was performed operating in single reaction monitoring mode and transitions shown in Table 3.1 (parent mass; fragment mass) were used for identification and quantification of the compounds.

Table 3.1: Quantification parameters of employed RNAP inhibitors utilized for compound quantification by LC-MS/MS.

RNAP-inhibitor	Retention time (min)	Parent mass (m/z)	Fragment mass (m/z)
229	4.52	368	115.2
230	4.46	410	141.1
502	4.57	428	215.1
567	1.80	432.8	225.8

3.2.8.4 Calculation of permeated compound amounts

The permeated amount of employed model fluorescent dyes as well as anti-infective compounds in transport experiments was calculated in all cases according to calibration curves created from samples of standard concentrations. Cumulative permeated amounts as a percentage were always normalized to the accurately-determined starting (apical) concentration.

3.2.9 Isothermal titration calorimetry (ITC)

The interaction of fluorescein, rhodamine 123 and rhodamine B isothiocyanate with PMB was investigated in order to further investigate permeation of these dyes across the PMB-treated IL. ITC experiments were performed using a Nano ITC^{2G} (TA instruments, New Castle, DE, USA) at 25 °C with 15 injections (fluorescent dye in syringe, PMB solution in cell) of 15 µl each, applying the following concentrations: fluorescein: 25 mM, PMB: 0.25 mM; rhodamine 123 and rhodamine B isothiocyanate: 10 mM, PMB: 0.2 mM. The dissociation constant (K_d), the change in Gibbs free energy (ΔG), enthalpy (ΔH) and entropy (ΔS), respectively, were subsequently determined from ITC binding curves via the software NanoAnalyze™ (Waters GmbH, Eschborn, Germany).

3.2.10   Statistical analysis

Presented numerical data represent mean ± SE. Student's t-test was employed where relevant to assess significant differences; *=$P < 0.05$, ***= $P<0.001$. All tests were calculated with the software SigmaPlot (version 12.5, see section 2.2.11).

3.3   Results and discussion

3.3.1   Model preparation

The OM model was designed in such a way as to obtain a structural mimic of the bacterial OM, employing physiologically-relevant raw material. A 90:10 (weight) ratio of POPE and POPG as a composition representative for *E. coli* [113, 123] was therefore used to form the IL, while LPS was used to form the OL. For the sake of a consistent PL deposition (as compared to the IM model preparation) it was initially attempt to deposit the PLs onto Transwell® filter inserts (the same support system which was used for the IM model) via the PVPA methodology. The approach was however not able to be adapted in this respect due to the inability to form liposomes containing such high amounts of POPE [124]. A hexane solution of the representative PLs was therefore used for the IL formation. For preparation of the OL, LPS was dissolved in water and nebulized on the beforehand formed IL, using a self-customized nebulization chamber, ensuring a selective LPS deposition onto the apical compartment of the Transwell® system as well as a consistent and sufficient outcome of LPS deposition (data not shown). The finalized OM model preparation procedure (Figure 3.1) therefore consists of a two-step approach, depositing the IL onto Transwell® filter inserts first, followed by the addition of the OL via five nebulization cycles on top to obtain the entire OM model structure.
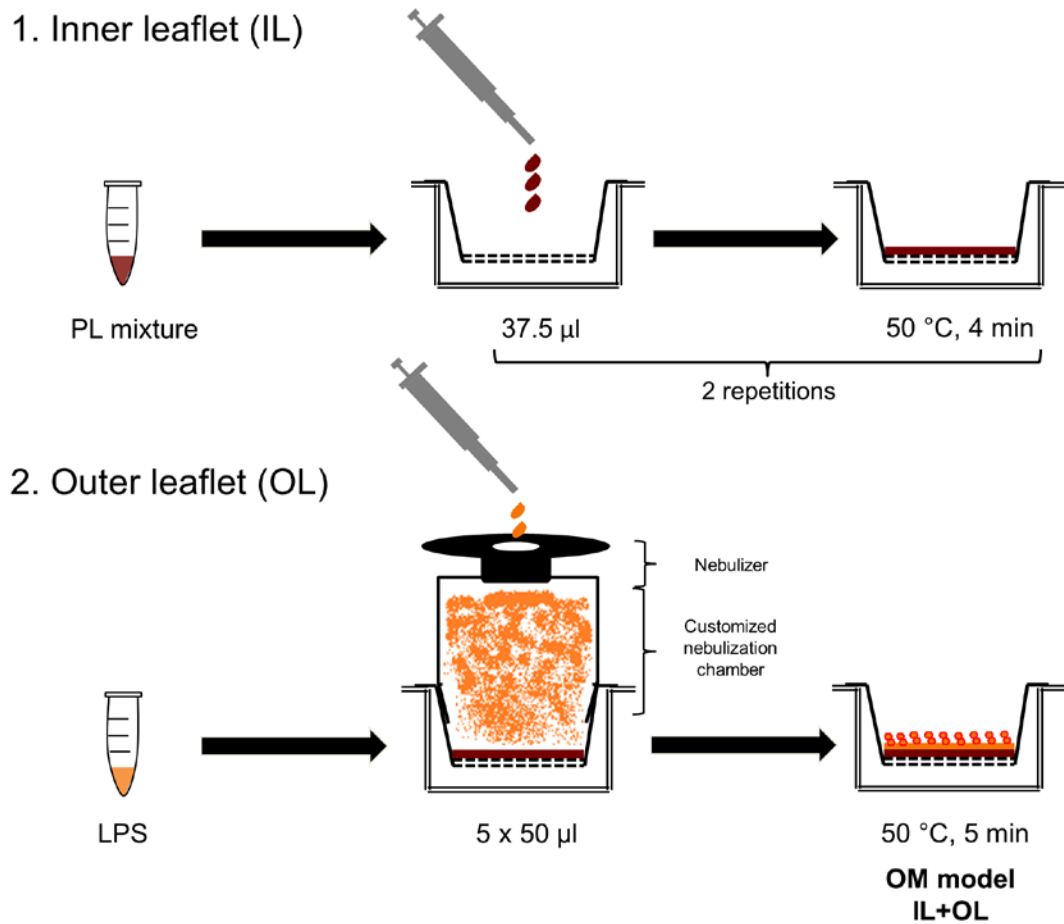
Figure 3.1: Schematic of the two-step OM modeling approach, building the IL first followed by the OL on a Transwell® filter insert to obtain the entire OM structure.

3.3.2   Model characterization

3.3.2.1   Model thickness assessment

The OM model was analyzed to obtain an initial indication of whether a successful combination of the PL-containing IL with the overlaid OL-representing LPS layer was achieved. Vertical cross-sections of both IL and OM model samples were placed on sample grids, and imaged and sized in their original orientation via SEM (Figure 3.2). IL samples revealed thickness values of approximately 26 µm (Figure 3.2A), whereas the OM model showed an increased thickness with values of around 41 µm (Figure 3.2B), implying a successful combination of IL and OL via the developed modeling procedure (Figure 3.1).
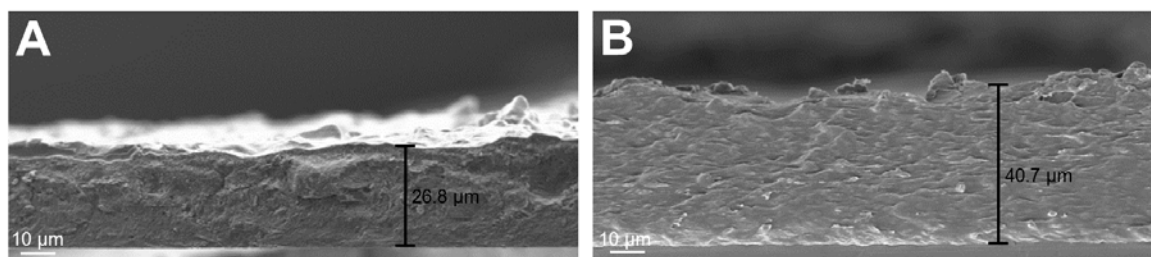
Figure 3.2: Vertical cross-sections of the IL (A) and entire OM model (B) without underlying Transwell® filter insert are shown, indicating a successful combination of IL and OL. Images are representative of n=3 investigations with mean z-dimension values of 28 ± 2 μm and 42 ± 5 μm for the IL and OM model samples respectively.

3.3.2.2   Model integrity assessment

The distribution and integrity of the deposited LPS layer of the OL was investigated using CLSM. Particular focus was placed in this case on characterizing the OL in greater detail, as the LPS component is known to be chiefly responsible for mediating the barrier function of the OM [114]. The OM model was therefore prepared using FITC-labeled LPS for imaging purposes, while IL samples were used as negative control. The entire model surface was subsequently imaged immediately after preparation, and after simulated transport experiments (KRB, pH 7.4, 5 h, 37 °C) to assess the stability of the LPS layer upon exposure to buffer (as would occur during permeability investigations). Images taken directly after preparation revealed an adequate LPS distribution and consistency of coverage, with minimal intensity variations being observed (Figure 3.3A). Images taken after simulated transport experiments revealed some loss of fluorescent intensity but indicated a continued integrity of the LPS layer (Figure 3.3B). The definition of 13 representative ROI across the entire model surface (Figure 3.3C) and quantification of fluorescence intensity within these ROI allowed for a more detailed analysis of the effect of permeability experiment conditions on LPS coverage and distribution. A drop in overall fluorescence intensity following model exposure to buffer ('post buffer') could again be observed with ROI analysis, but a continued integrity of the LPS layer was demonstrated by a consistent count level over the model surface (Figure 3.3D). The low level of fluorescence counts in the case of IL samples confirmed that the measured counts specifically arise from FITC-labeled LPS (Figure 3.3D). This further

provides evidence of the continued presence of appreciable amounts of LPS on buffer-exposed OM models as well as the absence of any interfering signal from present PLs of the IL.
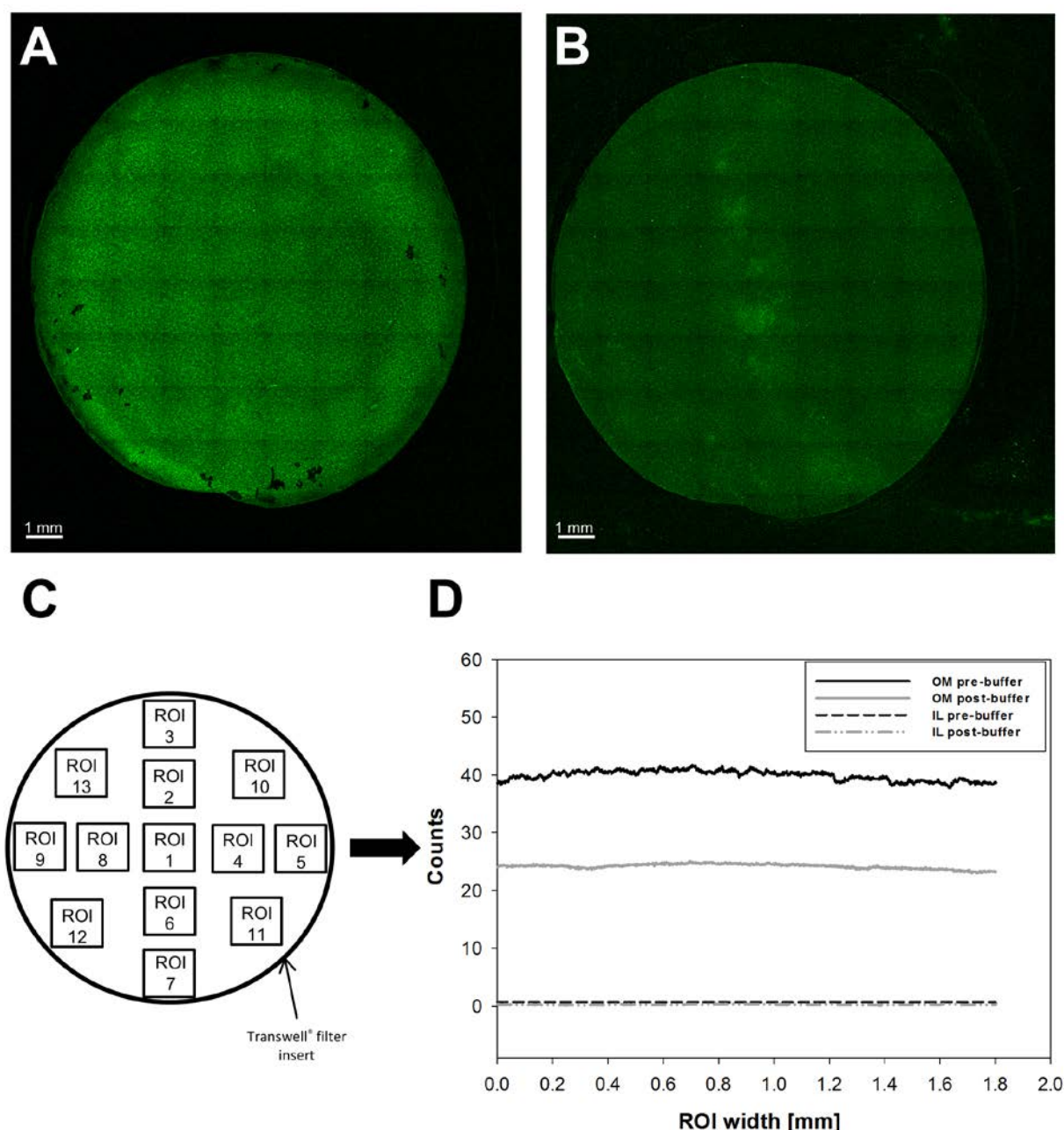
Figure 3.3: Representative CLSM images of the entire OM model surface showing FITC-labeled LPS in green immediately following model preparation (A) and after simulated transport experiment (B). The images reveal some loss of fluorescence intensity (B), which was further analyzed by the definition of 13 representative ROI with a width of 1.8 mm each, on model surfaces (C) used to quantify fluorescence intensity. Results of ROI analysis also indicate a drop in fluorescence comparing OM post-buffer to pre-buffer samples, but a continued LPS layer integrity; the absence of detected fluorescence in IL models also confirms that the measured counts specifically arise from FITC- labeled LPS within the OM model (D).

Correlative microscopy was additionally employed to obtain more detailed insights into the distribution of LPS after OM model preparation. SEM images showed a surface texture of investigated OM model samples (Figure 3.4A). CLSM images of the same sample revealed some point-wise variations in fluorescence intensity (Figure 3.4B) but an overall coverage of LPS, confirming the observations of the previous CLSM investigation also in higher resolution. The superimposed correlative microscopy image however indicated that the observed variations in fluorescence intensity seem to relate with a point-wise accumulation of LPS molecules most likely as a result of the IL surface texture (Figure 3.4C). Both characterization methods therefore revealed OM model suitability for permeability investigation conditions.
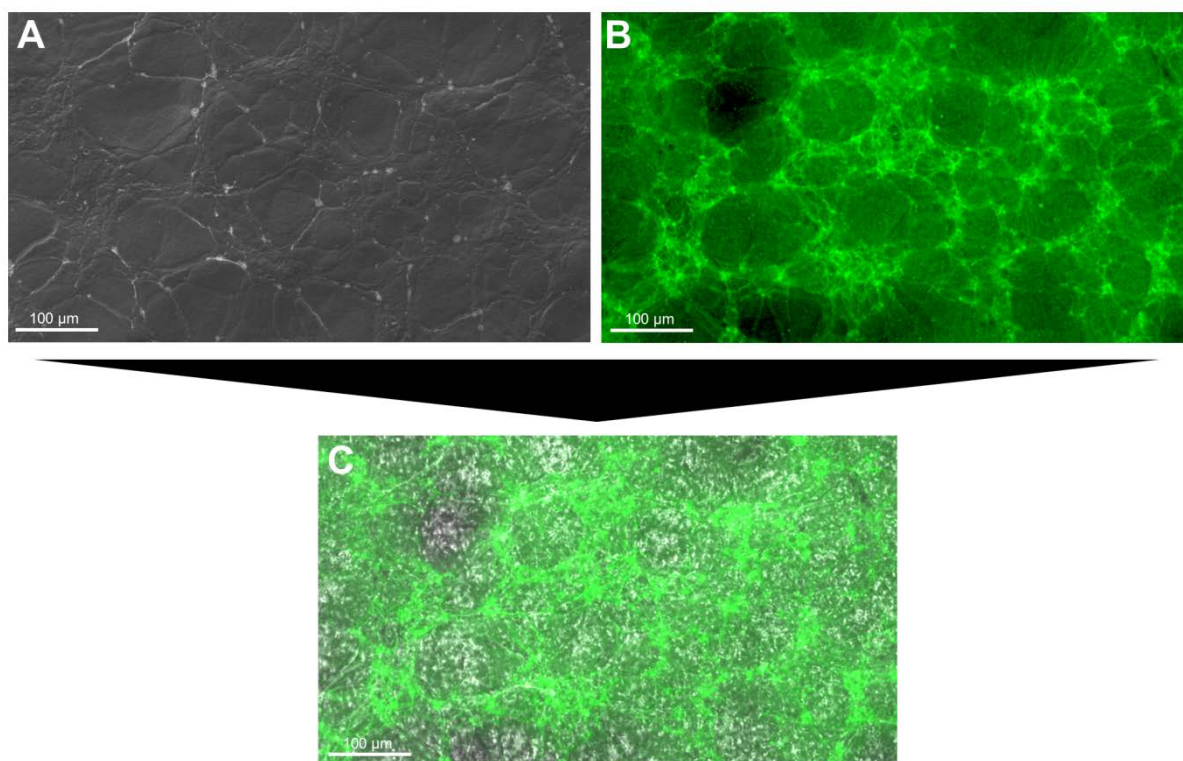
Figure 3.4: Representative SEM (A) as well as CLSM image (B) of the OM, showing FITC-labeled LPS in green. The superimposed correlative microscopy image (C) shows a sufficient coverage of the PL layer with LPS, in accordance with CLSM investigations as shown in Figure 3.3, in higher resolution. Images further provide evidence of some spot-wise LPS accumulation, potentially as a result of IL surface texture.

3.3.2.3   Model structure assessment

After initially investigating the combination of the PL-containing IL with the LPS-containing OL via SEM, as well as the integrity of the LPS layer via CLSM and correlative microscopy, the PL-LPS interactions within the OM model structure were further studied using x-ray diffraction. Initially, the equilibration behavior of the freshly prepared OM model on exposure to liquid conditions was assessed at 99% relative humidity, mimicking the conditions of transport studies. Analysis revealed an occurring membrane hydration over time resulting in the appearance of higher order Bragg peaks, indicating a higher degree of order within the membrane stacks (Figure 3.5A). In addition, a stretching in the head group region of OM model samples was observed (Figure 3.5B) in comparison to analyzed samples of the IL alone. This conclusively confirms the successful combination of IL and OL within the OM, and furthermore indicates an asymmetric OM structure.
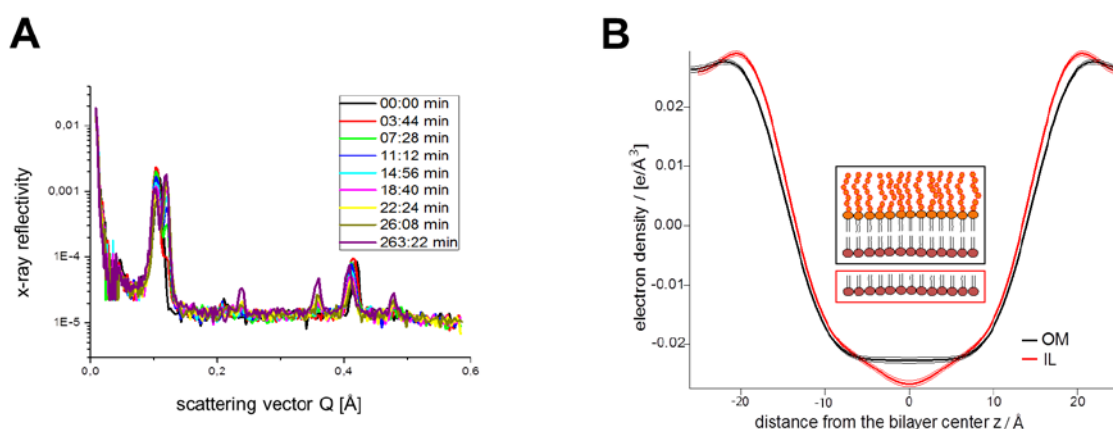
Figure 3.5: Membrane stacks of the OM model at room temperature and 99% relative humidity over time (A), revealing membrane hydration over time resulting in higher order Bragg peaks in the curves, indicative of a higher degree of order within the membrane stacks. Fourier profiles of the IL and OM after equilibration, calculated from x-ray diffraction structural investigations, revealing an interaction between LPS and PL visible as a stretching in the head group region. Electron densities are not scaled.

3.3.3 Permeability investigations

3.3.3.1 OM model barrier property assessment

After confirming a successful combination of the IL-mimicking PL layer with the OL-mimicking LPS layer into an asymmetric OM structure, it was deemed necessary to investigate the barrier properties of the OM model to confirm the suitability of the OM model to act as a permeation-limiting structure. Within this, the enhancement of barrier properties of the produced OM model in comparison to the OL or IL alone was particularly assessed. Thus, the permeability behavior of a set of readily-quantifiable permeability markers (fluorescein, rhodamine 123, rhodamine B isothiocyanate) with a range of lipophilicities and different charge at the employed pH of 7.4 (Table 2.4, section 2.3.4.1) was investigated in the OL, IL and OM models. As can be seen in Figure 3.6, the permeability of all tested marker compounds was significantly decreased in the case of the OM model in comparison to the OL and IL alone. The conducted permeation studies therefore confirm the importance of combining OL and IL structures for achieving a suitable OM mimic exhibiting barrier properties.
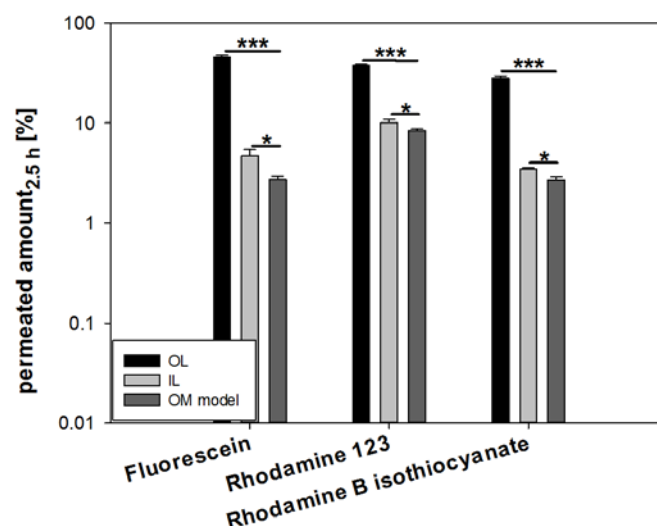
Figure 3.6. Permeated amounts of fluorescent dyes across the OL, IL and OM model are shown, revealing a significant decrease in permeated amounts in the case of the OM model, hence confirming the importance of a successful combination via the developed preparation procedure (Figure 3.1) to form an OM model with appreciable barrier properties. Values represent mean ± SE; n=3 for OL investigations and n=9 from 3 individual experiments for IL and OM model investigations; * = $P < 0.05$, *** = $P < 0.001$.

3.3.3.2 Functional similarity investigation of the OM model to the bacterial OM

Following confirmation of structural similarity, three consecutive experimental steps were defined to elucidate the functional similarity of the OM model to the bacterial OM. In a first step, the effect of EDTA, known to destabilize and permeabilize the native OM, was studied in the OM model. EDTA affects the native OM barrier by removing LPS molecules [116], as well as by chelating divalent cations such as calcium in surrounding media, which bridge adjacent LPS molecules within the OM structure and mediate a high OM stability. The removal of LPS molecules and divalent cations therefore results in a decreased OM integrity and subsequently higher permeation rates of tested substances [125-127]. For functional assessment of the OM model, EDTA was applied in conjunction with the permeability markers formerly used to investigate OM, IL and OL model barrier properties (section 3.3.3.1). Transport studies revealed a significant increase in permeation in the case of all compounds, especially in the case of fluorescein, across the OM model in the presence of EDTA (Figure 3.7A), indicating functional similarity of the OM model to the bacterial OM. The effect of EDTA on the IL model component alone was furthermore studied, to confirm the observed permeation enhancing-effect on the OM as being the result of an EDTA-LPS interaction. Interestingly, increased permeation rates of marker compounds in the presence of EDTA were also seen to occur in the case of the IL (Figure 3.7B). This observation is however not entirely unexpected, and is in accordance with previously described EDTA-mediated destabilization of lipid layers [128]. However, the observed increased permeation of rhodamine 123 and rhodamine b isothiocyanate was seen not to be statistically significant as compared to fluorescein (Figure 3.7B), indicating a more pronounced effect of EDTA with more hydrophilic dyes.

In a second experimental step aimed to investigate functional similarity, the effect of PMB on the OM model was assessed. PMB is likewise known to disorganize and destabilize the bacterial OM [107, 127, 129], interacting in an electrostatic manner with LPS present in the OL and most likely promoting its own insertion into the structure. This is accompanied by pore formation, resulting in a weakening of OM integrity. As can be seen in Figure 3.7A, PMB similarly affected the OM model,

resulting in a significantly increased permeability of all employed marker compounds and confirming functional similarity of the OM model to the native OM.
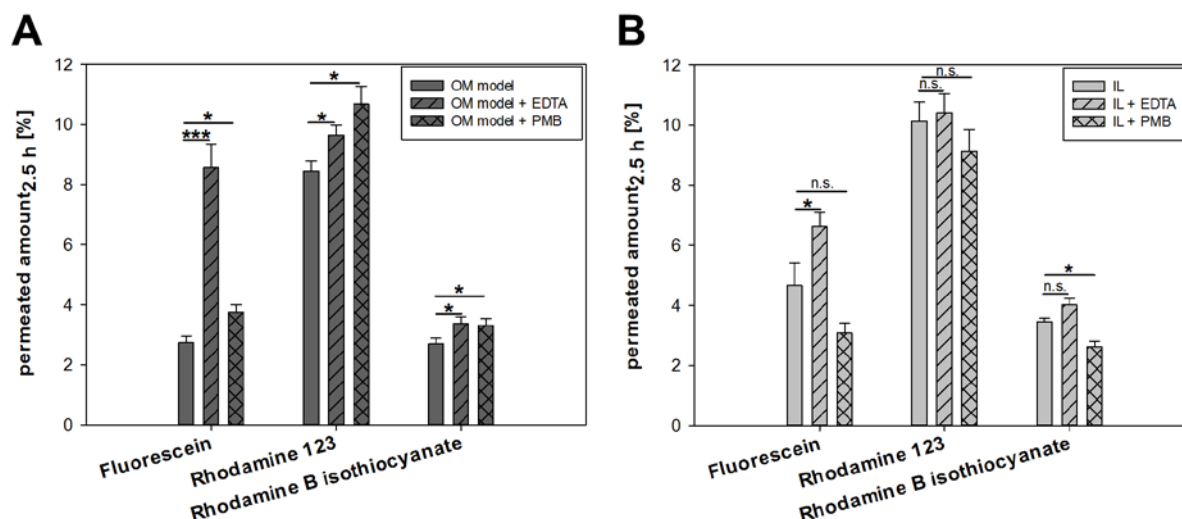
Figure 3.7: Permeated amounts of fluorescent marker compounds across the OM model are shown, in the presence and absence of EDTA and PMB (A). Data reveals a significant increase in marker compound permeation mediated by both EDTA and PMB. Permeated amounts of fluorescent dyes across the IL in the presence and absence of EDTA and PMB are additionally shown (B). Values represent mean ± SE; n=9 from 3 individual experiments; * = P < 0.05, *** = P < 0.001, n.s. = not significant.

The effect of PMB on the IL component of the OM alone was likewise investigated for comparison, in this case revealing a decrease in permeation of employed marker compounds in the presence of PMB (Figure 3.7B). A PMB-facilitated increase in permeation of marker compounds across the IL alone was not expected, due to the low amount of acidic POPG (the initial point of contact for PMB-mediated permeabilization of lipid layers) in the IL [107]; an explanation for the observed reduction in permeation was however not immediately evident. It was hypothesized that this may have occurred due to interaction between the permeability markers themselves and PMB. The interplay of PMB and employed permeability markers was therefore elucidated via binding affinity investigations, using ITC. Conducted experiments revealed the possibility of spontaneous interactions (negative ΔG, Table 3.2) between all permeability markers and PMB, which was potentially still present in trace amounts in the apical compartment of Transwells® (despite the employment of a washing step) at the point of marker compound addition. A statistically significant decrease in permeation across the IL (when the effect PMB

was studied) was only seen to occur in the case of rhodamine B isothiocyanate, the marker compound which interestingly showed the strongest interaction with PMB (as can be seen from the lowest K_D value, Table 3.2). The interactions between PMB and permeability markers were furthermore seen to be mainly hydrophobic-based (negative $T\Delta S$, positive ΔH, Table 3.2) with an additional impact of hydrogen bonds in the case of rhodamine B isothiocyanate (negative ΔH, Table 3.2) [130]. These interactions might therefore result in bulky structures of high molecular weight which are not able to permeate across the OM as well as less amounts of free permeability markers themselves, altogether leading to lower, observed permeation rates. These observations might be in contrast to the observed increase of marker permeation in presence of PMB across the OM model. However, the occurrence of such bulky structures consisting of PMB and the permeability marker which are not able to permeate might be limited due to the strong and favorable interactions of PMB with LPS, leading to higher amounts of free marker compounds.

Table 3.2: ITC results of investigated fluorescent permeability marker – PMB interactions. Values represent mean ± SE; n=3.

Compound	K_D (mM)[a]	ΔG (kJ mol^{-1})[b]	ΔH (kJ mol^{-1})[c]	ΔS (J (mol K)$^{-1}$)[d]
Fluorescein	0.18 ± 0.02	-17.12	8.93	88.37
Rhodamine 123	0.06 ± 0.001	-28.51	1.23	99.76
Rhodamine B isothiocyanate	0.02 ± 0.001	-51.37	-3.95	159.10

[a] Dissociation constant. [b] Change in Gibbs free energy. [c] Enthalpy change. [d] Entropy change

In a third step of assessing functional similarity of the OM model to the bacterial OM, the permeability of vancomycin, an antibiotic known to be inactive against Gram-negative bacteria due to its inability to permeate across the bacterial OM [131], was investigated. Vancomycin permeation across the OM model was seen to be very low, with approximately 0.3% of the initially added compound permeating from the apical to the basolateral compartment after 2.5 h (Figure 3.8). This conclusively demonstrates the functional similarity of the OM model to the native OM.
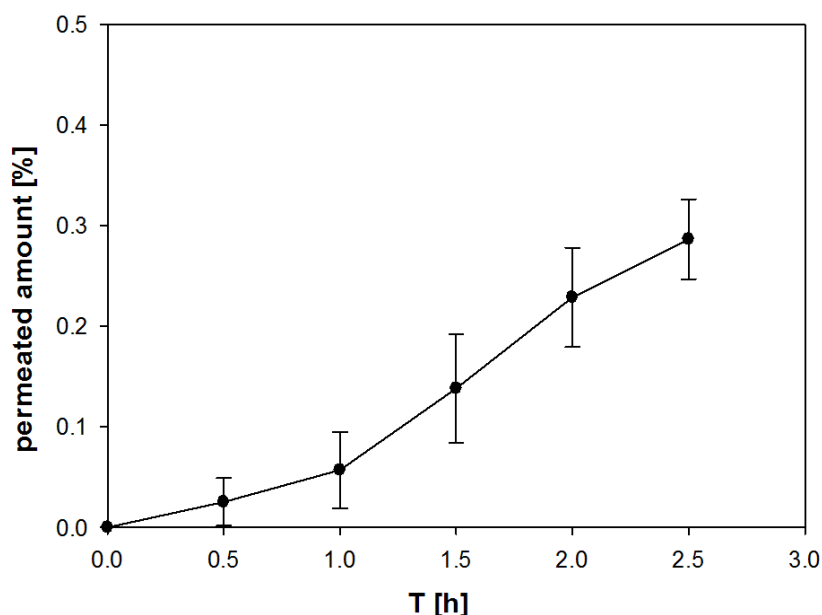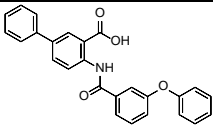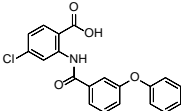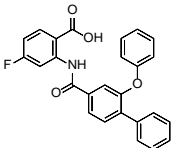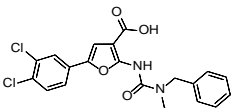
Figure 3.8: Permeation rate and extent of vancomycin across the OM model is shown, seen to be very low and therefore demonstrating functional similarity of the OM model to the native OM.

3.3.3.3 RNAP inhibitors

After confirming functional similarity of the OM model to the bacterial OM, a set of in-house synthesized RNAP inhibitors (Table 3.3) was defined in order to study the predictive value of permeation data gained from the OM model. The bacterial RNAP constitutes a multi-subunit enzyme which is responsible for transcription of bacterial proteins and essential for bacterial cell survival [132]. RNAP inhibitors are in general known to be inactive against wild type *E. coli* due to the permeation limiting ability of the bacterial OM, and in some cases due to pronounced active efflux (see minimum inhibitory concentration (MIC) in *E. coli* K12, Table 3.3) [119]. The compound class was therefore considered to be interesting for testing in the OM model, as the main permeation limiting structure in the Gram-negative bacterial cell envelope [119]. However, previously performed MIC assessment of the selected compound set in *E. coli* TolC mutants (exhibiting a non-functioning AcrA-AcrB-TolC efflux machinery) in fact showed a group of compounds which were still inactive (502, 567; Table 3.3) in addition to an active subset (229, 230; Table 3.3). The permeability of this set of 4 compounds across the OM model was therefore investigated in order to assess whether differences in passive OM model permeability could potentially provide an

explanation for observed compound activity differences. The permeability of tested RNAP inhibitors was generally seen to be low in magnitude (Table 3.3), highlighting the permeation limiting ability of the OM model with respect to these compounds in the same way as was already observed in the case of the native OM in previously conducted *in bacterio* studies [119]. Compounds active in *E. coli* TolC (compounds 229, 230) were seen to permeate to a greater extent across the OM model in comparison to the inactive compound 502, indicating passive OM model permeation data to be predictive for activity, although noted differences were small, due to the generally low level of permeability (Table 3.3). Interestingly, compound 567 was seen to permeate across the OM model to the greatest extent, despite its inactivity in *E. coli* TolC. This may be explained by the low intrinsic activity of compound 567, visible in its considerably higher IC_{50} value in comparison to the other compounds. Other bacterial cell envelope components in addition to the OM could also play a role in limiting cytoplasmic entry of the structurally-different compound 567, and so access to its target; for this reason, the current RNAP inhibitor compound set was additionally tested in the overall cell envelope model (see section 4.3.5.3).

Table 3.3: Results of previously performed cell-free and cell-based assays utilizing the selected RNAP inhibitors, together with the performed assessment of their permeability across the OM model.

Compound	Structure	log P[a]	IC$_{50}$ (µM)[b]	MIC in *E. coli* K12[c] (µg ml^{-1})	MIC in *E. coli* TolC[d] (µg ml^{-1})	Permeated amount$_{2.5\,h}$ OM model (%)[g]
229		7.90	13[e]	>50[e]	2.5[e]	2.28 ± 0.13
230		6.95	44[e]	>25[e]	2.3[e]	2.04 ± 0.15
502		7.92	13[e]	>25[e]	>25[e]	1.82 ± 0.10
567		6.84	60[f]	>50[f]	>50[f]	3.42 ± 0.31

[a] Calculated partition coefficient via the software ACD percepta (version 2016). [b] Half maximal inhibitory concentration of *E. coli* RNAP. [c] Minimum inhibitory concentration (MIC) in *E. coli* K12: intact cell envelope system. [d] *E. coli* TolC: mutant deficient in the AcrAB-TolC efflux system. [e] Values from Hinsberger *et al.* [118]. [f] Values from Elgaher *et al.* [119]. [g] Values represent mean ± SE; n=6 from two individual experiments.

3.4   Conclusion

This chapter describes the successful development of a stable and robust model of the Gram-negative bacterial OM, employing physiologically-relevant raw materials. The developed preparation procedure was shown to result in a model of asymmetric nature and so similar structure to the native bacterial OM; this structural similarity, together with a pronounced permeation limiting ability, led to the OM model being considered as appropriate for transport experiments aimed to provide quantitative data regarding the rate and extent of compound permeation. In addition, the permeabilizing effect of EDTA and PMB as well as the inability of the antibiotic vancomycin to cross the OM model confirmed a functional similarity to the bacterial OM. The investigation of the permeability behavior of a set of anti-infective compounds (RNAP inhibitors) furthermore highlighted the ability of the OM model to

work as a sufficient permeation limiting barrier as well as the ability to study anti-infective compound permeation in-depth, in a kinetically and time-resolved manner. The development of a model of the periplasmic space (PS) as a final individual envelope component and the subsequent combination of the three individually prepared models to produce an overall envelope model will be described in the following chapter.

3.5   Acknowledgements

4. Membrane combination and the overall cell envelope model

Personal contributions to this chapter were as follows:

- ➢ Model development
- ➢ Performance, analysis and interpretation of SEM investigations
- ➢ Analysis and interpretation of CLSM investigations
- ➢ Interpretation of bacterial uptake studies
- ➢ Performance, analysis and interpretation of all transport experiments
- ➢ Development of quantification methods
- ➢ Analysis and interpretation of all described results
- ➢ Writing of chapter

4.1   Introduction

The design of a PS model, as well as its subsequent combination with IM and OM models (developed in chapters 2 and 3 respectively) to produce an overall envelope model is reported in this chapter. In contrast to the membrane structures of the envelope, the PS is not considered to represent a transport barrier [47]. It rather constitutes a viscous compartment functioning as a spacer between IM and OM. An alginate gel layer was utilized to serve this purpose, again deposited on Transswell® filter inserts. The absence of a pronounced permeation limiting ability of the PS model was first demonstrated, hence indicating functional similarity to the native PS. Moreover, the suitability of the PS model to serve as a robust spacer between the IM and OM model in the course of the overall model preparation procedure was confirmed. Following this, the three individually developed envelope model components (IM, PS, OM) were combined in an ultimate step on a Transswell® filter insert, aiming for a structural envelope mimic, additionally allowing for an accurate, quantitative and time-resolved characterization of anti-infective compound permeation. The continued presence of three discrete, individual layers in the overall setup was examined as the basis for structural assessment. In addition, the predictive functional value of overall envelope model permeation data was investigated, comparing in a first step the permeability of a set of fluorescent permeability marker compounds in the envelope model to their uptake into *E. coli*. In further steps, the ability of the overall envelope model to probe and predict *in bacterio* activity of anti-infectives on the basis of their passive permeation was investigated, by studying the permeation behavior of two sets of novel anti-infective compounds (the previously mentioned RNAP inhibitors, as well as PqsD inhibitors).

4.2   Materials and Methods

4.2.1   Materials

POPE, POPG and lissamine rhodamine labeled 1,2-dipalmitoyl-*sn*-glycero-3-phosphoethanolamine (Liss Rhod PE) were sourced form Avanti Polar Lipids Inc. (see section 2.2.1). Transwell® permeable supports 3460 were purchased from Corning Inc. (see section 2.2.1). RNAP inhibitors were synthesized in-house as described in section 3.2.1. PqsD inhibitors (compounds 52, 249, 250, 368, 369 and 562) were also synthesized in house according to Storz *et al.* [133]. Protanal LF 10/60 FT (alginate) was sourced form FMC BioPolymer (Ayrshire, UK). FITC-labeled LPS were sourced from Sigma-Aldrich (St. Louis, MO, USA). Mobile phase components for UHPLC and LC-MS/MS were purchased from VWR (Radnor, PA, USA). All other reagents and chemicals were at least of analytical grade and were purchased from Sigma-Aldrich (St. Louis, MO, USA).

4.2.2   Model preparation

4.2.2.1   PS model

A 75 µl volume of a 2% (w/v) alginate solution was pipetted onto a Transwell® filter insert, ensuring the entire filter area was covered, followed by the addition of 25 µl of a 5% (w/v) calcium chloride solution. Filter inserts were then allowed to incubate for at least one hour at room temperature to allow for complete gel formation.

4.2.2.2   Overall envelope model

The overall cell envelope model was also prepared using a Transwell® filter insert as a supporting base. Within this, the IM model was prepared first as described in

section 2.2.4, followed by the deposition of the PS model (see section 4.2.2.1) on top. The IM and PS structures were then finally overlaid with the OM model (IL + OL), prepared as described in section 3.2.2, in order to form the overall cell envelope model.

4.2.3   SEM

The PS model robustness and stability in the context of the overall model preparation process were investigated. In this respect, preparation of the OM model (more specifically, the IL component) on top of the PS layer was simulated (see section 4.2.2.2), by adding 37.5 µl of hexane to the PS model surface in two cycles, followed by oven drying after each addition. PS samples were subsequently frozen in liquid nitrogen and imaged via SEM (Zeiss EVO HD 15, Carl Zeiss AG, Oberkochen, Germany) in order to investigate any solvent-mediated changes in the PS surface structure.

4.2.4   CLSM

The structure of the overall envelope model was investigated via CLSM (Leica TCS SP8 AOBS/DMI8, Leica Microsystems GmbH, Wetzlar, Germany). In order to facilitate imaging, each component of the envelope structure was fluorescently stained. Laurdan was utilized to stain the IM model, incorporated into the structure by adding 0.1 mol% laurdan to the PL solution used for liposome preparation and subsequent IM formation (see sections 2.2.3 and 2.2.4). The PS model was initially prepared on a separate Transwell® filter insert to the formed IM, and was stained using FITC-labeled concanavalin A as a marker known to specifically interact with alginate [134]. Staining was achieved by incubating the formed alginate gel with a 500 µg ml^{-1} solution of FITC-labeled concanavalin A for 1.5 h, followed by washing with KRB. The PS model was subsequently transferred onto the IM model. The OM model was then added on top, prepared as described in 4.2.2.2, with the addition of 0.05 mol% Liss Rhod PE to the IL-PL mixture, as well as the employment of FITC-

labeled LPS for preparation of the OL. The overall envelope model was subsequently fixed on an object slide using an adhesive fixing agent, cut out of the plastic support and imaged in an inverted orientation.

4.2.5   Bacterial uptake studies

The fluorescent marker compounds fluorescein, rhodamine 123 and rhodamine B were again employed for bacterial uptake studies. Within these studies, a 20 ml volume of lysogeny broth medium was initially inoculated with 0.8 ml of an *E. coli* (BW25113) overnight culture, followed by adjustment to an OD of 6 in 5 mM magnesium sulfate. Bacterial cells were subsequently incubated with 1 µM solutions of each fluorescent dye (in KRB) for 30 min. A 390 µl volume of the bacterial cell suspension was then added on top of 550 µl of a 1 M sucrose cushion, followed by centrifugation (9 min, 4.5 g) to remove adherent (rather than internalized) dye. The supernatant was discarded and the pellet resuspended in 5 mM magnesium sulfate, followed by sonication using a probe sonicator (Sonoplus mini 20, Bandelin electronic GmbH & Co. KG, Berlin, Germany) on ice in order to disrupt the bacterial cells. A second centrifugation step (15 min, 15.7 g, 4 °C) was performed to sediment cell fragments. The obtained supernatant was subsequently used for quantification of marker compounds, with a compound extraction being carried out prior to quantification. For this purpose a 300 µl volume of each internalized fluorescent dye sample was added to 900 µl of acetonitrile, vortexed and centrifuged (10 min, 15.7 g, 4 °C). A 1000 µl volume of the resulting supernatant was transferred into a fresh vial and dried by vacuum centrifugation. The dried fraction was subsequently re-dissolved in 50 µl acetonitrile (containing 0.1 % formic acid and 10 ng ml^{-1} naproxen as internal standard), followed by shaking and centrifugation (5 min, 15.7 g). The solution was then transferred into vials for quantification (see section 4.2.7.3 below).

4.2.6   Permeability investigations

4.2.6.1   PS model

The permeability behavior of fluorescein and rhodamine B isothiocyanate (see Table 2.1, section 2.2.10) was assessed in the PS model, in order to confirm the absence of any permeation barrier properties. Hence, the permeability of these dyes across the PS model was compared to the permeability across blank Transwell® filter inserts. Transport studies were performed according to the procedure described in section 2.2.9, taking basolateral compartment samples for dye quantification after 0, 0.5, 1, 1.5, 2, and 2.5 h.

4.2.6.2   Overall envelope model

Overall envelope model-permeated amounts of fluorescent dyes (fluorescein, rhodamine 123 and rhodamine B; Table 2.1, section 2.2.10), in-house synthesized PqsD-inhibitors (compounds 52, 249, 250, 368, 369, and 562) and RNAP inhibitors (compounds 229, 230, 502, and 567) were investigated. All analyte solutions were prepared in KRB (pH 7.4) at concentrations calculated in order to ensure sink conditions (fluorescent dyes: Table 2.1, RNAP inhibitors: 50 µM, PqsD inhibitors: 400 µM). DMSO (2% v/v) was added to solutions of PqsD and RNAP inhibitors to ensure complete compound solubility. Transport studies were performed according to the procedure described in section 2.2.9, with sample collection in the case of fluorescent dyes after 0, 0.5, 1, 1.5, 2, 2.5, 3.5 and 4.5 h, and after 0, 0.5, 1, 1.5, 2, and 2.5 h in the case of anti-infective compounds. A shorter experiment duration was employed here to exclude any impact of DMSO on model barrier properties.

4.2.7   Quantification of permeated compound/drug amounts

4.2.7.1   Fluorescence quantification

A Tecan Infinite® M200 plate reader was used to determine the permeated amount of fluorescent dyes across the overall envelope model (for quantification parameters see Table 2.1, section 2.2.10).

4.2.7.2   UHPLC quantification

A UHPLC (Dionex Ulitmate® 3000) with an Accucore™ column (RP 18, 150 mm x 2.1 mm, 2.6 µm, Thermo Fisher Scientific Co., Waltham, MA, USA) was used to quantify the permeated amount of PqsD inhibitors in the overall envelope model. A binary solvent mixture (A: water + 0.1% trifluoroacetic acid (TFA); B: acetonitrile + 0.1% TFA) was used in a gradient run with an increase of B from 50% to 100 % in 3.7 min. A solvent flow rate of 400 µl min^{-1} was used, and a column temperature of 30 °C. Resulting RTs were 2.21 min for compound 52, 2.96 min for compound 249, 2.68 min for compound 250, 1.44 min for compound 368, 1.76 min for compound 369 and 1.77 min for compound 562. All compounds were measured via UV detection at a wavelength of 204 nm.

4.2.7.3   LC-MS/MS quantification

RNAP inhibitors were quantified according to the method described in section 3.2.8.3.

Fluorescent dyes in the context of bacterial uptake studies were quantified via a multiple reaction monitoring method which was adjusted for each fluorescent compound. An AB Sciex QTrap 6500 (AB Sciex Germany GmbH, Darmstadt, Germany) coupled to an Agilent 1290 UHPLC (Agilent Technologies, Santa Clara,

CA, USA) was used for this purpose, with bacterial matrix always included in the samples. The fluorescent dye quantification was performed using a binary solvent mixture (A: water + 0.1% formic acid; B: acetonitrile + 0.1% formic acid). A gradient run was employed, increasing B from 1% to 10% in 1 min, followed by an increase to 100% in 3.5 min; the solvent composition was then kept constant for 1.10 min. The flow rate of the mobile phase was set to 700 µl min^{-1}. Data was subsequently analyzed using MultiQuant software (AB Sciex Germany GmbH, Darmstadt, Germany).

4.2.7.4 Calculation of permeated compound amounts

The permeated amount of employed model fluorescent dyes as well as anti-infective compounds in transport experiments was calculated in all cases according to calibration curves created from samples of standard concentrations. Cumulative permeated amounts as a percentage were always normalized to the accurately-determined starting (apical) concentration.

4.2.8 Statistical analysis

Presented numerical data represent mean ± SE. Student's t-test was employed where relevant to assess significant differences; ***= P<0.001. All tests were calculated with the software SigmaPlot (version 12.5, see section 2.2.11).

4.3 Results and Discussion

4.3.1 PS model preparation

The PS model was designed to exhibit similar characteristics to the native PS: namely, to represent a viscous compartment without any appreciable permeation

barrier properties [34]. The PS model should furthermore facilitate a combined deposition of IM and OM structures on single Transwell® inserts, while maintaining separation of these individual models − resulting in an overall cell envelope structure with three discrete components. A hydrophilic gel spacer was employed to fulfil these functions and so the role of the PS. The spacer was formed by adding alginate and calcium chloride solutions onto Transwell® filter inserts, followed by at least one hour of incubation at room temperature to allow gel formation to occur. Alginate as such constitutes a linear copolymer, consisting of L-guluronate and D-mannuronate. Addition of divalent cations such as calcium mediates a linking of adjacent guluronate blocks, leading to the so-called egg-box model of cross-linking, resulting in a gel structure [135].

4.3.2   PS model characterization

The required absence of PS model barrier properties was investigated by comparing the permeability of readily-quantifiable fluorescent dyes (fluorescein and rhodamine B isothiocyanate) across the PS model to their permeation across blank Transwell® filter inserts. Fluorescein and rhodamine B isothiocyanate were chosen as they show differences in lipophilicity as well as different charges at the employed experimental pH of 7.4 (Table 2.4, section 2.3.4.1). This would allow for detection of any noticeable impact of such physicochemical parameters on permeation behavior through the PS. The permeability of both fluorescent dyes across the PS model was seen to be slightly reduced in comparison to blank Transwell® inserts (Figure 4.1A, B). Fluorescent dye permeation was furthermore seen to be drastically reduced in the case of the IM and OM model in comparison to the PS model (Figure 4.1B, C). Therefore, an absence of pronounced permeation limiting ability of the PS model is demonstrated, while the IM and OM clearly constitute the major permeation limiting structures. Hence, the model can be expected to function as a two-membrane permeation barrier, which is in line with the native, Gram-negative bacterial cell envelope [47].
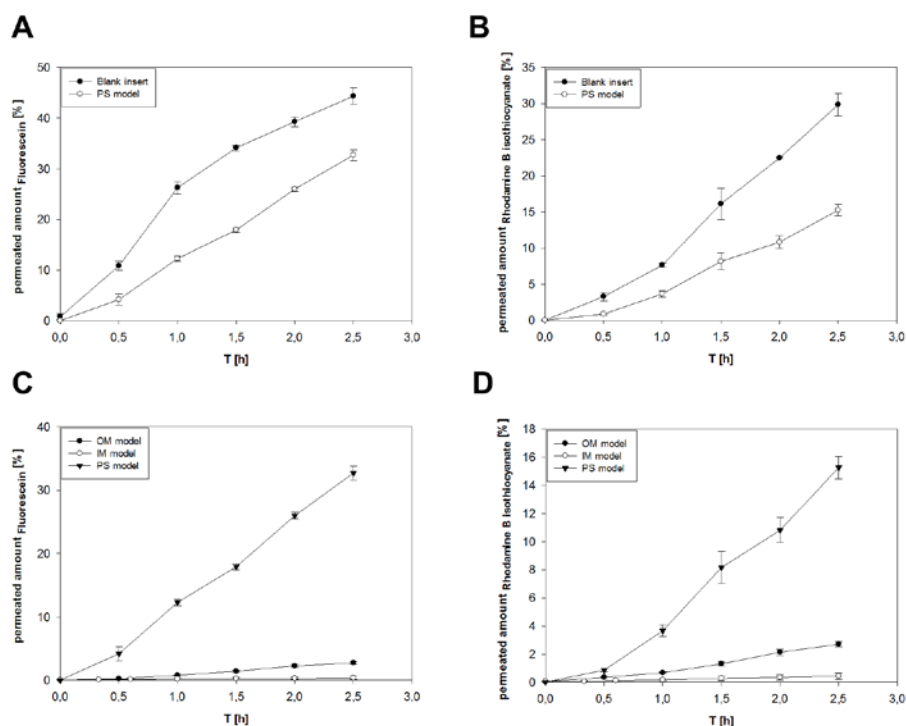
Figure 4.1: Permeated amounts of fluorescein (A) and rhodamine B isothiocyanate (B) across the PS model in comparison to blank Transwell® filter inserts are shown, revealing a negligible barrier function of the PS model. The comparison between permeated amounts of both fluorescent dyes across the OM, IM and PS model (C, D) respectively, is additionally shown. Values represent mean ± SE; n=3 for PS model and blank filter insert experiments; n=9 from 3 individual experiments for IM and OM model experiments.

Following confirmation of the functional similarity of the PS model to the bacterial PS in terms of a lack of permeation limiting ability, the stability and robustness of the PS model in the course of the overall model preparation procedure was assessed. Within this preparation procedure, the PS model has to withstand two cycles of hexane addition as a vehicle for dissolved PLs, followed by oven drying, in order to form the IL component of the OM (OM model addition on top of the PS, see section 4.2.2.2). Hexane was therefore added on top of the PS model and oven-dried as described, to simulate the OM model preparation procedure. PS model samples were subsequently imaged via SEM and compared to untreated (negative control) PS samples. Only a slight change in the PS surface structure due to the hexane addition was observed, with no clear indications of disrupted gel integrity (Figure 4.2). Observations altogether confirmed the suitability of the PS model to work as a robust spacer between IM and OM in the overall envelope model setup, without significantly contributing to the permeation-limiting function of the model.
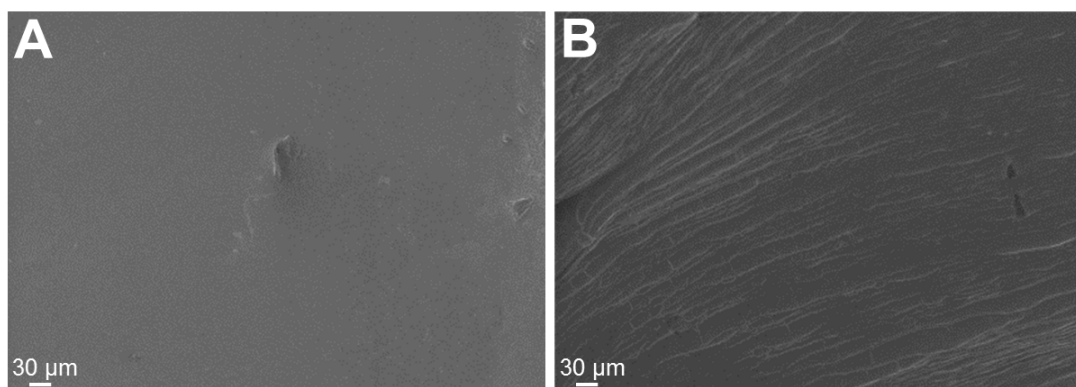
Figure 4.2: PS model without (A) and with hexane treatment (B), revealing some alteration in surface structure but no clear structural damage.

4.3.3   Overall envelope model preparation

In a final step, the three individually designed and characterized envelope component models (IM, PS, and OM) were combined on a Transwell® filter insert to produce an overall envelope model. The IM model was deposited first (see section 2.2.4), followed by the formation of the PS model (see section 4.2.2.1) directly on top. The OM model was then subsequently prepared on top of the formed PS (see section 3.2.2) to obtain the overall envelope model.

4.3.4   Overall envelope model characterization

Following formation of the overall envelope model, CLSM was employed to elucidate the continued existence of three discrete components (IM, PS, OM) within the structure. As mentioned in section 4.2.4, each individual component of the overall model was fluorescently labeled to allow for detection and identification. In order to achieve this staining, the preparation procedure of the overall envelope model was slightly altered compared to the procedure described in section 4.2.2.2, by preparing the PS model on a separate Transwell® filter insert rather than directly on top of the IM structure. This was introduced in order to ensure that PS model staining and subsequent washing did not interfere with nor alter the IM model. The PS model was then fluorescently stained and subsequently transferred on top of the IM model,

followed by OM component preparation. Obtained CLSM images indicated the presence of three discrete IM, PS and OM model layers (Figure 4.3A, B and C). However, a clear spatial differentiation of the layers in the combined image remains difficult (Figure 4.3D). This is due to objective-mediated limitations in resolution, as well as the altered overall model preparation procedure, in which incorporation of an additional PS transfer step was necessary for staining purposes (see section 4.2.4).
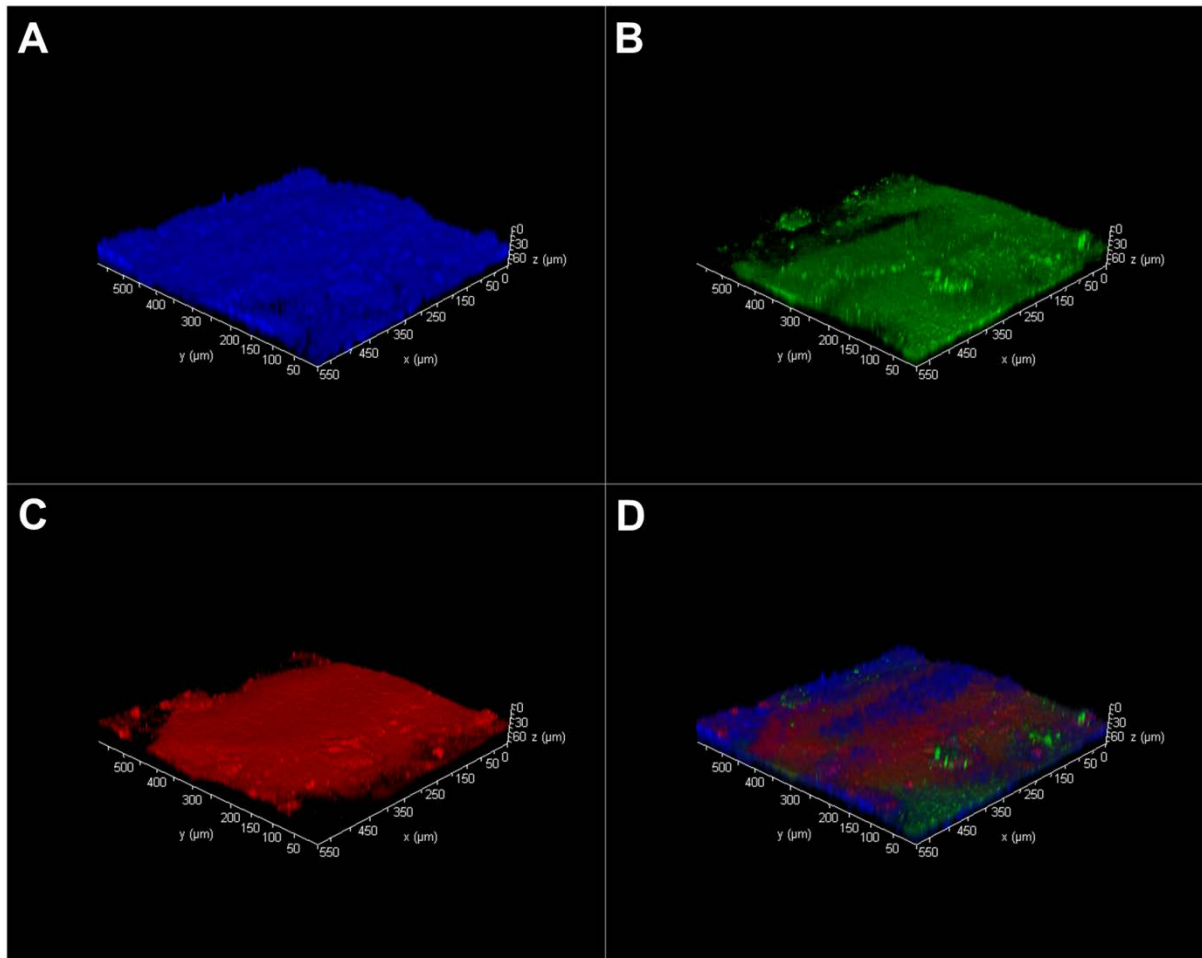
Figure 4.3: Z-stacks of overall envelope model samples, showing individual channels of the IM model in blue (A), the PS model in green (B) and the OM model in red (C) as well as the match of the channels (D). Analysis allowed for a differentiation between the three discrete model components, however a distinct spatial discrimination of the three layers in the combined image remains difficult.

4.3.5 Overall envelope model predictability assessment

Before the applicability and usefulness of the *in vitro* envelope model to serve as a tool in the development of new anti-infectives can be established, the ability of the model to provide predictive permeation data must first be demonstrated. Hence, three steps for assessing the predictability of model permeation data were defined, starting with a comparison of compound permeability across the overall envelope model to compound uptake into bacterial cells (*E. coli*). The second and third steps involved the permeability assessment of two sets of anti-infective compounds (PqsD and RNAP inhibitors) across the envelope model, followed by comparison of permeation behavior to previously obtained *in bacterio*-derived activity data. This comparison was carried out to elucidate the existence of any model permeability – *in bacterio* activity relationships.

4.3.5.1 Model permeability – *E. coli* uptake comparison

For an initial exploratory comparison, three fluorescent dyes (fluorescein, rhodamine 123 and rhodamine B) exhibiting a range of $logD_{(pH\ 7.4)}$ and different charges at the employed pH of 7.4 (Table 2.4, section 2.3.4.1) were defined, and their permeation across the overall envelope model was compared to their uptake into *E. coli.* While the *in vitro* model focuses purely on the assessment of passive permeation through the envelope membrane structures, *E. coli* cells obviously contain functioning active transport and efflux components as well as porins, capable of mediating transport. The selected dyes moreover allowed for the specific assessment of bacterial uptake without any data distortion due to bacterial killing, as might occur in the testing of antibiotics. Transport experiments revealed an increase of permeation/uptake with increasing dye lipophilicity in both, the *in vitro* model after the 2.5 h time point (Figure 4.4A) as well as *E. coli.* The permeation data from the maximum *in vitro* experiment runtime of 4.5 h corresponded even better to uptake *E. coli* data (Figure 4.4B). Furthermore, encouraging associations were noticed comparing the percentage of dye permeation across the *in vitro* envelope model after 2.5 h and 4.5 h, respectively, with the percentage compound uptake into *E. coli*

(Figure 4.4C, D). Differences in observed data comparing permeation across the model to uptake into *E. coli* might however be explained by an influence of protein-mediated as well as active transport or efflux processes in the case of *E. coli* data, whereas the *in vitro* model permeation data solely reflect passive trans-membrane permeation. While however being an encouraging first result, the small group of tested dyes must be expanded to the investigation of additional compounds to ultimately confirm an *in vitro* passive permeability – *in bacterio* uptake correlation.
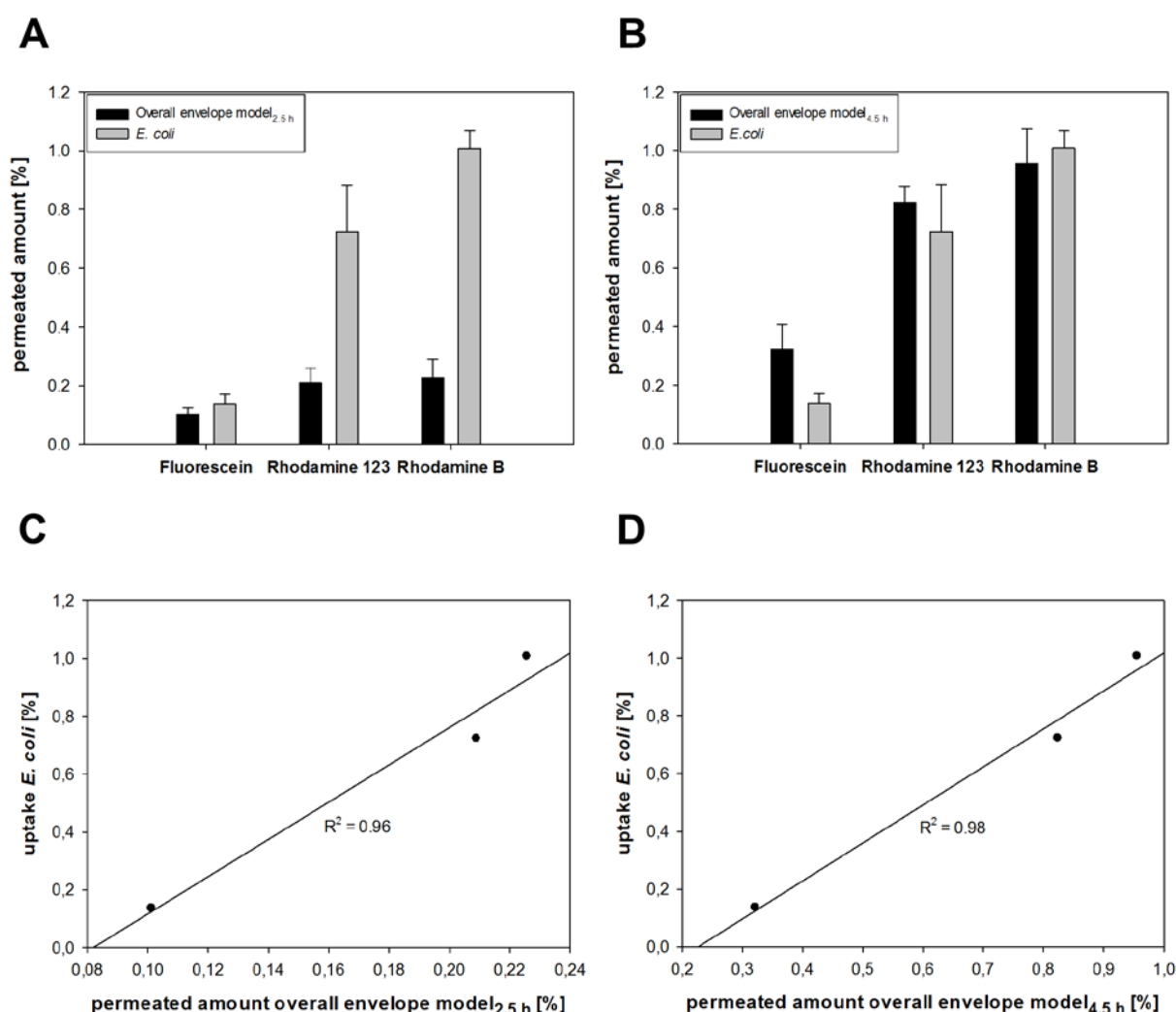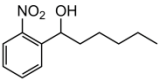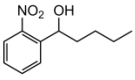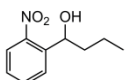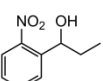
Figure 4.4: Comparison of permeability of employed fluorescent dyes across the overall envelope model with their uptake into *E. coli.* Data reveals the same trend at the 2.5 h time point of permeation studies in comparison to uptake data (A), as well as comparable permeation amounts at the 4.5 h time point of *in vitro* permeation studies in comparison to *E. coli* uptake (B). An appreciable association between the two data sets is furthermore indicated in the case of both *in vitro* experimental run times (C, D). Values represent mean ± SE; n=6 from 2 individual experiments.

4.3.5.2   PqsD inhibitors

In a second step, the focus shifted towards the permeability investigation of anti-infective compounds in the overall envelope model, and comparison of this permeation behavior to existing *in bacterio* activity data. A set of compounds of the PqsD inhibitor class was selected for this purpose. In general, this compound class interferes with the quorum sensing system of bacterial cell-to-cell communication, which in some bacteria such as *P. aeruginosa* is based on the *Pseudomonas Quinolone Signal (PQS)* as well as its precursor, 2-heptyl-4-quinolone (HHQ) [136]. Both substances are involved in regulating the production of virulence factors and in biofilm formation via activation of the transcriptional regulator PqsR [137-139]. Previous investigations have identified PqsD as a key enzyme in the biosynthesis of HHQ and PQS, making PqsD inhibitors an interesting group of anti-infective compounds [140, 141]. PqsD inhibitors are of particular interest in the context of the overall envelope model as they must permeate across the entire bacterial cell envelope structure in order to reach their intracellular target and do not affect bacterial growth. A set of in-house synthesized PqsD inhibitors (Table 4.1) was selected, on the basis of their comparable IC_{50} values, but in some cases a lack of *in bacterio* activity (see compounds 249 and 250, no HHQ inhibition, Table 4.1) [133]. The permeability of this compound set across the overall envelope model was then investigated, as a potential means to explain the differences in observed compound *in bacterio* activity.

Table 4.1: Important physiochemical parameters and activity in cell-free (IC$_{50}$) and cellular (HHQ inhibition) assays of employed PqsD inhibitors.

Compound	Structure	M_w (g mol^{-1})[a]	log P[b,c]	IC$_{50}$ (µM)[b,d]	HHQ inhibition (%)[b,e]
249		223.27	3.24	1.0	no inhibition
250		209.24	2.72	2.9	no inhibition
52		195.22	2.17	1.0	22
369		181.19	1.64	0.8	61
368		167.16	1.11	0.8	26
562		153.14	0.76	0.7	13

[a] Molecular weight. [b] Values from Storz *et al.* [133]. [c] Calculated partition coefficient (calculated by ACD/Labs 2012). [d] Half maximal inhibitory concentration. [e] Readout for compound activity determined in *P. aeruginosa* PA14 pqsH mutant at inhibitor concentrations of 250 µM. No inhibition was defined as <10 %.

Consistent with the above hypothesis, PqsD inhibitors which showed HHQ inhibition and therefore activity against *P. aeruginosa* (compounds 52, 368, 369 and 562) exhibited a significantly higher permeability across the envelope model than the non-active compounds (249, 250) – this can be clearly seen in Figure 4.5A, as well as in the kinetic permeation profiles in Figure 4.4B, which additionally highlight the ability of the overall model setup to allow for more detailed insight into permeation processes. Permeation data for compound 249 is absent in both figures, as at all time points permeated amounts were below the detection limit of the employed quantification assay. Moreover, it is of interest that an inverse correlation between PqsD inhibitor lipophilicity and permeation across the envelope model was observed, as this is in contrast to the direct correlation noted previously with tested fluorescent dyes (*in vitro – in bacterio* comparison; see section 4.3.5.1). This implies an impact of physicochemical parameters additional to lipophilicity on compound permeability. In addition, while active compounds in general showed a higher permeation in the

overall envelope model, the compound showing the highest activity against *P. aeruginosa* (compound 369) was not seen permeate with the highest amount across the envelope model. This interesting observation may be explained by a potential impact of active efflux processes − an aspect of further experimental interest. Nevertheless, clustering of the PqsD compound set based on their activity against *P. aeruginosa* and passive model permeation (Figure 4.5C) allowed for a clear distinction of two compound groups: low model permeability ~ no *in bacterio* activity, and high model permeability ~ *in bacterio* activity. This illustrates the impact of passive cell envelope permeability on *in bacterio* activity and so indicates a usefulness of data gained from the cell envelope model for the optimization of such novel anti-infectives compounds.
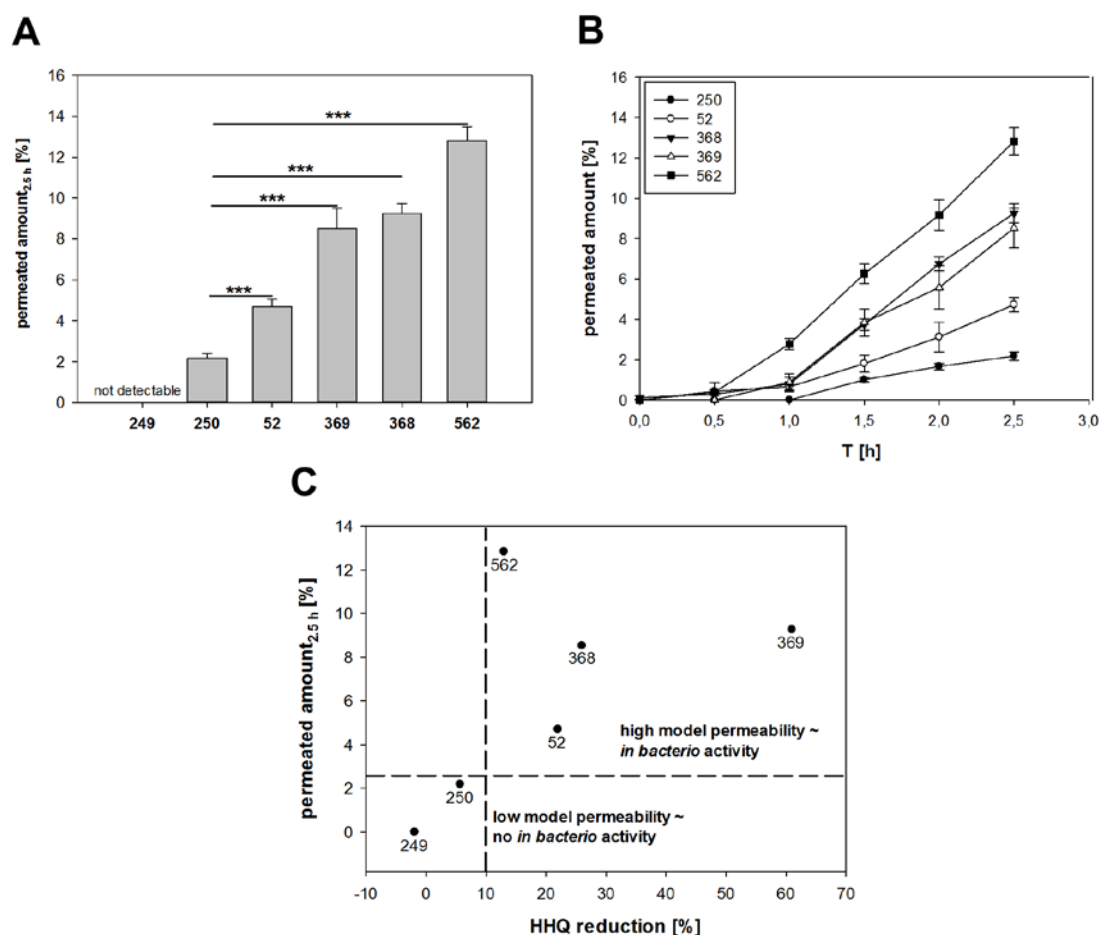
Figure 4.5: Permeability of PqsD inhibitors across the overall envelope model showing significantly higher permeation values in the case of *in bacterio* active compounds in comparison to non-active ones (A). Kinetic profiles highlight the ability of the overall envelope model setup to provide quantitative and kinetically-resolved permeation data (B). Compounds were furthermore clustered into two groups according to the permeation results and their pre-determined *in bacterio* activity (C). Values represent mean ± SE; n=6 from two individual experiments, *** = $P < 0.001$.

4.3.5.3 RNAP inhibitors

In a third step of the overall model predictability assessment, the same set of RNAP inhibitors which was already employed in the course of the OM model development (see section 3.3.3.3) was again utilized and tested additionally across the overall envelope model. This was done in order to elucidate the impact of the additional envelope components (IM and PS) on the previously assessed RNAP inhibitor permeability across the OM. Permeability experiment results revealed very small differences in permeation of tested compounds (Table 4.2) across the three-layered overall envelope model in comparison to the one-layer OM (as investigated in chapter 3, section 3.3.3.3). This is furthermore in agreement with previous cell-based investigations which showed the OM working as the major permeation barrier for these compounds [119]. Additionally, the same permeability behavior of tested RNAP inhibitors across the overall envelope model in comparison to the OM model could again be observed (Table 4.2). *E. coli* TolC-active compounds (229, 230) were again seen to permeate to a greater extent than the non-active compound 502.

Compound 567 again showed the highest permeability in the overall model despite its determined poor activity − this could be due to its high IC_{50}, as already mentioned in relation to the OM permeation studies; alternatively, the fact that its structural backbone is different to that of the other selected compounds (see Table 3.2, section 3.3.3.3) may mean that it is a substrate for alternative efflux systems to AcrA-AcrB-TolC. Knocking this system out (as in the TolC mutant) therefore would not show the same level of impact on its permeation as for the other compounds (229, 230 and 502). This demonstrates the ability of the envelope model to determine additional factors to permeability which influences antibiotic activity at an early stage, emphasizing the capability of the envelope model to act as an effective tool in testing novel antibiotic compounds.

Table 4.2: Results of previously performed cell-free and cell-based assays as well as permeability assessment across the OM as determined in chapter 3, and overall envelope model of employed RNAP inhibitors.

Compound	MIC in *E. coli* K12[a] (µg ml^{-1})	MIC in *E. coli* TolC[b] (µg ml^{-1})	Permeated amount$_{2.5\,h}$ OM model (%)[e]	Permeated amount$_{2.5\,h}$ overall envelope model (%)[e]
229	>50[c]	2.5[c]	2.28 ± 0.13	1.93 ± 0.15
230	>25[c]	2.3[c]	2.04 ± 0.15	1.39 ± 0.14
502	>25[c]	>25[c]	1.82 ± 0.10	1.17 ± 0.02
567	>50[d]	>50[d]	3.42 ± 0.31	2.91 ± 0.17

[a] E. coli K12: intact cell envelope system. [b] *E. coli* TolC: mutant deficient in the AcrAB-TolC efflux system. [c] Values from Hinsberger *et al.* [17]. [e] Values from Elgaher *et al.* [18]. [e] Values represent mean ± SE; n=6 from two individual experiments.

4.4   Conclusion

This chapter describes the preparation and characterization of a model of the PS, shown to be a functional mimic of the native PS, and furthermore designed to serve as a robust spacer between the IM and OM in the subsequently developed overall envelope model preparation procedure. Within this, all individually designed and developed envelope model components (IM, PS and OM) were successfully combined to form a stable and robust *in vitro* permeation model, mimicking the tripartite structure of the Gram-negative bacterial cell envelope. An initial exploratory study revealed permeation data from the overall envelope model to be predictive for bacterial (*E. coli*) uptake. The investigation of PqsD and RNAP inhibitor permeability across the overall envelope model was moreover seen to provide robust and in-depth characterization of anti-infective permeation, allowing for an information-rich determination (quantitative and time-resolved) of the influence of compound permeation on anti-infective efficacy on a case by case basis.

4.5   Acknowledgements

5.   General conclusion and summary

The presented work describes the successful development of an *in vitro* permeation model of the Gram-negative bacterial cell envelope. The model was designed in a step by step approach, modeling each component of the envelope barrier (IM, PS, and OM) individually and employing physiologically-relevant raw materials. The three components were combined in a final step, resulting in the overall envelope model structure. Herein, the commonly used Transwell® system was employed as a support for each of the individual prepared models, as well as the overall envelope model. This model setup and its divisible nature allows for a straight-forward permeability assessment in a quantitative, kinetically- and spatially-resolved manner, an advantage in comparison to existing *in vitro* and *in bacterio* approaches. During the development process each individual model was extensively characterized, investigating it microscopic and macroscopic structure as well as confirming its suitability for permeability experiment conditions. Moreover, the IM, PS and OM models were all designed to show functional similarity to the respective part of the native bacterial envelope. In order to confirm this similarity, the known bacterial membrane destabilizing and permeabilizing effects of PMB and EDTA were demonstrated in the IM and OM model, and OM model respectively; an appropriate absence of barrier properties in the PS model was also successfully demonstrated. Following combination of individual models, the structure of the combined overall envelope model was assessed, revealing the existence of three discrete layers. Permeation data derived from the overall envelope model was seen to be predictive of bacterial uptake, while the permeability investigation of two sets of novel anti-infective compounds (PqsD and RNAP inhibitors) showed the ability of the model to facilitate quantitative and in-depth characterization of anti-infective permeation, allowing for determination of the influence of compound permeation on anti-infective efficacy. Anti-infective efficacy was seen to be influenced by a complex interplay of compound-related factors (physicochemical parameters); through its provision of information-rich permeability data the developed overall envelope model clearly provides an ability to probe this interplay, and as such the developed model constitutes a useful tool for anti-infective compound development.

6.   Outlook

Additional employed methods such as scanning acoustic and photoacoustic microscopy showed initial promise in allowing for visualization of the discrete envelope model components, and as such is worthy of further investigation.

Furthermore, the overall envelope model, as developed and described in this thesis, can already be employed to investigate the passive permeability of small to middle scale anti-infective compound sets. To expand on this ability, two main strategic avenues in terms of future model advancement would be beneficial. On the one hand, an upscaling of the model preparation procedure employing a miniaturized support system would be valuable, as this would allow for a subsequent automatization and ability for high throughput screening capacity, enabling testing of large scale compound libraries. On the other hand, while the current ability of the overall envelope model to provide passive trans-membrane permeability data is already of considerable value, the incorporation of transport-mediating proteins as well as aspects of active efflux into the model would constitute a possible advancement. The insertion of proteins such as OMPs into the OM component of the overall membrane model could extend the validity of generated permeability data, while the incorporation of active efflux transporters would specifically allow for investigating alterations in levels of permeated anti-infective compounds as a function of the evolution of efflux-based resistance mechanisms.

In addition, the permeability assessment of a suitable compound set across the overall cell envelope model (in the current setup and especially after incorporation of transport-mediating proteins and aspects of active transport) would allow for elucidation of structure-permeability relationships for bacterial permeation, and the consequent definition of physiochemical parameters of anti-infectives which favor bacterial uptake. This could ultimately lead to the determination of rules for prediction of bacterial permeation [142] as well as to the definition of permeation-activity relationships.

7. References

[1] M. Schneider, M. Windbergs, N. Daum, B. Loretz, E.M. Collnot, S. Hansen, U.F. Schaefer, C.M. Lehr, Crossing biological barriers for advanced drug delivery, Eur. J. Pharm. Biopharm., 84 (2013) 239-241.

[2] L. Bartosova, J. Bajgar, Transdermal drug delivery *in vitro* using diffusion cells, Curr. Med. Chem., 19 (2012) 4671-4677.

[3] R.L. Bronaugh, R.F. Stewart, Methods for *in vitro* percutaneous absorption studies V: Permeation through damaged skin, J. Pharm. Sci., 74 (1985) 1062-1066.

[4] T.J. Franz, Percutaneous absorption on the relevance of *in vitro* data, J. Invest. Dermatol., 64 (1975) 190-195.

[5] M. di Cagno, H.A. Bibi, A. Bauer-Brandl, New biomimetic barrier Permeapad for efficient investigation of passive permeability of drugs, Eur. J. Pharm. Sci., 73 (2015) 29-34.

[6] H.A. Bibi, M. di Cagno, R. Holm, A. Bauer-Brandl, Permeapad for investigation of passive drug permeability: The effect of surfactants, co-solvents and simulated intestinal fluids (FaSSIF and FeSSIF), Int. J. Pharm., 493 (2015) 192-197.

[7] M. Kansy, F. Senner, K. Gubernator, Physicochemical high throughput screening: Parallel artificial membrane permeation assay in the description of passive absorption processes, J. Med. Chem., 41 (1998) 1007-1010.

[8] A. Avdeef, P. Artursson, S. Neuhoff, L. Lazorova, J. Grasjo, S. Tavelin, Caco-2 permeability of weakly basic drugs predicted with the double-sink PAMPA pKa (flux) method, Eur. J. Pharm. Sci., 24 (2005) 333-349.

[9] A. Avdeef, M. Strafford, E. Block, M.P. Balogh, W. Chambliss, I. Khan, Drug absorption *in vitro* model: filter-immobilized artificial membranes. 2. Studies of the permeability properties of lactones in *Piper methysticum* Forst, Eur. J. Pharm. Sci., 14 (2001) 271-280.

[10] F.T. Huque, K. Box, J.A. Platts, J. Comer, Permeability through DOPC/dodecane membranes: measurement and LFER modelling, Eur. J. Pharm. Sci., 23 (2004) 223-232.

[11] A. Avdeef, High-throughput Measurement of Permeability Profiles, in: Drug Bioavailability, Wiley, (2004) 46-71.

[12] A. Avdeef, Transport Model, in: Absorption and Drug Development, Wiley, (2003) 7-21.

[13] F. Wohnsland, B. Faller, High-throughput permeability pH profile and high-throughput alkane/water log P with artificial membranes, J. Med. Chem., 44 (2001) 923-930.

[14] K. Sugano, H. Hamada, M. Machida, H. Ushio, High throughput prediction of oral absorption: improvement of the composition of the lipid solution used in parallel artificial membrane permeation assay, J. Biomol. Screen., 6 (2001) 189-196.

REFERENCES

[15] K. Sugano, N. Takata, M. Machida, K. Saitoh, K. Terada, Prediction of passive intestinal absorption using bio-mimetic artificial membrane permeation assay and the paracellular pathway model, Int. J. Pharm., 241 (2002) 241-251.

[16] C. Zhu, L. Jiang, T.M. Chen, K.K. Hwang, A comparative study of artificial membrane permeability assay for high throughput profiling of drug absorption potential, Eur. J. Med. Chem., 37 (2002) 399-407.

[17] G. Ottaviani, S. Martel, P.A. Carrupt, Parallel artificial membrane permeability assay: a new membrane for the fast prediction of passive human skin permeability, J. Med. Chem., 49 (2006) 3948-3954.

[18] L. Di, E.H. Kerns, K. Fan, O.J. McConnell, G.T. Carter, High throughput artificial membrane permeability assay for blood-brain barrier, Eur. J. Med. Chem., 38 (2003) 223-232.

[19] X. Chen, A. Murawski, K. Patel, C.L. Crespi, P.V. Balimane, A novel design of artificial membrane for improving the PAMPA model, Pharm. Res., 25 (2008) 1511-1520.

[20] I.J. Hidalgo, T.J. Raub, R.T. Borchardt, Characterization of the human colon carcinoma cell line (Caco-2) as a model system for intestinal epithelial permeability, Gastroenterology, 96 (1989) 736-749.

[21] P. Artursson, J. Karlsson, Correlation between oral drug absorption in humans and apparent drug permeability coefficients in human intestinal epithelial (Caco-2) cells, Biochem. Biophys. Res. Commun., 175 (1991) 880-885.

[22] C.I. Grainger, L.L. Greenwell, D.J. Lockley, G.P. Martin, B. Forbes, Culture of Calu-3 cells at the air interface provides a representative model of the airway epithelial barrier, Pharm. Res., 23 (2006) 1482-1490.

[23] D.J. Giard, S.A. Aaronson, G.J. Todaro, P. Arnstein, J.H. Kersey, H. Dosik, W.P. Parks, *In vitro* cultivation of human tumors: establishment of cell lines derived from a series of solid tumors, J. Natl. Cancer. Inst., 51 (1973) 1417-1423.

[24] A. Kuehn, S. Kletting, C. de Souza Carvalho-Wodarz, U. Repnik, G. Griffiths, U. Fischer, E. Meese, H. Huwer, D. Wirth, T. May, N. Schneider-Daum, C.M. Lehr, Human alveolar epithelial cells expressing tight junctions to model the air-blood barrier, Altex, 33 (2016) 251-260.

[25] J. Susewind, C. de Souza Carvalho-Wodarz, U. Repnik, E.M. Collnot, N. Schneider-Daum, G.W. Griffiths, C.M. Lehr, A 3D co-culture of three human cell lines to model the inflamed intestinal mucosa for safety testing of nanomaterials, Nanotoxicology, 10 (2016) 53-62.

[26] G.E. Flaten, A.B. Dhanikula, K. Luthman, M. Brandl, Drug permeability across a phospholipid vesicle based barrier: a novel approach for studying passive diffusion, Eur. J. Pharm. Sci., 27 (2006) 80-90.

[27] G.E. Flaten, H. Bunjes, K. Luthman, M. Brandl, Drug permeability across a phospholipid vesicle-based barrier 2. Characterization of barrier structure, storage stability and stability towards pH changes, Eur. J. Pharm. Sci., 28 (2006) 336-343.

[28] G.E. Flaten, M. Skar, K. Luthman, M. Brandl, Drug permeability across a phospholipid vesicle based barrier: 3. Characterization of drug-membrane interactions and the effect of agitation on the barrier integrity and on the permeability, Eur. J. Pharm. Sci., 30 (2007) 324-332.

[29] G.E. Flaten, K. Luthman, T. Vasskog, M. Brandl, Drug permeability across a phospholipid vesicle-based barrier 4. The effect of tensides, co-solvents and pH changes on barrier integrity and on drug permeability, Eur. J. Pharm. Sci., 34 (2008) 173-180.

[30] E. Naderkhani, J. Isaksson, A. Ryzhakov, G.E. Flaten, Development of a biomimetic phospholipid vesicle-based permeation assay for the estimation of intestinal drug permeability, J. Pharm. Sci., 103 (2014) 1882-1890.

[31] A. Engesland, M. Skar, T. Hansen, N. Skalko-Basnet, G.E. Flaten, New applications of phospholipid vesicle-based permeation assay: permeation model mimicking skin barrier, J. Pharm. Sci., 102 (2013) 1588-1600.

[32] A. Engesland, N. Skalko-Basnet, G.E. Flaten, Phospholipid vesicle-based permeation assay and EpiSkin(R) in assessment of drug therapies destined for skin administration, J. Pharm. Sci., 104 (2015) 1119-1127.

[33] S.T. Buckley, S.M. Fischer, G. Fricker, M. Brandl, *In vitro* models to evaluate the permeability of poorly soluble drug entities: challenges and perspectives, Eur. J. Pharm. Sci., 45 (2012) 235-250.

[34] T.J. Silhavy, D. Kahne, S. Walker, The bacterial cell envelope, Cold Spring Harb. Perspect. Biol., 2 (2010) a000414.

[35] F. Graef, S. Gordon, C.-M. Lehr, Anti-infectives in drug delivery - Overcoming the Gram-negative bacterial cell envelope, in: How to Overcome the Antibiotic Crisis: Facts, challenges, technologies and future perspectives, Springer International Publishing, (2016) 475-496.

[36] M.L. Nelson, Grier, M.C., Barbaro, S. E., and Ismail M. Y., Polyfunctional antibiotics affecting bacterial membrane dynamics, Anti-Infect. Agents Med. Chem., 8 (2009) 3-16.

[37] L.A. Dever, T.S. Dermody, Mechanisms of bacterial resistance to antibiotics, Arch. Intern. Med., 151 (1991) 886-895.

[38] M. Palusinska-Szysz, A. Zdybicka-Barabas, B. Pawlikowska-Pawlega, P. Mak, M. Cytrynska, Anti-Legionella dumoffii activity of *Galleria mellonella* defensin and apolipophorin III, Int. J. Mol. Sci., 13 (2012) 17048-17064.

[39] W. Vollmer, D. Blanot, M.A. de Pedro, Peptidoglycan structure and architecture, FEMS Microbiol. Rev., 32 (2008) 149-167.

[40] C.W. Mullineaux, A. Nenninger, N. Ray, C. Robinson, Diffusion of green fluorescent protein in three cell environments in *Escherichia coli*, J. Bacteriol., 188 (2006) 3442-3448.

[41] C.R. Raetz, C. Whitfield, Lipopolysaccharide endotoxins, Annu Rev. Biochem., 71 (2002) 635-700.

[42] A. Kumar, H.P. Schweizer, Bacterial resistance to antibiotics: active efflux and reduced uptake, Adv. Drug. Deliv. Rev., 57 (2005) 1486-1513.

[43] A. Davin-Regli, J.M. Bolla, C.E. James, J.P. Lavigne, J. Chevalier, E. Garnotel, A. Molitor, J.M. Pages, Membrane permeability and regulation of drug "influx and efflux" in enterobacterial pathogens, Curr. Drug Targets, 9 (2008) 750-759.

REFERENCES

[44] F.C. Tenover, Mechanisms of antimicrobial resistance in bacteria, Am. J. Med., 119 (2006) S3-10; discussion S62-70.

[45] H. Nikaido, E.Y. Rosenberg, Porin channels in *Escherichia coli*: studies with liposomes reconstituted from purified proteins, J. Bacteriol., 153 (1983) 241-252.

[46] E. De, A. Basle, M. Jaquinod, N. Saint, M. Mallea, G. Molle, J.M. Pages, A new mechanism of antibiotic resistance in *Enterobacteriaceae* induced by a structural modification of the major porin, Mol. Microbiol., 41 (2001) 189-198.

[47] H.I. Zgurskaya, C.A. López, S. Gnanakaran, Permeability barrier of Gram-negative cell envelopes and approaches to bypass it, ACS Infect. Dis., 1 (2015) 512-522.

[48] M. Kreir, C. Farre, M. Beckler, M. George, N. Fertig, Rapid screening of membrane protein activity: electrophysiological analysis of OmpF reconstituted in proteoliposomes, Lab on a chip, 8 (2008) 587-595.

[49] T. Mach, C. Chimerel, J. Fritz, N. Fertig, M. Winterhalter, C. Futterer, Miniaturized planar lipid bilayer: increased stability, low electric noise and fast fluid perfusion, Anal. Bioanal. Chem., 390 (2008) 841-846.

[50] J.L. Gornall, K.R. Mahendran, O.J. Pambos, L.J. Steinbock, O. Otto, C. Chimerel, M. Winterhalter, U.F. Keyser, Simple reconstitution of protein pores in nano lipid bilayers, Nano Lett., 11 (2011) 3334-3340.

[51] J.M. Pages, C.E. James, M. Winterhalter, The porin and the permeating antibiotic: a selective diffusion barrier in Gram-negative bacteria, Nat. Rev. Microbiol., 6 (2008) 893-903.

[52] C. Danelon, E.M. Nestorovich, M. Winterhalter, M. Ceccarelli, S.M. Bezrukov, Interaction of zwitterionic penicillins with the OmpF channel facilitates their translocation, Biophys. J., 90 (2006) 1617-1627.

[53] E.M. Nestorovich, C. Danelon, M. Winterhalter, S.M. Bezrukov, Designed to penetrate: time-resolved interaction of single antibiotic molecules with bacterial pores, Proc. Natl. Acad. Sci. U.S.A., 99 (2002) 9789-9794.

[54] K.R. Mahendran, E. Hajjar, T. Mach, M. Lovelle, A. Kumar, I. Sousa, E. Spiga, H. Weingart, P. Gameiro, M. Winterhalter, M. Ceccarelli, Molecular basis of enrofloxacin translocation through OmpF, an outer membrane channel of *Escherichia coli* - when binding does not imply translocation, The journal of physical chemistry B, 114 (2010) 5170-5179.

[55] D.I. Fernandez, A.P. Le Brun, T.C. Whitwell, M.A. Sani, M. James, F. Separovic, The antimicrobial peptide aurein 1.2 disrupts model membranes via the carpet mechanism, Phys. Chem. Chem. Phys., 14 (2012) 15739-15751.

[56] A.I. Kuzmenko, H. Wu, F.X. McCormack, Pulmonary collectins selectively permeabilize model bacterial membranes containing rough lipopolysaccharide, Biochemistry, 45 (2006) 2679-2685.

[57] M. Luckey, H. Nikaido, Specificity of diffusion channels produced by lambda phage receptor protein of Escherichia coli, Proc. Natl. Acad. Sci. U. S. A., 77 (1980) 167-171.

[58] G. D'Errico, A. Silipo, G. Mangiapia, A. Molinaro, L. Paduano, R. Lanzetta, Mesoscopic and microstructural characterization of liposomes formed by the lipooligosaccharide from *Salmonella minnesota* strain 595 (Re mutant), Phys. Chem. Chem. Phys., 11 (2009) 2314-2322.

[59] J. Kubiak, J. Brewer, S. Hansen, L.A. Bagatolli, Lipid lateral organization on giant unilamellar vesicles containing lipopolysaccharides, Biophys. J., 100 (2011) 978-986.

[60] N. Modi, M. Winterhalter, U. Kleinekathofer, Computational modeling of ion transport through nanopores, Nanoscale, 4 (2012) 6166-6180.

[61] G. Fragneto, T. Charitat, J. Daillant, Floating lipid bilayers: models for physics and biology, Eur. Biophys. J., 41 (2012) 863-874.

[62] C. Rodrigues, P. Gameiro, M. Prieto, B. de Castro, Interaction of rifampicin and isoniazid with large unilamellar liposomes: spectroscopic location studies, Biochim. Biophys. Acta, 1620 (2003) 151-159.

[63] O. Ries, C. Carnarius, C. Steinem, C. Ducho, Membrane-interacting properties of the functionalised fatty acid moiety of muraymycin antibiotics, Med. Chem. Comm., 6 (2015) 879-886.

[64] C. Peetla, A. Stine, V. Labhasetwar, Biophysical interactions with model lipid membranes: applications in drug discovery and drug delivery, Mol. Pharmaceutics, 6 (2009) 1264-1276.

[65] T. Charitat, E. Bellet-Amalric, G. Fragneto, F. Graner, Adsorbed and free lipid bilayers at the solid-liquid interface, The European Physical Journal B - Condensed Matter and Complex Systems, 8 (1999) 583-593.

[66] D.I. Fernandez, A.P. Le Brun, T.H. Lee, P. Bansal, M.I. Aguilar, M. James, F. Separovic, Structural effects of the antimicrobial peptide maculatin 1.1 on supported lipid bilayers, Eur. Biophys. J., 42 (2013) 47-59.

[67] L.A. Clifton, C.L. Johnson, A.S. Solovyova, P. Callow, K.L. Weiss, H. Ridley, A.P. Le Brun, C.J. Kinane, J.R. Webster, S.A. Holt, J.H. Lakey, Low resolution structure and dynamics of a colicin-receptor complex determined by neutron scattering, J. Biol. Chem., 287 (2012) 337-346.

[68] A.P. Le Brun, L.A. Clifton, C.E. Halbert, B. Lin, M. Meron, P.J. Holden, J.H. Lakey, S.A. Holt, Structural characterization of a model gram-negative bacterial surface using lipopolysaccharides from rough strains of *Escherichia coli*, Biomacromolecules, 14 (2013) 2014-2022.

[69] L.A. Clifton, M.W. Skoda, E.L. Daulton, A.V. Hughes, A.P. Le Brun, J.H. Lakey, S.A. Holt, Asymmetric phospholipid: lipopolysaccharide bilayers; a Gram-negative bacterial outer membrane mimic, J. R. Soc. Interface., 10 (2013) 20130810.

[70] L.A. Clifton, M.W. Skoda, A.P. Le Brun, F. Ciesielski, I. Kuzmenko, S.A. Holt, J.H. Lakey, Effect of divalent cation removal on the structure of gram-negative bacterial outer membrane models, Langmuir, 31 (2015) 404-412.

[71] L.A. Clifton, S.A. Holt, A.V. Hughes, E.L. Daulton, W. Arunmanee, F. Heinrich, S. Khalid, D. Jefferies, T.R. Charlton, J.R. Webster, C.J. Kinane, J.H. Lakey, An accurate in vitro model of the *E. coli* envelope, Angew. Chem. Int. Ed., 54 (2015) 11952-11955.

[72] D. Mayers, Antimicrobial Drug Resistance: Mechanisms of Drug Resistance, Humana Press, 2009.

REFERENCES

[73] K. Murzyn, T. Rog, M. Pasenkiewicz-Gierula, Phosphatidylethanolamine-phosphatidylglycerol bilayer as a model of the inner bacterial membrane, Biophys. J., 88 (2005) 1091-1103.

[74] W. Zhao, T. Rog, A.A. Gurtovenko, I. Vattulainen, M. Karttunen, Role of phosphatidylglycerols in the stability of bacterial membranes, Biochimie, 90 (2008) 930-938.

[75] T. Lemmin, C. Bovigny, D. Lançon, M. Dal Peraro, Cardiolipin models for molecular simulations of bacterial and mitochondrial membranes, Journal of Chemical Theory and Computation, 9 (2013) 670-678.

[76] K.R. Pandit, J.B. Klauda, Membrane models of *E. coli* containing cyclic moieties in the aliphatic lipid chain, Biochim. Biophys. Acta., 1818 (2012) 1205-1210.

[77] R.D. Lins, T.P. Straatsma, Computer simulation of the rough lipopolysaccharide membrane of *Pseudomonas aeruginosa*, Biophys. J., 81 (2001) 1037-1046.

[78] T.J. Piggot, D.A. Holdbrook, S. Khalid, Electroporation of the *E. coli* and *S. aureus* membranes: molecular dynamics simulations of complex bacterial membranes, J. Phys. Chem. B, 115 (2011) 13381-13388.

[79] E.L. Wu, P.J. Fleming, M.S. Yeom, G. Widmalm, J.B. Klauda, K.G. Fleming, W. Im, *E. coli* outer membrane and interactions with OmpLA, Biophys. J., 106 (2014) 2493-2502.

[80] N.A. Berglund, T.J. Piggot, D. Jefferies, R.B. Sessions, P.J. Bond, S. Khalid, Interaction of the antimicrobial peptide polymyxin B1 with both membranes of *E. coli*: a molecular dynamics study, PLoS Comput. Biol., 11 (2015) e1004180.

[81] E. Hajjar, K.R. Mahendran, A. Kumar, A. Bessonov, M. Petrescu, H. Weingart, P. Ruggerone, M. Winterhalter, M. Ceccarelli, Bridging timescales and length scales: from macroscopic flux to the molecular mechanism of antibiotic diffusion through porins, Biophys. J., 98 (2010) 569-575.

[82] P.R. Singh, M. Ceccarelli, M. Lovelle, M. Winterhalter, K.R. Mahendran, Antibiotic permeation across the OmpF channel: modulation of the affinity site in the presence of magnesium, The journal of physical chemistry. B, 116 (2012) 4433-4438.

[83] M.T. Cronin, A.O. Aptula, J.C. Dearden, J.C. Duffy, T.I. Netzeva, H. Patel, P.H. Rowe, T.W. Schultz, A.P. Worth, K. Voutzoulidis, G. Schuurmann, Structure-based classification of antibacterial activity, J. Chem. Inf. Comput. Sci., 42 (2002) 869-878.

[84] R. O'Shea, H.E. Moser, Physicochemical properties of antibacterial compounds: implications for drug discovery, J. Med. Chem., 51 (2008) 2871-2878.

[85] T.D. Davis, C.J. Gerry, D.S. Tan, General platform for systematic quantitative evaluation of small-molecule permeability in bacteria, ACS Chem. Biol., 9 (2014) 2535-2544.

[86] H. Cai, K. Rose, L.H. Liang, S. Dunham, C. Stover, Development of a liquid chromatography/mass spectrometry-based drug accumulation assay in *Pseudomonas aeruginosa*, Anal. Biochem., 385 (2009) 321-325.

[87] Y. Zhou, C. Joubran, L. Miller-Vedam, V. Isabella, A. Nayar, S. Tentarelli, A. Miller, Thinking outside the "bug": a unique assay to measure intracellular drug penetration in gram-negative bacteria, Anal. Chem., 87 (2015) 3579-3584.

[88] S. Kascakova, L. Maigre, J. Chevalier, M. Refregiers, J.M. Pages, Antibiotic transport in resistant bacteria: synchrotron UV fluorescence microscopy to determine antibiotic accumulation with single cell resolution, PLoS One, 7 (2012) e38624.

[89] J.M. Pages, S. Kascakova, L. Maigre, A. Allam, M. Alimi, J. Chevalier, E. Galardon, M. Refregiers, I. Artaud, New Peptide-based antimicrobials for tackling drug resistance in bacteria: single-cell fluorescence imaging, ACS Med. Chem. Lett., 4 (2013) 556-559.

[90] B. Cinquin, L. Maigre, E. Pinet, J. Chevalier, R.A. Stavenger, S. Mills, M. Refregiers, J.M. Pages, Microspectrometric insights on the uptake of antibiotics at the single bacterial cell level, Sci. Rep., 5 (2015) 17968.

[91] M. Thein, G. Sauer, N. Paramasivam, I. Grin, D. Linke, Efficient subfractionation of Gram-negative bacteria for proteomics studies, J. Proteome Res., 9 (2010) 6135-6147.

[92] R.M. Epand, R.F. Epand, Bacterial membrane lipids in the action of antimicrobial agents, J. Pept. Sci., 17 (2011) 298-305.

[93] F. Müller-Landau, D.A. Cadenhead, B.M.J. Kellner, The nature of the liquid expanded/liquid condensed phase change in insoluble monolayers at the air/water interface, J. Colloid Interface Sci., 73 (1980) 264-266.

[94] T.-H. Chou, I.M. Chu, C.-H. Chang, Interaction of paclitaxel with DSPC in monolayers at the air/water interface at different temperatures, Colloids Surf., B, 25 (2002) 147-155.

[95] A.D. Bangham, M.M. Standish, J.C. Watkins, Diffusion of univalent ions across the lamellae of swollen phospholipids, J. Mol. Biol., 13 (1965) 238-252.

[96] F. Graef, B. Vukosavljevic, J.P. Michel, M. Wirth, O. Ries, C. De Rossi, M. Windbergs, V. Rosilio, C. Ducho, S. Gordon, C.M. Lehr, The bacterial cell envelope as delimiter of anti-infective bioavailability - an *in vitro* permeation model of the Gram-negative bacterial inner membrane, J. Control. Release, 243 (2016) 214-224.

[97] J.T. Davies, E.K. Rideal, Interfacial phenomena, Academic Press, New York, 1963.

[98] D. Marsh, Lateral pressure in membranes, Biochim. Biophys. Acta, 1286 (1996) 183-223.

[99] S.M. Fischer, G.E. Flaten, E. Hagesaether, G. Fricker, M. Brandl, *In-vitro* permeability of poorly water soluble drugs in the phospholipid vesicle-based permeation assay: the influence of nonionic surfactants, J. Pharm. Pharmacol., 63 (2011) 1022-1030.

[100] F. Leonard, E.M. Collnot, C.M. Lehr, A three-dimensional coculture of enterocytes, monocytes and dendritic cells to model inflamed intestinal mucosa *in vitro*, Mol. Pharm., 7 (2010) 2103-2119.

[101] S.P. Gantzsch, B. Kann, M. Ofer-Glaessgen, P. Loos, H. Berchtold, S. Balbach, T. Eichinger, C.M. Lehr, U.F. Schaefer, M. Windbergs, Characterization and evaluation of a modified PVPA barrier in comparison to Caco-2 cell monolayers for combined dissolution and permeation testing, J. Control. Release, 175 (2014) 79-86.

[102] A. Avdeef, Absorption and Drug Development: Solubility, Permeability, and Charge State, Wiley, 2012.

REFERENCES

[103] A. Malkia, L. Murtomaki, A. Urtti, K. Kontturi, Drug permeation in biomembranes: *in vitro* and *in silico* prediction and influence of physicochemical properties, Eur. J. Pharm. Sci., 23 (2004) 13-47.

[104] A.M. Marino, M. Yarde, H. Patel, S. Chong, P.V. Balimane, Validation of the 96 well Caco-2 cell culture model for high throughput permeability assessment of discovery compounds, Int. J. Pharm., 297 (2005) 235-241.

[105] A. Avdeef, The rise of PAMPA, Expert Opin. Drug Metab. Toxicol., 1 (2005) 325-342.

[106] R.E. Hancock, A. Bell, Antibiotic uptake into gram-negative bacteria, Eur. J. Clin. Microbiol. Infect. Dis., 7 (1988) 713-720.

[107] R. Daugelavicius, E. Bakiene, D.H. Bamford, Stages of polymyxin B interaction with the *Escherichia coli* cell envelope, Antimicrob. Agents Chemother., 44 (2000) 2969-2978.

[108] D.R. Storm, K.S. Rosenthal, P.E. Swanson, Polymyxin and related peptide antibiotics, Annu. Rev. Biochem., 46 (1977) 723-763.

[109] M. Teuber, J. Bader, Action of polymyxin B on bacterial membranes. Binding capacities for polymyxin B of inner and outer membranes isolated from *Salmonella typhimurium* G30, Arch. Microbiol., 109 (1976) 51-58.

[110] Y. Zhang, F. Chen, E. Sun, R. Ma, C. Qu, L. Ma, *In vitro* antibacterial activity of combinations of fosfomycin, minocycline and polymyxin B on pan-drug-resistant *Acinetobacter baumannii*, Exp. Ther. Med., 5 (2013) 1737-1739.

[111] D.R. Bowers, H. Cao, J. Zhou, K.R. Ledesma, D. Sun, O. Lomovskaya, V.H. Tam, Assessment of minocycline and polymyxin B combination against *Acinetobacter baumannii*, Antimicrob. Agents. Chemother., 59 (2015) 2720-2725.

[112] L.A. McDonald, L.R. Barbieri, G.T. Carter, E. Lenoy, J. Lotvin, P.J. Petersen, M.M. Siegel, G. Singh, R.T. Williamson, Structures of the muraymycins, novel peptidoglycan biosynthesis inhibitors, J. Am. Chem. Soc., 124 (2002) 10260-10261.

[113] E.J. Lugtenberg, R. Peters, Distribution of lipids in cytoplasmic and outer membranes of *Escherichia coli* K12, Biochim. Biophys. Acta, 441 (1976) 38-47.

[114] K. Takrouri, H.D. Cooper, A. Spaulding, P. Zucchi, B. Koleva, D.C. Cleary, W. Tear, P.J. Beuning, E.B. Hirsch, J.B. Aggen, Progress against *Escherichia coli* with the oxazolidinone class of antibacterials: Test case for a general approach to improving whole-cell Gram-negative activity, ACS Infect. Dis., 2 (2016), 405-426.

[115] H. Nikaido, Molecular basis of bacterial outer membrane permeability revisited, Microbiol. Mol. Biol. Rev., 67 (2003) 593-656.

[116] H.L. Alakomi, A. Paananen, M.L. Suihko, I.M. Helander, M. Saarela, Weakening effect of cell permeabilizers on Gram-negative bacteria causing biodeterioration, Appl. Environ. Microbiol., 72 (2006) 4695-4703.

[117] K.S. Rosenthal, D.R. Storm, Disruption of the *Escherichia coli* outer membrane permeability barrier by immobilized polymyxin B, J. Antibiot., 30 (1977) 1087-1092.

[118] S. Hinsberger, K. Husecken, M. Groh, M. Negri, J. Haupenthal, R.W. Hartmann, Discovery of novel bacterial RNA polymerase inhibitors: pharmacophore-based virtual screening and hit optimization, J. Med. Chem., 56 (2013) 8332-8338.

[119] W.A.M. Elgaher, M. Fruth, M. Groh, J. Haupenthal, R.W. Hartmann, Expanding the scaffold for bacterial RNA polymerase inhibitors: design, synthesis and structure-activity relationships of ureido-heterocyclic-carboxylic acids, RSC Advances, 4 (2014) 2177-2194.

[120] J.R. Howse, J. Bowers, E. Manzanares-Papayanopoulos, I.A. McLure, R. Steitz, Neutron reflectivity studies of critical adsorption: the correspondence between a critical adsorption profile and specular neutron reflection, Phys. Rev. E. Stat. Phys. Plasmas Fluids Relat. Interdiscip. Topics, 59 (1999) 5577-5581.

[121] T. Hauss, S. Dante, T.H. Haines, N.A. Dencher, Localization of coenzyme Q10 in the center of a deuterated lipid membrane by neutron diffraction, Biochim. Biophys. Acta, 1710 (2005) 57-62.

[122] M.J. Jesus Valle, F.G. Lopez, A.S. Navarro, Development and validation of an HPLC method for vancomycin and its application to a pharmacokinetic study, J. Pharm. Biomed. Anal., 48 (2008) 835-839.

[123] M. Ishinaga, R. Kanamoto, M. Kito, Distribution of phospholipid molecular species in outer and cytoplasmic membrane of *Escherichia coli*, J. Biochem., 86 (1979) 161-165.

[124] H. Zhang, Thin-Film Hydration Followed by Extrusion Method for Liposome Preparation, in: Liposomes: Methods and protocols, Springer, (2017) 17-22.

[125] R.E. Hancock, The bacterial outer membrane as a drug barrier, Trends Microbiol., 5 (1997) 37-42.

[126] M. Vaara, Agents that increase the permeability of the outer membrane, Microbiol. Rev., 56 (1992) 395-411.

[127] H. Nikaido, M. Vaara, Molecular basis of bacterial outer membrane permeability, Microbiol. Rev., 49 (1985) 1-32.

[128] V. Prachayasittikul, C. Isarankura-Na-Ayudhya, T. Tantimongcolwat, C. Nantasenamat, H.J. Galla, EDTA-induced membrane fluidization and destabilization: biophysical studies on artificial lipid membranes, Acta. Biochim. Biophys. Sin. , 39 (2007) 901-913.

[129] Z. Yu, W. Qin, J. Lin, S. Fang, J. Qiu, Antibacterial mechanisms of polymyxin and bacterial resistance, BioMed. Research International, 2015 (2015) 11.

[130] X. Du, Y. Li, Y.L. Xia, S.M. Ai, J. Liang, P. Sang, X.L. Ji, S.Q. Liu, Insights into protein-ligand interactions: Mechanisms, models, and methods, Int. J. Mol. Sci., 17 (2016).

[131] U.S. Eggert, N. Ruiz, B.V. Falcone, A.A. Branstrom, R.C. Goldman, T.J. Silhavy, D. Kahne, Genetic basis for activity differences between vancomycin and glycolipid derivatives of vancomycin, Science, 294 (2001) 361-364.

[132] I. Chopra, Bacterial RNA polymerase: a promising target for the discovery of new antimicrobial agents, Curr. Opin. Investig. Drugs., 8 (2007) 600-607.

REFERENCES

[133] M.P. Storz, G. Allegretta, B. Kirsch, M. Empting, R.W. Hartmann, From *in vitro* to *in cellulo*: structure-activity relationship of (2-nitrophenyl)methanol derivatives as inhibitors of PqsD in Pseudomonas aeruginosa, Org. Biomol. Chem., 12 (2014) 6094-6104.

[134] M. Strathmann, J. Wingender, H.C. Flemming, Application of fluorescently labelled lectins for the visualization and biochemical characterization of polysaccharides in biofilms of *Pseudomonas aeruginosa*, J. Microbiol. Methods., 50 (2002) 237-248.

[135] K.Y. Lee, D.J. Mooney, Alginate: properties and biomedical applications, Prog. Polym. Sci., 37 (2012) 106-126.

[136] E.C. Pesci, J.B. Milbank, J.P. Pearson, S. McKnight, A.S. Kende, E.P. Greenberg, B.H. Iglewski, Quinolone signaling in the cell-to-cell communication system of *Pseudomonas aeruginosa*, Proc. Natl. Acad. Sci. U. S. A., 96 (1999) 11229-11234.

[137] C. Lu, B. Kirsch, C. Zimmer, J.C. de Jong, C. Henn, C.K. Maurer, M. Musken, S. Haussler, A. Steinbach, R.W. Hartmann, Discovery of antagonists of PqsR, a key player in 2-alkyl-4-quinolone-dependent quorum sensing in *Pseudomonas aeruginosa*, Chem. Biol., 19 (2012) 381-390.

[138] C. Lu, C.K. Maurer, B. Kirsch, A. Steinbach, R.W. Hartmann, Overcoming the unexpected functional inversion of a PqsR antagonist in *Pseudomonas aeruginosa*: an *in vivo* potent antivirulence agent targeting pqs quorum sensing, Angew. Chem. Int. Ed., 53 (2014) 1109-1112.

[139] M.P. Storz, C.K. Maurer, C. Zimmer, N. Wagner, C. Brengel, J.C. de Jong, S. Lucas, M. Musken, S. Haussler, A. Steinbach, R.W. Hartmann, Validation of PqsD as an anti-biofilm target in *Pseudomonas aeruginosa* by development of small-molecule inhibitors, J. Am. Chem. Soc., 134 (2012) 16143-16146.

[140] L.A. Gallagher, S.L. McKnight, M.S. Kuznetsova, E.C. Pesci, C. Manoil, Functions required for extracellular quinolone signaling by *Pseudomonas aeruginosa*, J. Bacteriol., 184 (2002) 6472-6480.

[141] Y.M. Zhang, M.W. Frank, K. Zhu, A. Mayasundari, C.O. Rock, PqsD is responsible for the synthesis of 2,4-dihydroxyquinoline, an extracellular metabolite produced by *Pseudomonas aeruginosa*, J. Biol. Chem., 283 (2008) 28788-28794.

[142] K. Lewis, Antibiotics: Recover the lost art of drug discovery, Nature, 485 (2012) 439-440.

8. Appendices

8.1   Abbreviations

ADME	absorption, distribution, metabolism, excretion
AMPs	antimicrobial peptides
BM-PAMPA	biomimetic-PAMPA
CL	1,1',2,2'-tetra-(9Z-octadecenoyl) cardiolipin (sodium salt)
CLSM	confocal laser scanning microscopy
Cryo-SEM	cryogenic scanning electron microscopy
DMSO	dimethylsulfoxide
DOPC	dioleoylphosphatidylcholine
DPPC	dipalmitoylphosphatidylcholine
DS-PAMPA	double-sink PAMPA
DUV	deep ultraviolet
EDTA	ethylenediaminetetraacetic acid
ER	electrical resistance
FITC	fluorescein isothiocyanate
hAELVi	human Alveolar Epithelial Lentivirus immortalized
HDM-PAMPA	hexadecane membrane PAMPA
HHQ	2-heptyl-4-quinolone (HHQ)
IL	inner leaflet
IM	inner membrane
ITC	isothermal titration calorimetry
KRB	Krebs-Ringer buffer
LB	Langmuir-Blodgett
LC	liquid condensed
LC-MS/MS	liquid chromatography-tandem mass spectrometry
LE	liquid expanded

Liss Rhod PE	lissamine rhodamine labeled 1,2-dipalmitoyl-*sn*-glycero-3-phosphoethanolamine
Log D(pH 7.4)	distribution coefficient at pH 7.4
LPS	lipopolysaccharides
LS	Langmuir-Schaefer
MIC	minimum inhibitory concentration
MD	molecular dynamic
OD	optical density
OL	outer leaflet
OM	outer membrane
OMP	outer membrane protein
PAMPA	parallel artificial membrane permeability assay
P_{app}	apparent permeability coefficient
PBS	phosphate-buffered saline
PC	phosphatidylcholine
PE	phosphatidylethanolamine
PG	phosphatidylglycerol
PL	phospholipid
PMB	polymyxin B
POPE	1-hexadecanoyl-2-(9*Z*-octadecenoyl)-*sn*-glycero-3-phosphoethanolamine
POPG	1-hexadecanoyl-2-(9*Z*-octadecenoyl)-*sn*-glycero-3-phospho-(1'-*rac*-glycerol) (sodium salt)
PQS	*Pseudomonas* Quinolone Signal
PS	periplasmic space
PVDF	polyvinylidene fluoride
PVPA	phospholipid-vesicle based permeation assay
RNAP	RNA polymerase
ROI	region of interest
RT	retention time
SAR	structure-activity relationship
SE	standard error of the mean

SEM   scanning electron microscopy

SLBs   supported lipid bilayers

TFA   trifluoracetic acid

UHPLC   ultra-high performance liquid chromatography

XRD   X-ray diffractometer

8.2 Figures

8.3   Tables

Curriculum vitae

PERSONAL DATA

Date of birth	15.05.1987
Birthplace	Bamberg
Family status	married

DOCTORAL STUDIES

Since 09/2013   **Helmholtz Institute for Pharmaceutical Research Saarland (HIPS), Helmholtz Center for Infection Research (HZI), Department of Drug Delivery (Head: Prof. Dr. Claus-Michael Lehr), Saarbrücken**

PhD in pharmaceutical technology
- Topic: Modeling the Gram-negative bacterial cell envelope: A new approach for permeability investigations of anti-infectives
- Supervisor of student laboratory courses
- Supervisor of one master thesis student and one pharmaceutical research internship student
- Lecturer in the course 'Drug Delivery' for biotechnology master students

INTERNSHIPS

05/2012 – 11/2012   **Novartis Pharma Stein AG, Process Unit Packaging, Stein**
- Line leader at a secondary packaging line
- Responsible for a job change optimization project (secondary packaging line)
- Support in a six-sigma (IQP) optimization project (paste project; including self-organized experiments)
- Support of process experts
- Rapid route cause investigations in the context of deviations and complaints

11/2011 – 05/2012   **'Engel – Apotheke' (community pharmacy), Münster**
As part of the mandatory pharmacy internship

07/2010 – 10/2010   **Sanofi - Aventis Deutschland GmbH, Department New Lantus Plant, Frankfurt a. M.**
Lead of an optimization project on a vial filling line
- Determination of the silicone content in the vials
- Detailed analysis of the silicone cleaning mechanism

08/2008 – 10/2008   **Dr. Robert Pfleger Chemische Fabrik GmbH, Bamberg**
As part of the mandatory pharmacy internship

EDUCATION

01/2013   **Pharmacist Licensure ('Approbation')**
Grade: 2.08

04/2007 – 11/2011   **Westfälische Wilhelms-University, Münster**
Studies of Pharmacy
Grade second state examination: 1.2

02/2010 – 07/2010   **University of Barcelona**
Erasmus semester

09/1997 – 06/2006   '**Dientzenhofer Gymnasium' (High School), Bamberg**
Degree: Abitur (Grade: 2.5)

FURTHER ACTIVITIES

11/2014 and 01/2016   **Attendance of workshops for doctoral researchers offered by the doctoral training program of Saarland University (GradUS)**
- Project management
- Leadership skills for doctoral researchers

03/2015 – 02/2016   **Participation in lectures as part of the doctoral training program of Saarland University (GradUS)**
- 3D analysis of micro and nanostructures
- Nano-biomaterials

10/2009 – 10/2011   Member of the Student Council of the Faculty of Pharmacy at Münster University

FURTHER SKILLS AND INTERESTS

Languages   German (native), English (fluent), French (beginner),
Spanish (beginner)

IT   Advanced skills in Microsoft$^®$ Word, Excel and Powerpoint,
Sigma Plot, Origin, Chromeleon (HPLC), Endnote

112

Scientific output

Articles published in Peer-reviewed journals

F.Graef, B. Vukosavljevic, J.-P. Michel, M. Wirth, O. Ries, C. De Rossi, M. Windbergs, V. Rosilio, C. Ducho, S. Gordon and C.-M. Lehr, The Bacterial Cell Envelope as Delimiter of Anti-Infective Bioavailability – An In Vitro Permeation Model of the Gram-Negative Bacterial Inner Membrane, *J. Control Release*, 2016

S. Seif, **F. Graef**, S. Gordon, M. Windbergs, Monitoring Drug Release from Electrospun Fibers Using an In Situ Fiber-Optic Probe, *Dissolut. Techn.*, 2016

Book chapter

F. Graef, S. Gordon, C.-M. Lehr, Anti-infectives in Drug Delivery − Overcoming the Gram-Negative Bacterial Cell Envelope, *Curr. Top. Microbiol. Immunol.*, 2016; and Anti-infectives in Drug Delivery − Overcoming the Gram-Negative Bacterial Cell Envelope, in: *How to Overcome the Antibiotic Crisis: Facts, Challenges, Technologies and Future Perspectives*, Springer International Publishing, 2016

Oral presentations

Controlled Release Society (CRS) German chapter meeting 2015, Basel, Switzerland

'Towards a drug permeation model of the Gram-negative bacterial envelope'

Globalization of Pharmaceutics Education Network (GPEN) 2014, Helsinki, Finland

'Modeling the Gram-negative bacterial cell envelope: A new approach for permeability investigation of anti-infectives'

Poster presentations

HIPS Symposium 2016, Saarbrücken, Germany

'Pseudobacterial nanocarriers for intracellular delivery of anti-infective drugs'

World Meeting on Pharmaceutics, Biopharmaceutics and Pharmaceutical Technology (PBP) 2016, Glasgow, Scotland

'An *in vitro* permeation model of the Gram-negative bacterial outer membrane for permeability investigations in early drug discovery'

Controlled Release Society (CRS) Annual Meeting 2015, Edinburgh, Scotland

'Designing a permeation model of the Gram-negative bacterial cell envelope'

HIPS Symposium 2014, Saarbrücken, Germany

'Modeling the Gram-negative bacterial cell envelope – a new approach

for permeability investigation of novel anti-infectives in early drug discovery'

Acknowledgements

‘‘Wer glaubt etwas zu sein

hat aufgehört etwas zu werden. ”

-Sokrates-